Multi-User Detection of Overloaded Systems with Low-Density Spreading

Mitchell Fantuz, B.A.Sc.

Thesis submitted in partial fulfillment of the requirements for the

Master of Applied Science degree in Electrical and Computer Engineering

Ottawa-Carleton Institute for Electrical and Computer Engineering

Faculty of Engineering

School of Information Technology and Engineering

University of Ottawa

Abstract

Future wireless networks will have applications that require many devices to be connected to the network. Non-orthogonal multiple access (NOMA) is a promising multiple access scheme that allows more users to simultaneously transmit in a common channel than orthogonal signaling techniques. This overloading allows for high spectral efficiencies which can support the high demand for wireless access. One notable NOMA scheme is low-density spreading (LDS), which is a code domain multiple access scheme. Low density spreading operates like code division multiple access (CDMA) in the sense that users use a spreading sequence to spread their data, but the spreading sequences have a low number of nonzero chips, hence the term low-density. The message passing algorithm (MPA) is typically used for multi-user detection (MUD) of LDS systems. The MPA detector has complexity that is exponential to the number of users contributing to each chip. LDS systems suffer from two inherent problems: high computational complexity, and vulnerability to multipath channels. In this thesis, these two problems are addressed. A lower complexity MUD technique is presented, which offers complexity that is proportional to the number of users squared. The proposed detector is based on minimum mean square error (MMSE) and parallel interference cancellation (PIC) detectors. Simulation results show the proposed MUD technique achieves reductions in multiplications and additions by 81.84% and 67.87% with a loss of about 0.25 dB with overloading at 150%. In addition, a precoding scheme designed to mitigate the effects of the multipath channel is also presented. This precoding scheme applies an inverse channel response to the input signal before transmission. This allows for the received signal to eliminate the multipath effects that destroy the low-density structure.

Acknowledgments

At this time, I would like to express thanks and gratitude to the individuals who helped with the completion of this thesis.

I would like to express my sincere appreciation to my supervisor Dr. Claude D'Amours. His technical knowledge, guidance and constructive suggestions gave me the skills and foundation to make this possible. I feel fortunate to have him not only as my supervisor, but as a mentor.

I would also like to offer my special thanks to the many individuals at NordiaSoft for our partnership in the NSERC Engage program. This program gave me the opportunity to develop some of this work on their tools and framework, as well as provide funding to make this possible.

To my loved ones, thank you for your constant support throughout the writing of this thesis. Also, thank you for putting up with my frequent complaining throughout my studies.

Table of Contents

List of Figures

List of Tables

List of Acronyms

1G	First Generation
2G	Second generation
4G	Fourth Generation
3G	Third Generation
5G	Fifth Generation
AWGN	Additive White Gaussian Noise
BER	Bit Error Rate
BPSK	Binary Phase Shift Keying
CDMA	Code Division Multiple Access
CP	Cyclic Prefix
DFT	Discrete Fourier Transform
FDE	Frequency Domain Equalization
FDMA	Frequency Domain Multiple Access
IDFT	Inverse Discrete Fourier Transform
IoT	Internet of Things
LDPC	Low Density Parity Check
LDS-CDMA	Low-Density Spreading CDMA
LDS-OFDM	Low-Density Spreading Orthogonal Frequency Domain Multiplexing
LLR	Log Likelihood Ratio
LPMA	Lattice Partition Multiple Access
M2M	Machine-to-Machine

MAI	Multiple Access Interference
MAP	Maximum a Posteriori Probability
MC-CDMA	Multicarrier CDMA
MIMO	Multiple-Input Multiple-Output
MMSE	Minimum Mean Square Error
mmWaves	Millimeter Waves
MPA	Message Passing Algorithm
MUD	Multi-User Detection
NOMA	Non-Orthogonal Multiple Access
OFDMA	Orthogonal Frequency Domain Multiple Access
OMA	Orthogonal Multiple Access
PDMA	Pattern Division Multiple Access
PIC	Parallel Interference Cancellation
SCMA	Sparse Code Multiple Access
SIC	Successive Interference Cancellation
SNR	Signal to Noise Ratio
TDMA	Time Domain Multiple Access
V2X	Vehicle to Everything
ZF	Zero Forcing

List of Symbols

$\left(\widetilde{\mathbf{R}}_k^T\right)^T$	Column k of $\widetilde{\mathbf{R}}$
$(\cdot)^+$	Moore-Penrose pseudoinverse
$(\cdot)^*$	Conjugation operator
$(\cdot)^H$	Hermitian transpose
$(\cdot)^T$	Transpose operator
$\widetilde{H}_{\mathrm{inv}_{k,i}}$	Normalized inverse channel frequency response at frequency bin i
U_{PIC_k}	Decision variable for user k after the PIC detector
$\hat{b}_k$	Final estimated bit for user k
b_{soft_k}	Soft bit for user k
$(\cdot)'$	Frequency-nonselective fading channel parameter
$(\cdot)''$	Precoding in multipath channel parameter
$\mathrm{DFT}_{N_{\mathrm{DFT}}}\{\cdot\}$	Discrete Fourier Transform of length N_{DFT}
$\mathrm{erf}(\cdot)$	Error function
$\exp(\cdot)$	Exponential function
h_k	Frequency-nonselective fading channel gain for user k
$\mathcal{L}^t_{u_k \to f_n}(x)$	Message sent from variable node k to function node n
$\mathcal{L}^t_{f_n \to u_k}(x)$	Message sent from function node n to variable node k
$\tanh(\cdot)$	Hyperbolic tangent operator
$\mathbf{H}_k$	Frequency domain of $\mathbf{h}_k$
$\widetilde{\mathbf{S}}$	Spreading matrix after separation of real and imaginary parts
$\widetilde{\mathbf{U}}$	Vector of decision variables split into real and imaginary components

$\mathbf{U}_{\mathrm{MMSE}}$	Decision variables after MMSE filter
$\mathbf{U}_{\mathrm{ZF}}$	Decision variables after zero forcing filter
$\mathbf{W}_{\mathrm{MMSE}}$	MMSE filter
$\mathbf{W}_{\mathrm{ZF}}$	Zero forcing filter
$\mathbf{Y}_k$	Frequency domain of $\mathbf{y}_k$
$\hat{\mathbf{b}}$	Vector of final estimated bits
$\mathbf{b}_{\mathrm{soft}}$	Vector of soft bits
$\mathbf{h}_k$	Multipath channel for user k
$\tilde{\mathbf{n}}$	Noise vector split into real and imaginary parts
$\mathbf{s}_k$	Spreading code for user k
$\mathbf{w}_k$	MMSE filter for user k
$\mathbf{y}_k$	Vector of grouped parallel spread bits
$\mathbf{z}_k$	Transmitted signal for user k after precoding
A_k	Amplitude of user k
$E_{\mathbf{H}_{\mathrm{inv}}}$	Energy of the inverse channel frequency response
$H_{\mathrm{inv}_k}(i)$	Inverse channel frequency response at frequency bin i
I_{MMSE_k}	Multiple access interference for decision variable k after the MMSE detector
I_{PIC_k}	Multiple access interference for decision variable k after the PIC detector
$M_n(\mathbf{x})$	Metrics computed at function node n
N_{MMSE_k}	Noise for decision variable k after the MMSE detector
N_{PIC_k}	Noise decision k after the PIC detector
N_{syms}	Number of parallel symbols used for precoding
$R_{k,i}$	Cross correlation between the spreading codes of user k and i
U_{MMSE_k}	Decision variable for user k after the MMSE detector

U_k	Decision variable for user k
$Y_{k,i}$	ith frequency bin of $\mathbf{Y}_k$
b_k	Bit for user k
d_c	Number of nonzero chips in a spreading code
d_f	Number of users contributing to a chip
f_n	Function node n
p_k	Probability that bit k is $+1$
r_n	Received signal at chip n
u_k	Variable node k
x_k	Transmitted symbol for user k
$\mathcal{X}_k$	Constellation set for user k
α_k	Coefficient for U_{MMSE_k} to compute soft bits
$\beta_{k,i}$	Coefficient for bit i after the MMSE detector
γ_k	Effective channel gain of user k
ζ_k	Set of nonzero values in the spreading code for user k
$\lambda_{k,i}$	Coefficient of residual MAI from bit i affecting decision variable k
ξ_n	Set of users that contribute to chip n
σ^2	Noise power
$\Im(\cdot)$	Imaginary part
$\Re(\cdot)$	Real part
$\mathrm{sgn}(\cdot)$	sgn function
$\mathbf{A}$	Diagonal matrix of users' amplitudes
$\mathbf{G}$	Indicator matrix
$\mathbf{H}$	Diagonal matrix of users' channel gains
$\mathbf{P}$	Diagonal matrix of the power transmitted from each user

$\mathbf{R}$	Cross correlation matrix
$\mathbf{S}$	Spreading matrix
$\mathbf{U}$	Vector of decision variables
$\mathbf{n}$	Noise vector
$\mathbf{r}$	Received signal vector
$\mathbf{x}$	Vector of transmitted symbols
$E[\cdot]$	Expectation operator
K	Number of Users
L	Length of multipath channel
$LLR(\cdot)$	Log likelihood ratio operator
M	Constellation size
N	Spreading code length
$P(\cdot)$	Probability function
$Q(\cdot)$	Q function
$p(\cdot)$	Probability mass function
$\mathbf{\Gamma}$	Diagonal matrix of effective channel gains
$\mathbf{\Upsilon}$	Diagonal matrix of received powers for each user
η	Overloading factor

Chapter 1
Introduction

1.1 Motivation and Background

The evolution from Fourth Generation (4G) to Fifth Generation (5G) cellular mobile communication systems is not incremental. The goal for 5G systems is to increase the aggregate data rate in a network 1000 times and increase cell edge rates 100 times compared to current 4G systems [1]. In addition, roundtrip latencies should be reduced by a factor of 15 to meet the demands of low latency applications such as two-way gaming, and cloud-based technologies [1]. To meet these high demands for increased data rates, 5G developers will have to find new technologies and methodologies for mobile networks. Some of these new technologies include device-centric architectures, millimeter waves (mmWave), massive multiple input multiple output (MIMO), smarter devices, and native support for machine-to-machine (M2M) communication [2].

Typical cellular systems have relied upon cell-centric models, where devices would enter and leave cells depending on their location. Devices would establish a connection to centralized base stations and would send data via uplink and receive data via downlink. The introduction of more devices, and increased spectrum with 5G will make it difficult to continue this cell-centric structure. Device-centric architectures will look to tackle these issues [3]. There is an enormous amount of unused spectrum in the mm wave bands (30-300 GHz) that can potentially be used for 5G [4]. MmWaves have not been considered for previous cellular networks due to their high propagation losses in outdoor conditions. But, new signal processing techniques and technologies are changing that notion [5]. Massive MIMO will use large amounts of antennas at base stations to allow for more advanced beamforming, spatial multiplexing, and spatial modulations [6].

The number of connected devices to a network could be in the tens or hundreds of billions due to applications such as Internet of Things (IoT), smart cities and devices, vehicle

to everything (V2X) and M2M communications that will need to be supported in 5G [1], [7]. The massive increase in devices on a network will require improvements to previous multiple access methods.

Determining how to allocate resources to users and how to allow users to access these resources is the core of cellular network design. Users access shared resources depending on the multiple access method implemented. In first-generation (1G) cellular networks, frequency domain multiple access (FDMA) was used. In this method, non-overlapping frequency channels were assigned to each user to separate them. Analog frequency modulation was used to transmit users' voice conversations on their respective channel. Second generation (2G) networks mainly used time domain multiple access (TDMA) to separate users. TDMA assigned time slots for different users, and each user could only transmit during its own time slot. This enhancement allowed for digital signaling and the introduction of mobile internet applications.

Advances in internet applications created the need for even higher data rates, and that is when third generation (3G) networks were introduced. 3G networks used code division multiple access (CDMA), which assigned users unique codes to spread their information. These unique codes have rates much higher than the signal bandwidth. These codes have good cross-correlation and autocorrelation properties which allowed users signals to be separable in the code domain. The development of 4G allowed for applications with high bandwidth requirements such as streaming and gaming applications. 4G systems make use of an advanced form of FDMA, orthogonal frequency domain multiple access (OFDMA). OFDMA allowed users to transmit their data on overlapping orthogonal subcarriers, in the frequency domain.

The multiple access methods described do not utilize any overloading, and in some cases, take advantage of orthogonality in the resources in which they use. The multiple access schemes that do take advantage of orthogonality between resources are referred to as orthogonal multiple access (OMA). OMA methods are attractive as they, when implemented correctly, can perfectly separate users without any multiple access interference (MAI). The downside to OMA schemes is that the maximum capacity is limited to the number of orthogonal resources. When the number of users exceeds this limit, MAI is inevitable.

To meet the data rate and capacity requirements for 5G systems, techniques beyond OMA will need to be explored. Non-orthogonal multiple access (NOMA) is a promising alternative that will be able to meet these demands [8]. NOMA allows for more users than orthogonal resources, and thus, each user's data will overlap over these resources, and they can no longer be orthogonal to one another. NOMA schemes are uniquely designed to limit the

MAI in a multiple access system. NOMA offers key features over OMA such as high spectral efficiency, ultra-high connectivity, and low transmission latency [9].

NOMA schemes can be broken down into 3 categories: power-domain NOMA, NOMA multiplexing in multiple domains and code-domain NOMA [9]. Power-domain NOMA is novel compared to other multiple access schemes due to how it separates users in the power domain instead of separation done typically in the time, frequency or space domains. Power-domain NOMA assigns users different power levels, based on each user's channel conditions, and will separate them through successive interference cancelation (SIC) [10]. SIC will estimate the transmitted information of the strongest user first, and then subtract that user's contribution to the total received signal. With the strongest user's signal eliminated, the second strongest user will be estimated next and so forth until each user's symbols have been estimated. NOMA multiplexing in multiple domains brings subcategories such as pattern division multiple access (PDMA) and lattice partition multiple access (LPMA). Pattern division multiple access uses nonorthogonal patterns in the code, power and space domains to use SIC [11]. The various domains used allow for the receiver to use a mix of different detection schemes. LPMA uses the power domain and code domain to multiplex users [12]. The difference between PDMA and LPMA is that LPMA assigns users multilevel lattice codes and power levels based on their channel state information.

Code-domain NOMA is similar to CDMA, in the sense that users share the same time-frequency resources but are assigned different codes to separate them [13]. Low-density spreading CDMA (LDS-CDMA) uses time domain resources for spreading, while low density spreading orthogonal frequency domain multiplexing (LDS-OFDM) spreads the symbols from each user on orthogonal subcarriers.

LDS was first introduced in [14] in a downlink scenario, but the primary advantages of LDS lie capability in uplink scenarios. Conventional CDMA systems have spreading sequences which consist of chips that are all nonzero. At the receiver, each sampled chip will then have a contribution from every user that is transmitting. LDS-CDMA differs in the sense that majority of the spreading chips are zero, with a few being nonzero [15]. Hence why it is termed low density. At the receiver of an LDS-CDMA scheme, each sampled chip will now only have contribution from a few users, instead of every user.

LDS-CDMA or LDS-OFDM is extended further to another code-domain NOMA scheme called sparse code multiple access (SCMA). SCMA still uses low density spreading sequences to spread each user's information, like LDS-CDMA, but combines modulation and

spreading into one functional unit, as shown in Figure 1.1 [16]. The combined symbol mapping and spreading block will take m bits and assign them to a spreading signature from a given codebook. Each user is given a unique codebook which contains 2^m codewords, one for each possible sequence of m message bits. Figure 1.1 shows an example of an SCMA system that has 6 users and 4 chips. 2 bits are mapped to a low density codeword which in this case, has 2 nonzero chips.

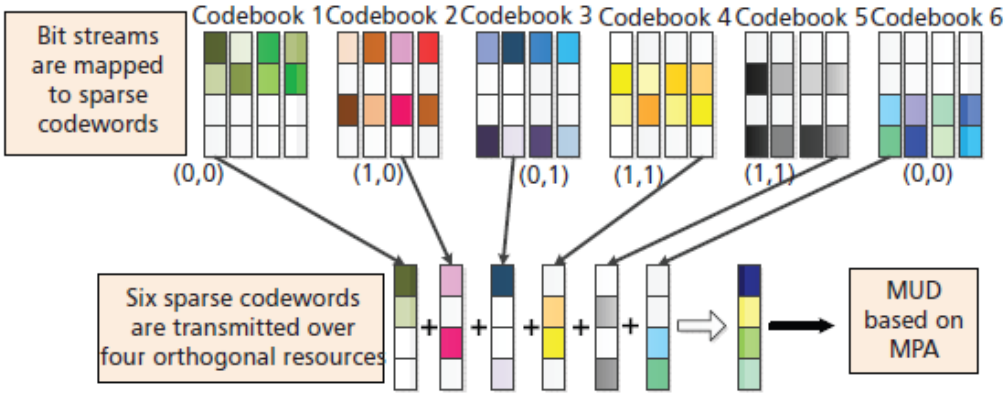

Figure 1.1: SCMA transmission [13]

The codebooks are designed such that each position of non-zero chips in a signature is fixed for every codeword in a codebook. This allows the receiver in a multiuser system to always know which users are contributing to each chip, like the LDS-CDMA structure. One of the advantages of SCMA in comparison to LDS-CDMA is that the codebooks can be designed to achieve a coding/shaping gain that the LDS-structure cannot achieve. The maximum achievable shaping gain with an optimized codebook is 1.53 dB [16]. Design of optimal codebooks is still an open problem, and some suboptimal design methods have been studied in [16], [17], [18]. A main focus of some suboptimal methods involve the design of a mother constellation, and performing operations on the mother constellation, such as phase rotation, complex conjugate, or vector permutations to derive the constellations used for the different codebooks [17], [18]. Other methods include designing codebooks based on permutation and have different nonzero positions for each codeword in a given codebook [19].

1.2 Thesis Objectives

LDS systems are being considered for 5G networks because of their high spectral efficiency. The overloading capability of LDS systems allow them to use less resources than current multiple access schemes. With the massive increase in connected devices on the network expected with 5G, this efficient spectrum usage is crucial. In addition, they offer near optimal MUD with reduced complexity, compared to the MAP detector. These benefits make LDS systems very attractive for 5G and other future networks. With these great benefits to LDS systems, there are still limiting factors to LDS-CDMA implementation. The two biggest limitations LDS systems face are:

- The high complexity involved with the detection of LDS systems using the message passing algorithm (MPA)
- Multipath fading channels

In this thesis, both of these problems with LDS systems will be addressed. The objectives of this thesis are:

- To find an alternative to the current MPA detection scheme that offers a reduction in computational complexity while keeping near bit error rate (BER) performance.
- To develop a scheme to allow for LDS systems to operate in multipath channels with acceptable BER performance.

1.3 Contribution of Thesis

The following are the main contributions of this thesis:

- An alternative MUD for LDS systems that doesn't involve MPA is proposed. This MUD is based on the joint linear minimum mean square error (MMSE) and parallel interference cancellation (PIC) detectors. The received signal is despread, and then separated into real and imaginary parts. From here, the PIC-MMSE detector operates on each user's decision variables after despreading. This detector has much lower complexity compared to the exponential complexity of MPA.
- An approximate BER is derived for the proposed PIC-MMSE detector.

- Simulations and complexity analysis are presented for the proposed PIC-MMSE and MPA detectors.
- A precoding scheme to combat LDS-CDMA signals in multipath environments based on frequency domain equalization (FDE) is introduced. Each user's signal is precoded such that the effects of the multipath channel are suppressed.
- Simulation results for the precoding scheme are presented to test its BER performance using the PIC-MMSE and MPA detectors. Errors in channel state information are also included in the simulation results.

  In addition, the work in this thesis has led to a publication to the Canadian Conference on Electrical and Computer Engineering (CCECE) 2019.

1.4 Thesis Organization

The remainder of this thesis is organized as follows:

Chapter 2 gives an overview of LDS systems. This overview includes the motivation behind the low-density structure, and the various factors that play into the performance of LDS systems. The design of spreading and the derivation of the MPA algorithm is also given. The BER performance is given through simulations for various system models and channel types.

Chapter 3 introduces the proposed PIC-MSE detector. In addition, other conventional detectors such as the MMSE, zero forcing (ZF) and PIC detectors are applied to LDS systems. An approximate expression for the BER is derived and verified through simulation results. Other simulation results for the BER performance in the AWGN and frequency-nonselective fading channels of the conventional detectors are given for various numbers of users and spreading factors.

Chapter 4 introduces a proposed precoding scheme designed for multipath channels. The precoding scheme introduced removes the effects of the multipath channel by applying an inverse channel frequency response to the transmitted signal. The BER performance of the precoding scheme is tested for the MPA and proposed PIC-MMSE detector through simulation results.

Chapter 5 gives conclusions and future work.

Chapter 2
Message Passing Algorithm for the Detection of Low Density Spread Signals

2.1 Introduction

Low density signatures offer advantages compared to their dense counterparts. LDS systems are a NOMA scheme which allows for overloading of orthogonal resources. The overloaded LDS systems are attractive for 5G due to the high spectral efficiency they offer, with relatively low complexity detection using MPA. The MPA algorithm, although less complex than maximum likelihood detection, still has complexity that is exponential.

The optimal MUD scheme is to find the joint maximum a posteriori probability (MAP) density function of all the transmitted symbols. The MAP detector must search every possible combination of symbols for each user. This search algorithm has complexity $O(M^K)$, where M is the constellation size and K is the total number of users. The complexity of the optimal MUD scheme is unfeasible and is too high for practical systems. Therefore, a suboptimal MUD scheme known as the message passing algorithm (MPA) is typically used [15].

This chapter provides a detailed description of LDS systems. This includes the system model for both the additive white Gaussian noise (AWGN) and frequency-nonselective fading channels, spreading code design, MPA detection and simulation results.

2.2 System Model

In this section, the general system model will be given for both the AWGN and frequency-nonselective fading channels.

2.2.1 AWGN Channel

Consider a fully synchronous CDMA system with K users and the spreading sequences are complex with a length of N chips. The discrete time system model for an LDS system is modelled as shown in (2.1), where $\mathbf{r} = [r_1, r_2, \dots r_N]^T \in \mathbb{C}^N$ is the received signal, $\mathbf{s}_k = \left[\mathrm{s}_{1,k}, \mathrm{s}_{2,k} \dots \mathrm{s}_{N,k}\right]^T \in \mathbb{C}^N$ is user k's spreading code, $\mathrm{x}_k \in \mathcal{X}_k$ is the symbol user k is transmitting and $\mathbf{n} = [n_1, n_2 \dots n_N]^T \in \mathbb{C}^N$ is the complex additive white Gaussian noise with covariance matrix $\sigma^2\mathbf{I}$, where $\mathbf{I}_\mathrm{N}$ is the identity matrix with size N by N. The amplitude for user k is A_k.

$$\mathbf{r} = \sum_{k=1}^{K} \mathbf{s}_k A_k x_k + \mathbf{n} \tag{2.1}$$

Each user's symbols are taken from the same constellation, such that $\mathcal{X}_k = \mathcal{X}, k = 1,2, \dots K$ and the constellation size is given as $M = |\mathcal{X}|$. This thesis will deal with overloaded systems, in other words, systems with a load factor $\eta = \frac{K}{N} > 1$. The signal model can be written in a compact vector/matrix notation as:

$$\mathbf{r} = \mathbf{SAx} + \mathbf{n} \tag{2.2}$$

where $\mathbf{S} = [\mathbf{s}_1, \mathbf{s}_2, \dots \mathbf{s}_K]^T \in \mathbb{C}^{N \times K}$ is the sparse spreading matrix, $\mathbf{x} = [x_1, x_2, \dots x_K]^T \in \boldsymbol{\mathcal{X}}^K$ is the vector of each user's symbols, and $\mathbf{A}$ is a diagonal matrix with each user's amplitude and is given as:

$$\mathbf{A} = \begin{bmatrix} A_1 & 0 & \cdots & 0 \\ 0 & A_2 & 0 & \vdots \\ \vdots & 0 & \ddots & 0 \\ 0 & \cdots & 0 & A_K \end{bmatrix} \tag{2.3}$$

The block diagram for the transmitter model for an LDS system is shown in Figure 2.1.

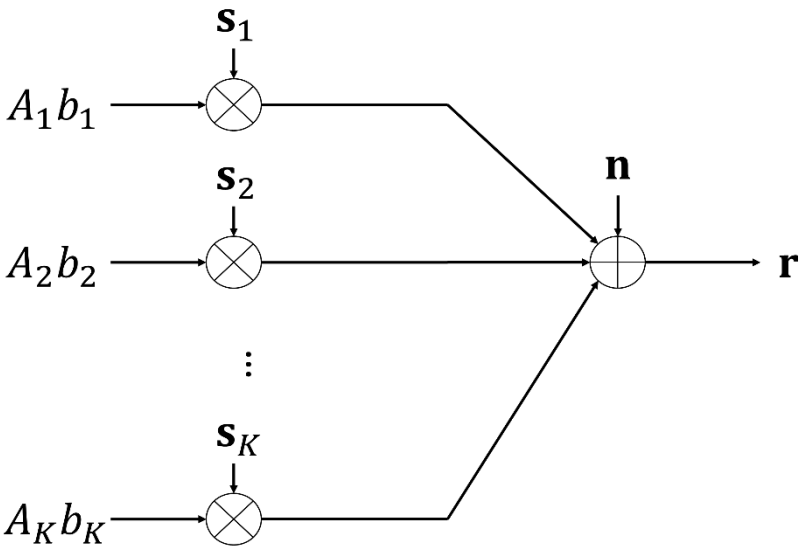

Figure 2.1: Transmitter diagram for an LDS-CDMA system in the AWGN channel

2.2.2 Frequency-Nonselective Fading Channel

The system model in (2.1) and (2.2) is altered by including the channel gains. The transmitter model is given in Figure 2.2. These channel gains are complex Gaussian random variables with zero mean and unit variance. The magnitude of the channel gains are Rayleigh distributed, and their phase is uniformly distributed on $[0,2\pi]$. The system model in the frequency-nonselective fading channel is:

$$\mathbf{r} = \sum_{k=1}^{K} \mathbf{s}_k h_k A_k x_k + \mathbf{n} \tag{2.4}$$

where h_k is the channel gain for user k. The received signal can be written in a compact vector/matrix notation as:

$$\mathbf{r} = \mathbf{SHAx} + \mathbf{n} \tag{2.5}$$

where **H** is a diagonal matrix containing the channel gains from each user, and is given as:

$$\mathbf{H} = \begin{bmatrix} h_1 & 0 & \cdots & 0 \\ 0 & h_2 & 0 & \vdots \\ \vdots & 0 & \ddots & 0 \\ 0 & \cdots & 0 & h_K \end{bmatrix} \tag{2.6}$$

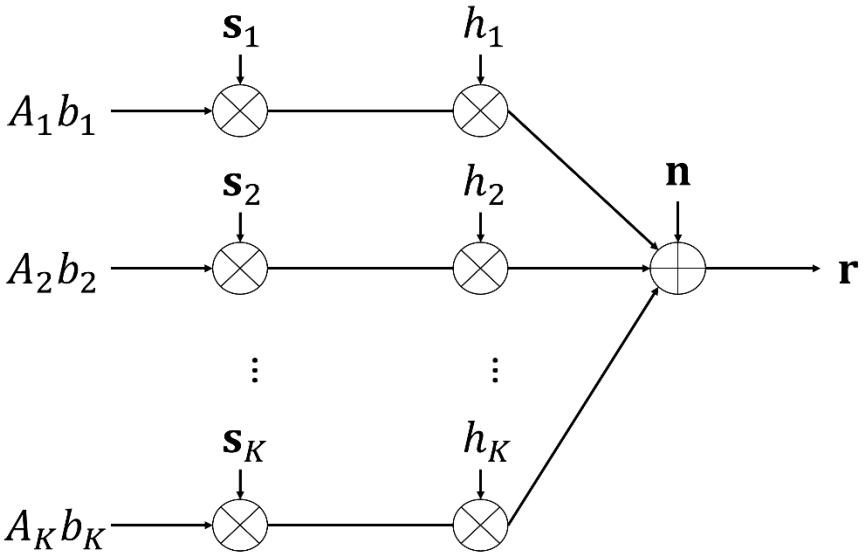

Figure 2.2: Transmitter diagram for an LDS-CDMA system in the frequency-nonselective fading channel

2.3 Spreading Sequence Design

The spreading sequences set used for an LDS system is crucial to its BER performance. There are important factors that go into designing spreading sequence set. These are:

1. The location and number of nonzero chips in each spreading code
2. Unique decodability
3. Minimum distance between possible received signals

To indicate the location and positions of nonzero chips, an indicator matrix is used. This indicator matrix shows the location of nonzero chips for different users. For example, (2.7) shows an indicator matrix $\mathbf{G}_{4\times6}$, for a 6 user, 4 chip overloaded LDS system. The columns represent each user's spreading code, and the rows show which users are contributing to that chip. For example, with the indicator matrix in (2.7), chip 2 (row 2) has contributions from users 2, 3 and 6 (columns 2, 3 and 6). The set of users that contribute to chip n is given by ξ_n and the set of nonzero chips in user k's spreading code is given by ζ_k. When examining the indicator matrix, ξ_n is the number of 1s in row n, and ζ_k is the number of 1s in column 1. In this example, $\xi_1 = \{1,3,5\}$ and $\zeta_3 = \{1,3\}$.

$$\mathbf{G}_{4\times6} = \begin{bmatrix} 1 & 0 & 1 & 0 & 1 & 0 \\ 1 & 0 & 0 & 1 & 0 & 1 \\ 0 & 1 & 1 & 0 & 0 & 1 \\ 0 & 1 & 0 & 1 & 1 & 0 \end{bmatrix} \tag{2.7}$$

Indicator matrices can also be grouped depending on the number of nonzero values in each row and column. A regular indicator matrix has the same number of 1's in each row (each chip has the same number of users contributing to it) and each column has the same number of 1's (each spreading code contains the same number of nonzero chips). Otherwise, the indicator matrix is irregular. For regular indicator matrices, let d_v represent the number of nonzero chips per spreading code and d_f represent the number of users contributing to each chip. Using the example indicator matrix in (2.7), $d_v = 2$ and $d_f = 3$. In addition, a regular indicator matrix must also satisfy that the ratio between the number of nonzero chips per code, and number of interfering users per chip must be equal to the overloading factor:

$$\eta = \frac{K}{N} = \frac{d_f}{d_v} \tag{2.8}$$

Desirable properties of an indicator matrix are very similar to the requirements of low-density parity check codes (LDPC) [15]. LDPC codes were first introduced by Gallager in [20], and are widely used today. The design of LDPC matrices has been extensively researched since its conception [21]. In most cases, these LDPC matrices can be used as indicator matrices for LDS systems.

Choosing the positions of the nonzero chips in LDS systems highly depends on the decoding algorithm being used. A desirable property of an LDPC matrix is the girth of the matrix. The girth measures the minimum number of cycles in the Tanner graph representation of the LDPC matrix. The larger the girth, the better the performance. The MPA detector which is typically used in LDS systems, is based on the sum product algorithm which is also used in the decoding of LDPC codes. The similar decoding/detection scheme between LDS systems and LDPC codes means the girth is also a desirable quality for indicator matrices in LDS systems [22]. We will further discuss the impact that the girth plays in the detection of LDS systems later in this chapter. When other detectors besides the typical MPA detector are used, better performance can be obtained by using different designs.

The sequences chosen must be uniquely decodable. Uniquely decodable codes ensure that in a noiseless transmission, no two combinations of input symbols yield the same received signal [23]. That is $\forall \mathbf{x}_1, \mathbf{x}_2 \in \mathcal{X}$ and $(\mathbf{x}_1 \neq \mathbf{x}_2)$, then $(\mathbf{S}\mathbf{x}_1 \neq \mathbf{S}\mathbf{x}_2)$. No matter the decoding scheme used, uniquely decodable codes are necessary to separate users' symbols. It is proven in that [24] that uniquely decodable systems exist for highly overloaded systems.

However, uniquely decodable codes does not ensure desirable performance. A set of codes may be uniquely decodable, but the distance between two possible received signals may be small. In a noisy channel, it will be harder to distinguish between possible sets of symbols if the distance between their received noiseless signal is small. The values of the nonzero chips in the codes helps maximize the distance between two possible codes. While the value of the nonzero chips should be chosen to maximize the distance between possible received signals, these values may also affect the unique decodability. A tradeoff for chip values was presented in [23], where the nonzero values in each row are chosen to be:

$$a_i = \exp\left(j\frac{2\pi}{P}i\right), \qquad i = 0,1,\ldots d_f - 1 \tag{2.9}$$

with P chosen such that:

$$P = Md_f \tag{2.10}$$

The spreading matrix for the example indicator in (2.7) that uses these values for the nonzero chips matrix would become:

$$\mathbf{S}_{4\times 6} = \begin{bmatrix} a_0 & 0 & a_1 & 0 & a_2 & 0 \\ a_0 & 0 & 0 & a_1 & 0 & a_2 \\ 0 & a_0 & a_1 & 0 & 0 & a_2 \\ 0 & a_0 & 0 & a_1 & a_2 & 0 \end{bmatrix}$$
$$= \begin{bmatrix} 1 & 0 & e^{\frac{j\pi}{3}} & 0 & e^{\frac{j2\pi}{3}} & 0 \\ 1 & 0 & 0 & e^{\frac{j\pi}{3}} & 0 & e^{\frac{j2\pi}{3}} \\ 0 & 1 & e^{\frac{j\pi}{3}} & 0 & 0 & e^{\frac{j2\pi}{3}} \\ 0 & 1 & 0 & e^{\frac{j\pi}{3}} & e^{\frac{j2\pi}{3}} & 0 \end{bmatrix} \quad (2.11)$$

2.4 MUD Detection of LDS Systems using Message Passing Algorithm

2.4.1 AWGN Channel

The block diagram for the receiver model is shown in Figure 2.3. The received signal that is received at the base station is decoded using the iterative message passing algorithm. This suboptimal MPA MUD scheme is very similar to the sum product algorithm described in [25]. MPA detection is derived from the optimal MAP detector.

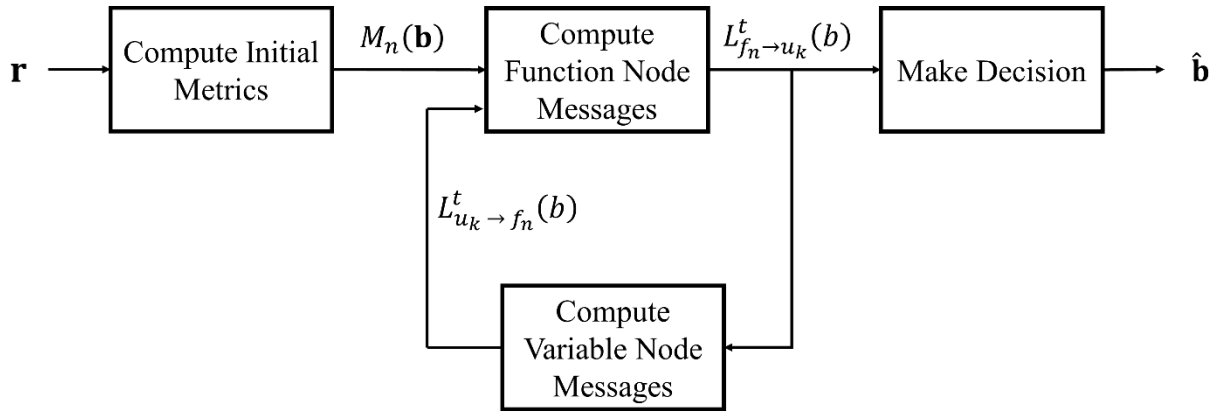

Figure 2.3: MPA detection diagram for an LDS-CDMA system

MAP detection maximizes the joint a posteriori probability mass function. This is done by exhaustive search, shown in (2.12), where $\hat{\mathbf{x}}$ is the estimated symbol vector, and $p(\cdot)$ is the probability mass function.

$$\hat{\mathbf{x}} = \underset{\mathbf{x} \in \boldsymbol{\mathcal{X}}^K}{\arg\max}\big(p(\mathbf{x}|\mathbf{r})\big) \tag{2.12}$$

Using Bayes rule, the probability mass function in (2.12) can be rewritten as:

$$p(\mathbf{x}|\mathbf{r}) = \frac{p(\mathbf{r}|\mathbf{x})P(\mathbf{x})}{P(\mathbf{r})} \tag{2.13}$$

where $P(\cdot)$ is the probability function. In addition, $P(\mathbf{r}) = \sum_{x \in X^K} p(\mathbf{r}|\mathbf{x})\, P(\mathbf{x})$. Because the noise vector is uncorrelated and identically independently distributed (i.i.d.), the total channel observation function can be rewritten as:

$$p(\mathbf{r}|\mathbf{x}) = \prod_{n=1}^{N} p(r_n|\mathbf{x}) \tag{2.14}$$

where $p(r_n|\mathbf{x})$ is the observation at chip n and is:

$$p(r_n|\mathbf{x}) = \frac{1}{\sqrt{2\pi\sigma^2}} \exp\left(-\frac{1}{2\sigma^2} \left| r_n - \sum_{k=1}^{K} s_{n,k} h_k A_k x_k \right|^2 \right) \tag{2.15}$$

By assuming the signals sent from each user are equiprobable, that is $P(\mathbf{x}) = \frac{1}{M^K}$, and dropping redundant terms, the MAP detector in (2.12) simplifies to:

$$\hat{\mathbf{x}} = \underset{\mathbf{x} \in \boldsymbol{\mathcal{X}}^K}{\arg\max} \left\{ \prod_{n=1}^{N} p(r_n|\mathbf{x}) \right\} \tag{2.16}$$

This allows for the MAP detection done in (2.12) to be rewritten as a marginalized product of functions. Due to the signatures spreading the user symbols being low density, the number of users contributing to chip n decreases from N to d_f, and (2.15) can be rewritten as:

$$p(r_n|\mathbf{x}) = \frac{1}{\sqrt{2\pi\sigma^2}} \exp\left(-\frac{1}{2\sigma^2} \left| r_n - \sum_{k \in \xi_n} s_{n,k} A_k x_k \right|^2 \right) \tag{2.17}$$

This allows for the number of unique metrics to be decreased from M^K to M^{d_f}. This reduction of metrics does simplify the MAP detection, but the exhaustive search of M^K possible combinations of user's symbols is still highly complex in practical implementations.

MPA uses belief propagation to approximate the marginalized product of functions in (2.16). MPA is broken down into function nodes and variable nodes. There are N function nodes, representing each received chip, and K variable nodes, representing each user's symbol. A factor graph is a bipartite graph in which function nodes and variable nodes are connected by edges, and pass messages to each other through these edges. A variable and function node are connected by an edge if the symbol represented by that variable node contributes to the chip represented by that function node. This can also be seen by examining the indicator matrix. A visual example of a factor graph is shown in Figure 2.4, where 6 users spread their data onto spreading sequences which have a length of 4 chips. As can be seen, each variable node is connected to $d_v = 2$ function nodes, and each function node is connected to $d_f = 3$ variable nodes.

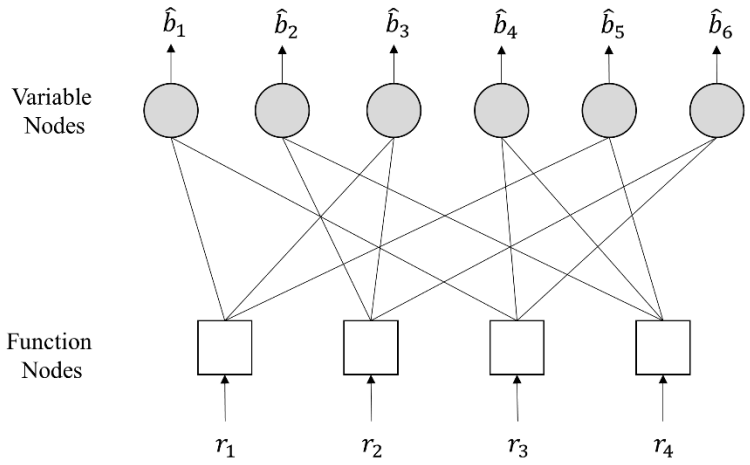

Figure 2.4: Factor graph representation of an LDS system with 6 users and 4 chips

The MPA detector works iteratively where the function and variable nodes send messages to each other along the edges that connect them. These messages represent the inference of a user's symbol and measure the reliability of this inference with soft-values. In the general case, the message sent from function node n to variable node k at iteration t is $\mathcal{L}^t_{f_n \to u_k}$, and is represented by a vector, of length M, for each possible symbol value. The message $L^t_{f_n \to u_k}$ includes the local inference made at node n, $M_n(\mathbf{x})$, as well as the product from the messages received from the other connected variable nodes, $\mathcal{L}^{t-1}_{u_k \to f_n}(x)$, which are

from the previous iteration. During the first iteration, when $t = 1$, $\mathcal{L}^0_{u_k \to f_n}(x) = \frac{1}{M}$. The local inference made at node n is simply $p(r_n|\mathbf{x})$. At each variable node, an estimate of that user's symbol can be made based on the product of all the received messages from the connected function nodes. After an estimate has been made at each variable node, the variable nodes send messages back to the function nodes. This ends one iteration. The message equations are shown in (2.19) and (2.20). The iterative algorithm is repeated until a fixed number of iterations has been reached, or all the messages exchanged have saturated.

$$M_n(\mathbf{x}) = \exp\left(-\frac{1}{2\sigma^2}\left|r_n - \sum_{k\in\xi_n} s_{n,k}A_k x_k\right|^2\right) \tag{2.18}$$

$$\mathcal{L}^t_{f_n\to u_k}(x) = \sum_{\tilde{\mathbf{x}}:\tilde{x}_k = x}\left(M_n(\tilde{\mathbf{x}})\prod_{\tilde{k}\in\xi_n\setminus k}\mathcal{L}^{t-1}_{u_k\to f_n}(\tilde{x}_{\tilde{k}})\right) \tag{2.19}$$

$$\mathcal{L}^t_{u_k\to f_n}(x) = \prod_{\tilde{n}\in\zeta_k}\mathcal{L}^t_{f_n\to u_k}(x) \tag{2.20}$$

$$\hat{x}_k = \underset{\tilde{x}}{\arg\max}\left\{\prod_{n\in\zeta_k}\mathcal{L}^t_{f_n\to u_k}(x)\right\} \tag{2.21}$$

2.4.2 Frequency-Nonselective Fading Channel

The messages sent from function nodes to variable nodes $\mathcal{L}^t_{f_n\to u_k}(x)$, and from variable nodes to function nodes $\mathcal{L}^t_{u_k\to f_n}(x)$ are the same as shown in (2.19) and (2.20) respectively for the AWGN channel, with a slight change to how the initial metrics in (2.18) are computed. This alteration is to include the channel gains:

$$M_n(\mathbf{x}) = \exp\left(-\frac{1}{2\sigma^2}\left|r_n - \sum_{k\in\xi_n} h_k A_k s_{n,k} x_k\right|^2\right) \tag{2.22}$$

2.5 Complexity of the MPA Detector

The sparse structure of LDS allows for each function node to only be connected to a few variable nodes, and hence, reduces the number of possible combinations of symbols interfering at that given chip. With conventional structure, every user would have contributed to that chip, and this increases the complexity of the algorithm exponentially. If each chip contains d_f number of contributing users, the MPA MUD scheme has complexity $O\left(M^{d_f}\right)$ compared to $O(M^K)$ that optimal MAP detection uses. For very sparse signatures, $d_c \ll K$ the reduction in complexity is significantly reduced [15]. In fact, the suboptimal MPA after a certain number of iterations will asymptotically approach the optimal MAP detection scheme [26].

Although the receiver complexity of LDS-CDMA/OFDM or SCMA systems is reduced drastically with the use of MPA rather than MAP detection, the complexity is still exponential to the number of interfering users at each chip. For very large systems, this still may be impractical. Even if d_f is kept low while number of user's increases, the girth of the factor graph increases. While this increase in girth results in better performance, it requires more iterations, and therefore more computations. Various adjustments to the MPA MUD have been made to either reduce the number of iterations or reduce the number of computations required per iteration. Channel coding is one means of reducing computational complexity [27]. By feeding the soft outputs from each user's channel decoder back into the factor graph, less MPA iterations are needed. Depending on how the channel coding is implemented, higher latencies may occur. Grouping users based on their signatures, or other properties, is another means of reducing computational complexity [28], [29]. In addition to grouping and channel coding, improvements can be made by applying weight factors to codewords with higher probability and smaller factors to codewords with lower probability [30]. An author of [31] proposes using an irregular indicator matrix, which can allow for MPA to act as a SIC detector. The irregular structure allows for some users to use fewer active chips in their spreading codes, which means those active chips have more energy, assuming each spreading code is normalized to have the same energy. This difference in energy per chip between users means some messages from stronger users being passed will be more reliable than the messages being passed by weaker users. These stronger users will have their messages trickle down to assist in the interference removal of weaker users, like SIC detection. The problem with this is that errors can propagate to weaker users if strong users have unreliable messages.

2.6 Simulation Results

In this section the performance of the MPA detector is discussed. MATLAB was used for simulations, and the following assumptions are made:

- Each user transmits with unit energy per bit
- For the frequency nonelective fading channel simulations:
    - All channel gains are independent complex Gaussian random variables with zero mean and unit variance that are constant during each signaling interval
    - The channel gains are known perfectly at the receiver
    - BPSK modulation is used

In the performance analysis, 2 different spreading matrices were considered. The first is a 9 user 6 chip system (150% loading) from [23] shown in (2.23) and the second is a 16 user 12 chip (133% loading) system in (2.24) whose indicator matrix is from [10], but the values for each chip in the spreading sequence are chosen following the methodology described in [23].

$$\mathbf{S}_{6\times 9} = \begin{pmatrix} 0 & 0 & a_2 & 0 & 0 & 0 & a_1 & 0 & a_0 \\ 0 & a_2 & 0 & a_1 & 0 & 0 & a_0 & 0 & 0 \\ 0 & 0 & a_1 & a_0 & 0 & a_2 & 0 & 0 & 0 \\ a_0 & 0 & 0 & 0 & a_1 & 0 & 0 & 0 & a_2 \\ a_2 & 0 & 0 & 0 & 0 & a_0 & 0 & a_1 & 0 \\ 0 & a_2 & 0 & 0 & a_0 & 0 & 0 & a_2 & 0 \end{pmatrix} \tag{2.23}$$

where $a_0 = 1, a_1 = \exp\left(j\frac{\pi}{3}\right), a_2 = \exp\left(j\frac{2\pi}{3}\right)$.

$$\mathbf{S}_{12\times16} = \begin{pmatrix} 0 & 0 & b_0 & 0 & 0 & 0 & 0 & b_1 & 0 & b_2 & 0 & 0 & b_3 & 0 & 0 & 0 \\ 0 & 0 & 0 & b_0 & 0 & 0 & b_1 & 0 & 0 & 0 & 0 & 0 & b_2 & 0 & b_3 & 0 \\ 0 & b_0 & 0 & 0 & b_1 & 0 & b_1 & 0 & 0 & b_3 & 0 & 0 & 0 & 0 & 0 & 0 \\ 0 & 0 & 0 & b_0 & 0 & b_1 & 0 & 0 & 0 & 0 & b_2 & 0 & 0 & b_3 & 0 & 0 \\ 0 & 0 & b_0 & 0 & 0 & 0 & 0 & 0 & b_1 & 0 & 0 & 0 & 0 & 0 & b_2 & b_3 \\ b_0 & 0 & 0 & 0 & 0 & b_1 & 0 & 0 & 0 & b_2 & 0 & 0 & 0 & 0 & b_3 & 0 \\ 0 & 0 & 0 & b_0 & 0 & 0 & 0 & b_1 & b_2 & 0 & 0 & b_3 & 0 & 0 & 0 & 0 \\ 0 & b_0 & 0 & 0 & 0 & b_1 & 0 & 0 & 0 & 0 & 0 & b_2 & 0 & 0 & 0 & b_3 \\ b_0 & 0 & 0 & 0 & 0 & b_1 & 0 & 0 & 0 & 0 & 0 & 0 & 0 & b_2 & 0 & b_3 \\ 0 & 0 & b_0 & 0 & b_1 & 0 & 0 & 0 & 0 & 0 & 0 & b_2 & 0 & b_3 & 0 & 0 \\ 0 & b_0 & 0 & 0 & 0 & 0 & 0 & 0 & a_1 & 0 & b_2 & 0 & b_3 & 0 & 0 & 0 \\ b_0 & 0 & 0 & 0 & b_1 & 0 & 0 & b_2 & 0 & 0 & b_3 & 0 & 0 & 0 & 0 & 0 \end{pmatrix} \tag{2.24}$$

where $b_0 = 1$, $b_1 = \exp\left(j\frac{\pi}{4}\right)$, $b_2 = \exp\left(j\frac{\pi}{2}\right)$, and $b_3 = \exp\left(j\frac{3\pi}{4}\right)$.

Figure 2.5 and Figure 2.6 show the BER for both the 6x9 and the 12x16 systems over the AWGN channel while varying the number of iterations used by the MPA detector. It is evident how important the number of iterations is to the BER of MPA detection. At least 2 iterations are required for both the 6x9 and 12x16 systems to achieve acceptable performance. In fact, both the 6x9 and 12x16 systems converge to the single user bound. Both the 6x9 system and the 12x16 systems converge after 3 iterations.

Figure 2.7, and Figure 2.8 show the BER of the 6x9 and the 12x16 systems over the slow, frequency-nonselective fading channel as well as the single user bound for both cases. The performance improves compared to the AWGN channel, and both systems converge to the single user bound in less iterations compared to the AWGN channel. This is because the fading applied to each user gives diversity at the receiver. Different users will have different signal strengths, and this helps separate them.

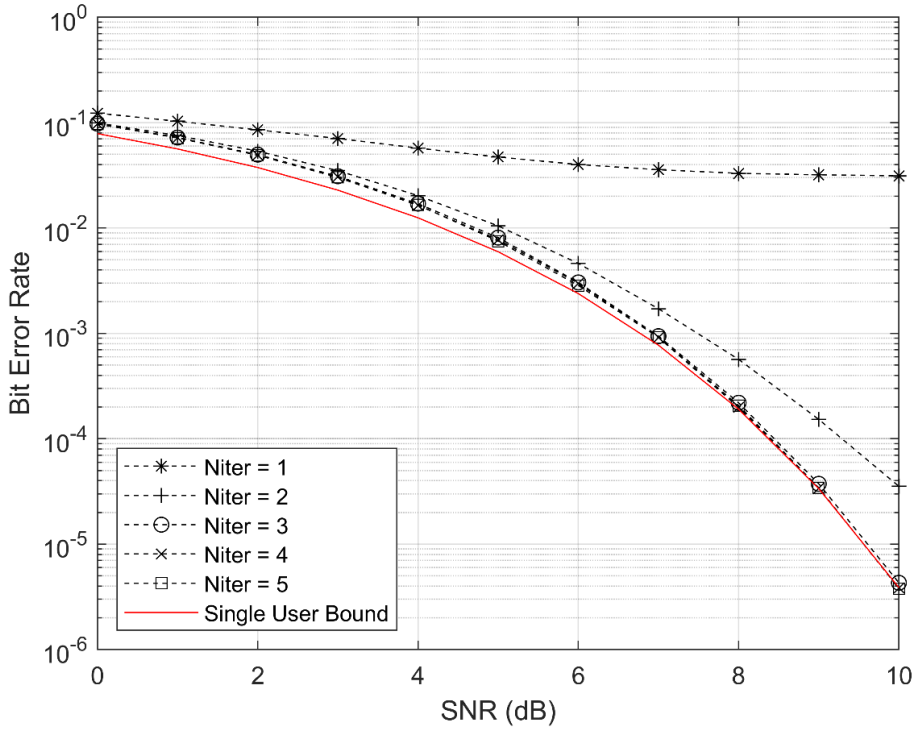

Figure 2.5: BER performance of the MPA detector of a system with 9 users and 6 chips in the AWGN channel with varying numbers of iterations

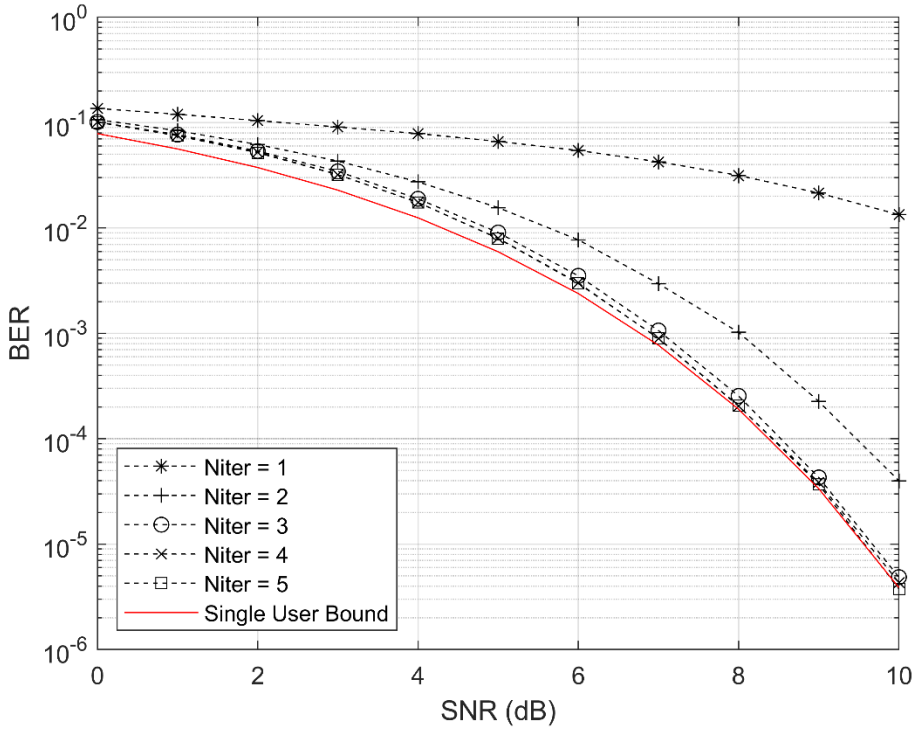

Figure 2.6: BER performance of the MPA detector of a system with 16 users and 12 chips in the AWGN channel with varying numbers of iterations

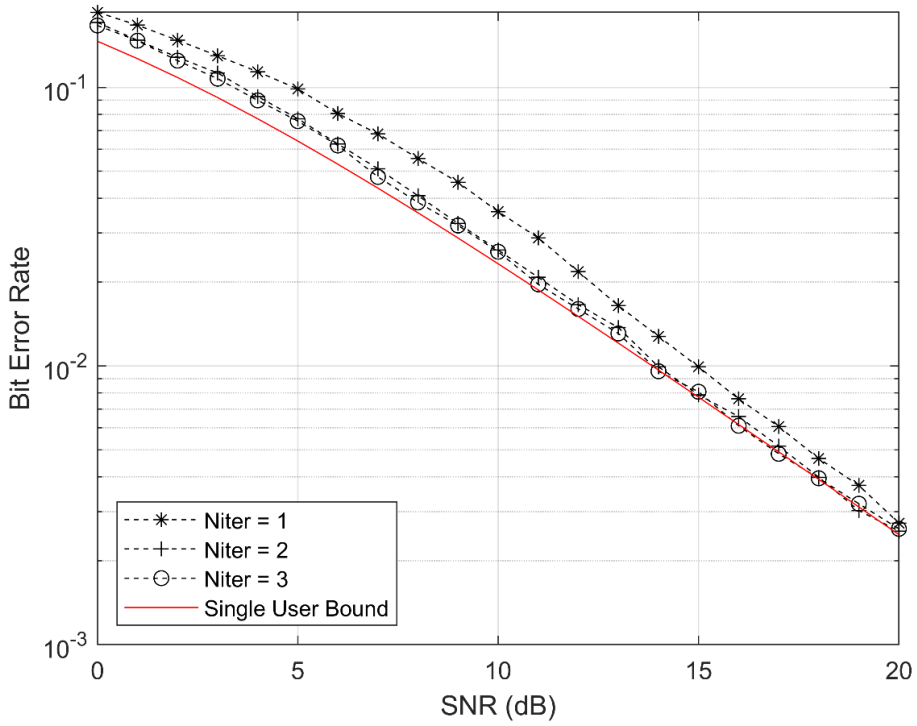

Figure 2.7: BER performance of the MPA detector of a system with 9 users and 6 chips in the frequency-nonselective fading channel with varying numbers of iterations

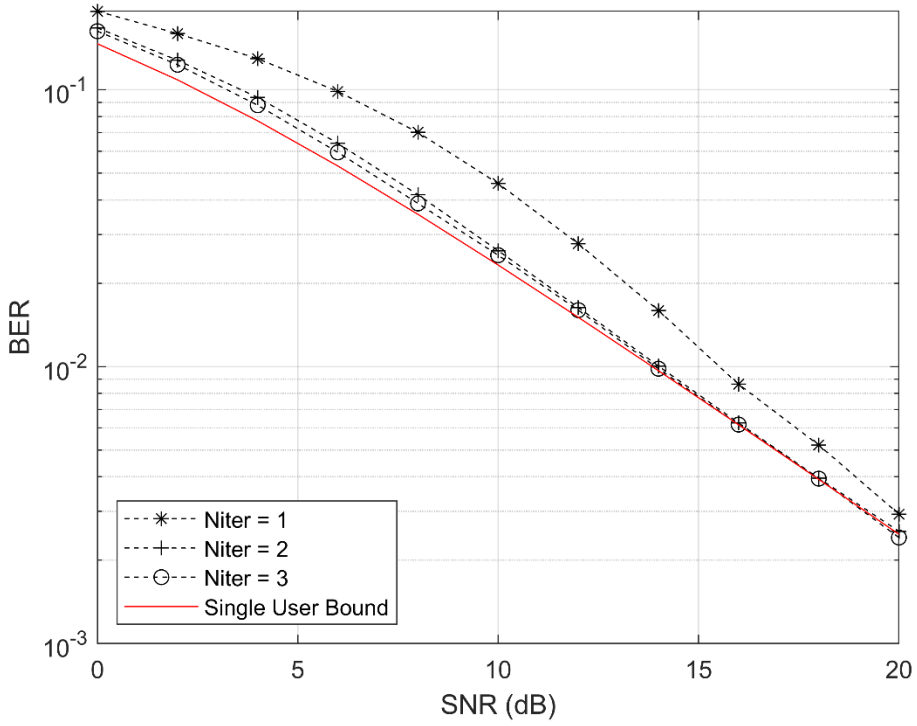

Figure 2.8: BER performance of the MPA detector of a system with 16 users and 12 chips in the frequency-nonselective fading channel with varying numbers of iterations

2.7 Summary

This chapter discussed the present work done with LDS systems. The system model, spreading sequence design, MPA detector, complexity analysis and simulation results were discussed. LDS systems use spreading sequences that have a small number of nonzero chips. This small number of chips allows for effective MUD in overloaded systems with the MPA detector.

The MPA detector is a well performing detection scheme, that uses belief propagation to estimate the optimum MAP detector. The complexity of the MPA detector is reduced from $O(M^K)$ to $O\left(M^{d_f}\right)$ compared to the MAP detector. The MPA detector provides great performance, as with system loads of 133% and 150% it approaches the single user bound in both the AWGN and frequency-nonselective fading channels.

Chapter 3
PIC-MMSE Detector for Low Density Spread Signals

3.1 Introduction

Multiuser detection in CDMA systems has been widely researched for the past few decades [32]. Conventional MUD methods start by despreading the received signal with each user's spreading code. This despreading creates decision variables for each user which contain the desired symbol from that respective user, as well as MAI and noise. The goal of a MUD is to take these decision variables and manipulate them to mitigate the MAI and noise and achieve better performance.

These detectors can be separated into linear and nonlinear detectors. Linear detectors will take the decision variables and apply a linear function, typically matrix multiplication. Some linear detectors include the decorrelating and MMSE detectors. Linear detectors offer good performance compared to optimum detectors with lower complexity. The problem with using linear detectors is that they give poor performance in overloaded conditions. Decision driven detection schemes such as PIC or SIC are examples of nonlinear detectors. The performance of these detectors rely heavily on the quality of the initial estimates being used for interference cancellation.

In this chapter, an alternative MUD technique for LDS systems is proposed. This proposed detector is based off the MMSE and PIC detectors. It combines them in a multistage manor, where the MMSE detection is done first, and the PIC detector uses the decision variables from the MMSE detector to cancel out the interference. This proposed detector has complexity that is much less than the MPA detector, and provides the same spectral efficiency.

3.2 Preprocessing: Despreading and Separation of Real and Imaginary Parts

3.2.1 AWGN Channel

The received signal is despread for the conventional detectors as well as the proposed PIC-MMSE detector. This despreading is done by correlating the received signal with each user's spreading code to get a decision variable for each user. Also, the detectors described in this chapter are for BPSK modulation. In this chapter, the transmitted symbol for user k, $x_k$will be changed to b_k, where $b_k \in \{-1, +1\}$ is the bit to be transmitted from user k. The decision variable for user k is:

$$\begin{aligned} U_k &= \mathbf{s}_k^H \mathbf{r} \\ &= A_k b_k + \sum_{\substack{i=1 \\ i \neq k}}^{K} R_{k,i} A_i b_i + \mathbf{s}_k^H \mathbf{n} \end{aligned} \tag{3.1}$$

where $(\cdot)^H$ is the Hermitian transpose operator and the term $R_{k,i}$ is the correlation between user k's spreading code and user i's spreading code. The vector notation for all K decision variables is:

$$\begin{aligned} \mathbf{U} &= \mathbf{S}^H \mathbf{r} \\ &= \mathbf{S}^H \mathbf{S} \mathbf{A} \mathbf{b} + \mathbf{S}^H \mathbf{n} \end{aligned} \tag{3.2}$$

where $\mathbf{U}$ is a $K \times 1$ vector of the decision variables. The correlation matrix $\mathbf{R}$ contains the cross correlations between the spreading codes from all the users and is defined as:

$$\mathbf{R} = \mathbf{S}^H \mathbf{S} \tag{3.3}$$

The despreading applied has less terms than conventional CDMA systems because those spreading sequences contain all nonzero values and LDS systems contain only a few chips that are nonzero.

The ZF, MMSE and PIC detectors in the next sections are altered from their original counterparts and are intended for BPSK modulation. The major difference is to separate the real and imaginary parts of $\mathbf{U}$, such that:

$$\begin{aligned}\widetilde{\mathbf{U}} &= \begin{bmatrix}\Re(\mathbf{U})\\ \Im(\mathbf{U})\end{bmatrix} \\ &= \begin{bmatrix}\Re(\mathbf{R}) & -\Im(\mathbf{R})\\ \Im(\mathbf{R}) & \Re(\mathbf{R})\end{bmatrix}\begin{bmatrix}\Re(\mathbf{Ab})\\ \Im(\mathbf{Ab})\end{bmatrix} + \begin{bmatrix}\Re(\mathbf{S}^H) & -\Im(\mathbf{S}^H)\\ \Im(\mathbf{S}^H) & \Re(\mathbf{S}^H)\end{bmatrix}\begin{bmatrix}\Re(\mathbf{n})\\ \Im(\mathbf{n})\end{bmatrix}\end{aligned} \tag{3.4}$$

where $\Re(\cdot)$ and $\Im(\cdot)$ denote the real and imaginary parts respectively. (3.4) can be rewritten in a more compact form:

$$\begin{aligned}\widetilde{\mathbf{U}} &= \begin{bmatrix}\Re(\mathbf{R})\\ \Im(\mathbf{R})\end{bmatrix}\mathbf{Ab} + \tilde{\mathbf{S}}\begin{bmatrix}\Re(\mathbf{n})\\ \Im(\mathbf{n})\end{bmatrix} \\ &= \widetilde{\mathbf{R}}\mathbf{Ab} + \tilde{\mathbf{S}}\tilde{\mathbf{n}}\end{aligned} \tag{3.5}$$

where:

$$\widetilde{\mathbf{R}} = \begin{bmatrix}\Re(\mathbf{R})\\ \Im(\mathbf{R})\end{bmatrix} \tag{3.6}$$

$$\tilde{\mathbf{S}} = \begin{bmatrix}\Re(\mathbf{S}^H) & -\Im(\mathbf{S}^H)\\ \Im(\mathbf{S}^H) & \Re(\mathbf{S}^H)\end{bmatrix} = \begin{bmatrix}\Re(\mathbf{S}^T) & \Im(\mathbf{S}^T)\\ -\Im(\mathbf{S}^T) & \Re(\mathbf{S}^T)\end{bmatrix} \tag{3.7}$$

$$\tilde{\mathbf{n}} = \begin{bmatrix}\Re(\mathbf{n})\\ \Im(\mathbf{n})\end{bmatrix} \tag{3.8}$$

The separation of real and imaginary parts gives an extra dimension for the detectors to use to get a better estimate on each user's symbol. In addition, the correlation matrix $\mathbf{R}$ will rank, that is at most, equal to N. This is because the spreading matrix $\mathbf{S}$ will have at most, N independent spreading codes due to the system being overloaded. In general, when the rank of $\mathbf{R}$ is less than K, the BER performance using linear detectors is reduced. The separation of real and imaginary parts produces the updated correlation matrix $\widetilde{\mathbf{R}}$ which will have at most, a rank of $2N$. If there are N spreading codes that are orthogonal, and the overloading factor is less than 200%, the rank of $\widetilde{\mathbf{R}}$ will be greater than K, and the system will be separable.

3.2.2 Frequency-Nonselective Fading Channel

The adjustment for the frequency-nonselective fading channel is shown in this subsection. The notation $(\cdot)'$ throughout this chapter identifies this variable is for the frequency-nonselective channel. In addition to despreadng, the decision variables are multiplied by the conjugate of the channel gains. After despreading, the decision variable for user k is:

$$\begin{aligned} U'_k &= h_k^* \mathbf{s}_k^H \mathbf{r} \\ &= |h_k| A_k b_k + \sum_{\substack{i=1 \\ i \neq k}}^{K} R_{k,i} h_k^* h_i A_i b_i + h_k^* \mathbf{s}_k^H \mathbf{n} \end{aligned} \tag{3.9}$$

where $(\cdot)^*$ is the conjugation operator. The vector of decision variables is:

$$\begin{aligned} \mathbf{U}' &= \mathbf{H}^H \mathbf{S}^H \mathbf{r} \\ &= \mathbf{H}^H \mathbf{S}^H \mathbf{S} \mathbf{H} \mathbf{A} \mathbf{b} + \mathbf{H}^H \mathbf{S}^H \mathbf{n} \\ &= \mathbf{H}^H \mathbf{R} \mathbf{H} \mathbf{A} \mathbf{b} + \mathbf{H}^H \mathbf{S}^H \mathbf{n} \end{aligned} \tag{3.10}$$

After the separation of real and imaginary parts of $\mathbf{U}'$:

$$\begin{aligned} \tilde{\mathbf{U}}' &= \begin{bmatrix} \Re(\mathbf{U}) \\ \Im(\mathbf{U}) \end{bmatrix} \\ &= \begin{bmatrix} \Re(\mathbf{H}^H \mathbf{R} \mathbf{H}) & -\Im(\mathbf{H}^H \mathbf{R} \mathbf{H}) \\ \Im(\mathbf{H}^H \mathbf{R} \mathbf{H}) & \Re(\mathbf{H}^H \mathbf{R} \mathbf{H}) \end{bmatrix} \begin{bmatrix} \Re(\mathbf{A}\mathbf{b}) \\ \Im(\mathbf{A}\mathbf{b}) \end{bmatrix} + \begin{bmatrix} \Re(\mathbf{H}^H \mathbf{S}^H) & -\Im(\mathbf{H}^H \mathbf{S}^H) \\ \Im(\mathbf{H}^H \mathbf{S}^H) & \Re(\mathbf{H}^H \mathbf{S}^H) \end{bmatrix} \begin{bmatrix} \Re(\mathbf{n}) \\ \Im(\mathbf{n}) \end{bmatrix} \end{aligned} \tag{3.11}$$

(3.11) can be rewritten in a more compact form:

$$\begin{aligned} \tilde{\mathbf{U}}' &= \begin{bmatrix} \Re(\mathbf{H}^H \mathbf{R} \mathbf{H}) \\ \Im(\mathbf{H}^H \mathbf{R} \mathbf{H}) \end{bmatrix} \mathbf{A}\mathbf{b} + \tilde{\mathbf{S}}' \begin{bmatrix} \Re(\mathbf{n}) \\ \Im(\mathbf{n}) \end{bmatrix} \\ &= \tilde{\mathbf{R}}' \mathbf{A}\mathbf{b} + \tilde{\mathbf{S}}' \tilde{\mathbf{n}} \end{aligned} \tag{3.12}$$

where:

$$\tilde{\mathbf{R}}' = \begin{bmatrix} \Re(\mathbf{H}^H \mathbf{R} \mathbf{H}) \\ \Im(\mathbf{H}^H \mathbf{R} \mathbf{H}) \end{bmatrix} \tag{3.13}$$

$$\tilde{\mathbf{S}}' = \begin{bmatrix} \Re(\mathbf{H}^H \mathbf{S}^H) & -\Im(\mathbf{H}^H \mathbf{S}^H) \\ \Im(\mathbf{H}^H \mathbf{S}^H) & \Re(\mathbf{H}^H \mathbf{S}^H) \end{bmatrix} \tag{3.14}$$

3.3 Conventional Multiuser Detectors

In this section, some conventional multiuser detectors are presented. The first subsection describes linear detectors such as the ZF, or decorrelating detector, and the MMSE detector. The second subsection describes a nonlinear detector known as the PIC detector.

3.3.1 Zero Forcing and Minimum Mean Square Error Detectors

This section describes the ZF and MMSE filters to apply to the decision variables in (3.2). Both detectors are linear and apply a matrix multiplication as filtering. The forms of these detectors are:

$$\mathbf{U}_{\mathrm{ZF}} = \mathbf{W}_{\mathrm{ZF}}\widetilde{\mathbf{U}} \tag{3.15}$$

$$\mathbf{U}_{\mathrm{MMSE}} = \mathbf{W}_{\mathrm{MMSE}}\widetilde{\mathbf{U}} \tag{3.16}$$

The ZF was first described in [33]. The ZF detector linearly transforms the decision variables by applying the inverse of the correlation matrix, if it is invertible. When the correlation matrix is invertible, the ZF detector completely removes the MAI, and decorrelates each user from each other. In the case of overloaded systems, the correlation matrix will be rank deficient, and won't be invertible. The separation of real and imaginary parts adds another dimension to the correlation matrix that will increase its rank. The ZF detector has the form:

$$\mathbf{W}_{\mathrm{ZF}} = \left(\widetilde{\mathbf{R}}\right)^{+} \tag{3.17}$$

where $(\cdot)^{+}$ is the Moore-Penrose pseudoinverse. The ZF decision variables are:

$$\mathbf{U}_{\mathrm{ZF}} = \mathbf{A}\mathbf{b} + \left(\widetilde{\mathbf{R}}\right)^{+}\tilde{\mathbf{n}} \tag{3.18}$$

With the ZF detector, the MAI is eliminated. At first glance, this appears to be ideal, but the multiplication of the inverse correlation matrix with the noise vector increases the noise variance.

The MMSE detector on the other hand looks to minimize the minimum mean square error between the transmitted bits and the filtered signal, like the MMSE equalizer used to suppress inter-symbol interference (ISI) in fading channels [34]. The MMSE detector has been proven to show that in the case of overloaded systems, the detector is unable to achieve an acceptable BER [35]. The minimum mean square error is achieved by minimizing:

$$\mathbf{W}_{\mathrm{MMSE}} = \arg\min_{\mathbf{W}} \left\{ E\left[\left| \mathbf{b} - \mathbf{W}\widetilde{\mathbf{U}} \right|^2 \right] \right\} \tag{3.19}$$

where $E[\cdot]$ is the expectation operator. It is shown in [36] the minimization required in (3.19) can be found by forcing the error vector $\left(\mathbf{b} - \mathbf{W}_{\mathrm{MMSE}}\widetilde{\mathbf{U}}\right)$ to be orthogonal to the vector of split decision variables $\widetilde{\mathbf{U}}$:

$$\begin{aligned} \mathbf{0} &= E\left[\left(\mathbf{Ab} - \mathbf{W}_{\mathrm{MMSE}}\widetilde{\mathbf{U}}\right)\widetilde{\mathbf{U}}^T\right] \\ &= E\left[\mathbf{Ab}\left(\widetilde{\mathbf{R}}\mathbf{Ab} + \tilde{\mathbf{S}}\tilde{\mathbf{n}}\right)^T - \mathbf{W}_{\mathrm{MMSE}}\left(\widetilde{\mathbf{R}}\mathbf{Ab} + \tilde{\mathbf{S}}\tilde{\mathbf{n}}\right)\left(\widetilde{\mathbf{R}}\mathbf{Ab} + \tilde{\mathbf{S}}\tilde{\mathbf{n}}\right)^T\right] \\ &= E\left[\mathbf{Abb}^T\mathbf{A}^T\widetilde{\mathbf{R}}^T + \mathbf{Ab}\tilde{\mathbf{n}}^T\tilde{\mathbf{S}}^T\right. \\ &\qquad \left. - \mathbf{W}_{\mathrm{MMSE}}\left(\widetilde{\mathbf{R}}\mathbf{Abb}^T\mathbf{A}^T\widetilde{\mathbf{R}}^T + \widetilde{\mathbf{R}}\mathbf{Ab}\tilde{\mathbf{n}}^T\tilde{\mathbf{S}}^T + \tilde{\mathbf{S}}\tilde{\mathbf{n}}\mathbf{b}^T\mathbf{A}^T\widetilde{\mathbf{R}}^T + \tilde{\mathbf{S}}\tilde{\mathbf{n}}\tilde{\mathbf{n}}^T\tilde{\mathbf{S}}^T\right)\right] \\ &= \mathbf{P}\widetilde{\mathbf{R}}^T - \mathbf{W}_{\mathrm{MMSE}}\left(\widetilde{\mathbf{R}}\mathbf{P}\widetilde{\mathbf{R}}^T + \frac{\sigma^2}{2}\tilde{\mathbf{S}}\tilde{\mathbf{S}}^T\right) \end{aligned} \tag{3.20}$$

The MMSE filter has the result:

$$\mathbf{W}_{\mathrm{MMSE}} = \mathbf{P}\widetilde{\mathbf{R}}^T\left(\widetilde{\mathbf{R}}\mathbf{P}\widetilde{\mathbf{R}}^T + \frac{\sigma^2}{2}\tilde{\mathbf{S}}\tilde{\mathbf{S}}^T\right)^+ \tag{3.21}$$

where $\mathbf{P}$ is:

$$\begin{aligned} \mathbf{P} &= \mathbf{A}\mathbf{A}^T \\ &= \begin{bmatrix} A_1^2 & 0 & \cdots & 0 \\ 0 & A_2^2 & 0 & \vdots \\ \vdots & 0 & \ddots & 0 \\ 0 & \cdots & 0 & A_K^2 \end{bmatrix} \end{aligned} \tag{3.22}$$

The MMSE filter for user k, is the kth row in $\mathbf{W}_{\mathrm{MMSE}}$:

$$\mathbf{w}_k = P_k\widetilde{\mathbf{R}}_k^T\left(\widetilde{\mathbf{R}}\mathbf{P}\widetilde{\mathbf{R}}^T + \frac{\sigma^2}{2}\tilde{\mathbf{S}}\tilde{\mathbf{S}}^T\right)^+ \tag{3.23}$$

where $\widetilde{\mathbf{R}}_k^T$ is row k in $\widetilde{\mathbf{R}}^T$.

3.3.2 Parallel Interference Cancellation

Subtractive interference cancellation is a nonlinear detection scheme that uses bit estimates to subtract out the MAI [37]. Interference cancellation can be broken down into two

categories, successive interference cancelation, and parallel interference cancellation [38]. SIC will subtract out each user's MAI sequentially, starting with the user with the highest power level. After the user with the highest power has had its interference removed, then the user with the next highest power level will have its interference removed. This continues until every user has had their interference removed. PIC detection on the other hand subtracts each user's interference all at once in parallel. The decision variables after the parallel removal can be fed back into the detector, allowing for PIC in multiple stages. In general, the PIC detector takes the initial estimates of the decision variables after despreading and uses these estimates to subtract each user's interference from each other. The PIC detector has the form:

$$U_{\mathrm{PIC}_k} = U_k - \sum_{\substack{i=1 \\ i \neq k}}^{K} R_{k,i} A_i \hat{b}_i \tag{3.24}$$

where $\hat{b}_i$ is the estimated bit from user i to be used for interference cancellation. The estimated bits used for interference cancellation can either be hard or soft bits. Soft bits allow for the PIC detector to cancel only partial amounts of the MAI in the case that the estimated bits are not reliable. This is found to perform better than hard bits, as hard bits can increase MAI when the estimated hard bits are incorrect [38].

Figure 1.1 shows the different decision methods used for PIC detection. These are hard, soft linear or soft nonlinear [39].

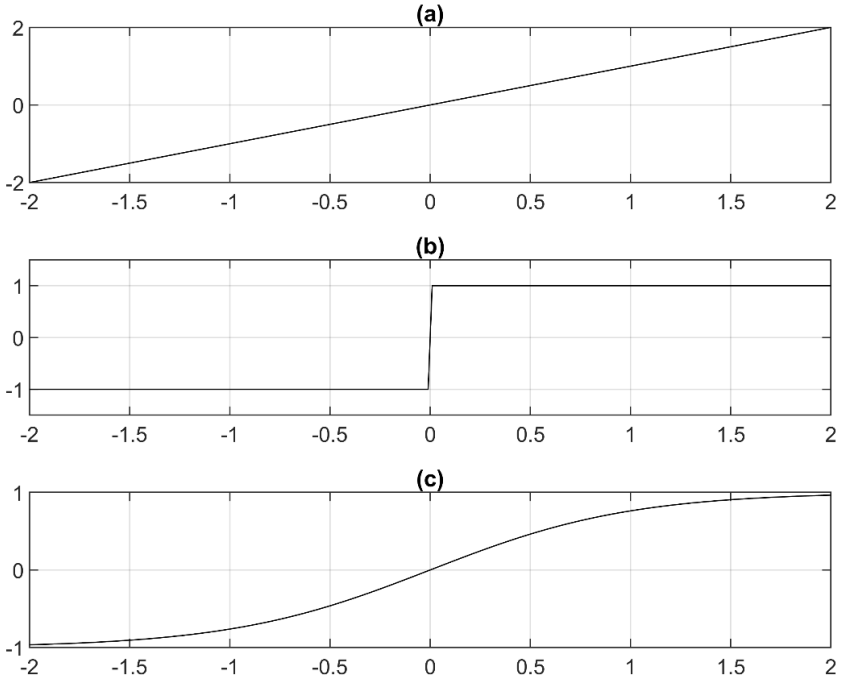

Figure 3.1: Various decision functions used for bit cancellation in PIC detectors. (a) is the linear function, (b) is the hard decision and (c) is the nonlinear hyperbolic tangent function

3.4 Proposed PIC-MMSE Detector

The proposed detector combines the MMSE detector described in (3.21) and the PIC detector in (3.24). The block diagram for the complete detection process is shown in Figure 3.2.

The block that computes the soft bits takes the decision variables from the MMSE filter, $\mathbf{U}_{\mathrm{MMSE}}$ and converts them to the soft bits $\mathbf{b}_{\mathrm{soft}}$. The values of $\mathbf{b}_{\mathrm{soft}}$ are normalized such that $b_{\mathrm{soft}_k} \in [-1, 1]$. In fact, $\mathbf{b}_{\mathrm{soft}}$ approximates the probability of each bit.

The following subsections will describe the PIC-MMSE detector in the AWGN and frequency-nonselective fading channels.

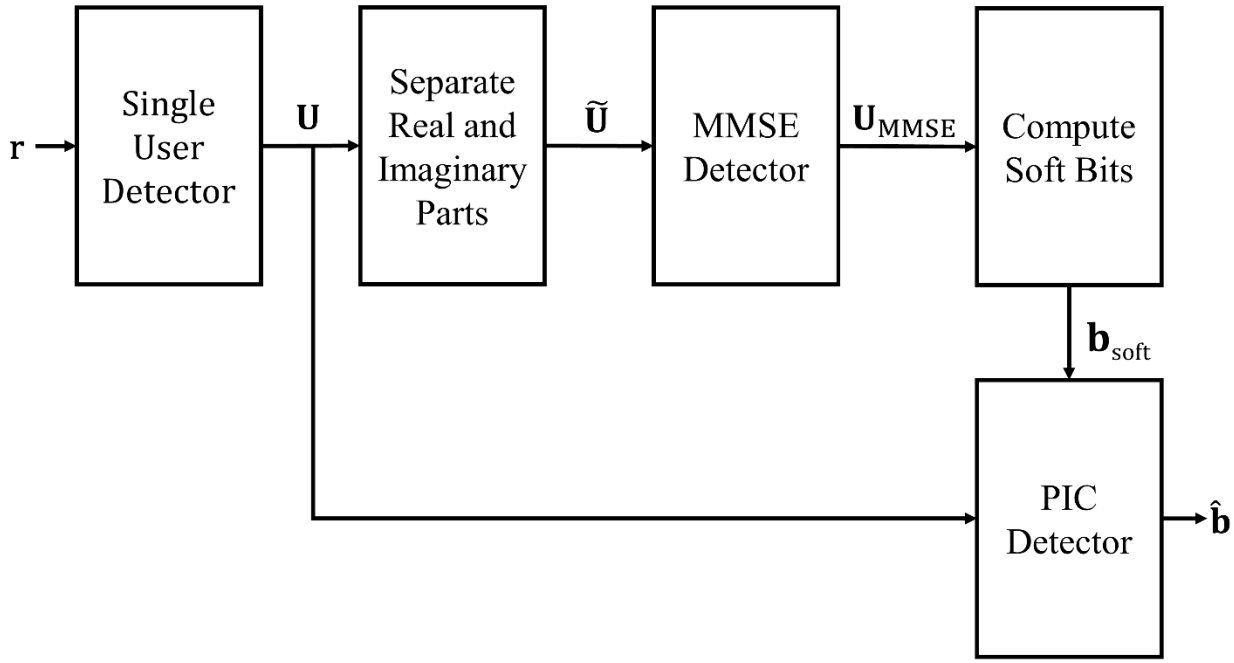

Figure 3.2: Block diagram of the proposed PIC-MMSE detector.

3.4.1 AWGN Channel

The computation of $\mathbf{b}_{\text{soft}}$ starts with first finding the likelihood and probability of each bit. The decision variables after the MMSE detector are:

$$\begin{aligned}\mathbf{U}_{\text{MMSE}} &= \mathbf{W}_{\text{MMSE}}\tilde{\mathbf{U}} \\ &= \mathbf{P}\tilde{\mathbf{R}}^T\left(\tilde{\mathbf{R}}\mathbf{P}\tilde{\mathbf{R}}^T + \frac{\sigma^2}{2}\tilde{\mathbf{S}}\tilde{\mathbf{S}}^T\right)^+\tilde{\mathbf{U}} \\ &= \mathbf{P}\tilde{\mathbf{R}}^T\left(\tilde{\mathbf{R}}\mathbf{P}\tilde{\mathbf{R}}^T + \frac{\sigma^2}{2}\tilde{\mathbf{S}}\tilde{\mathbf{S}}^T\right)^+\left(\tilde{\mathbf{R}}\mathbf{A}\mathbf{b} + \tilde{\mathbf{S}}\tilde{\mathbf{n}}\right) \\ &= \mathbf{P}\tilde{\mathbf{R}}^T\left(\tilde{\mathbf{R}}\mathbf{P}\tilde{\mathbf{R}}^T + \frac{\sigma^2}{2}\tilde{\mathbf{S}}\tilde{\mathbf{S}}^T\right)^+\tilde{\mathbf{R}}\mathbf{A}\mathbf{b} + \mathbf{P}\tilde{\mathbf{R}}^T\left(\tilde{\mathbf{R}}\mathbf{P}\tilde{\mathbf{R}}^T + \frac{\sigma^2}{2}\tilde{\mathbf{S}}\tilde{\mathbf{S}}^T\right)^+\tilde{\mathbf{S}}\tilde{\mathbf{n}}\end{aligned} \tag{3.25}$$

The decision variable for user k can be written as:

$$\begin{aligned} U_{\mathrm{MMSE}_k} &= \mathbf{w}_k \tilde{\mathbf{U}} \\ &= \mathbf{w}_k \left(\tilde{\mathbf{R}}_k^T\right)^T A_k b_k + \sum_{\substack{i=1 \\ i \neq k}}^{K} \mathbf{w}_k \left(\tilde{\mathbf{R}}_i^T\right)^T A_i b_i + \mathbf{w}_k \tilde{\mathbf{S}} \tilde{\mathbf{n}} \\ &= \beta_{k,k} b_k + \sum_{\substack{i=1 \\ i \neq k}}^{K} \beta_{k,i} b_i + \mathbf{w}_k \tilde{\mathbf{S}} \tilde{\mathbf{n}} \\ &= \beta_{k,k} b_k + I_{\mathrm{MMSE}_k} + N_{\mathrm{MMSE}_k} \end{aligned} \tag{3.26}$$

The term $\left(\tilde{\mathbf{R}}_k^T\right)^T$ is column k of $\tilde{\mathbf{R}}$**.** The definition of the other terms in (3.26):

$$\begin{aligned} \beta_{k,i} &= \mathbf{w}_k \left(\tilde{\mathbf{R}}_i^T\right)^T A_i \\ &= P_k \tilde{\mathbf{R}}_k^T \left(P_k \tilde{\mathbf{R}} \tilde{\mathbf{R}}^T + \frac{\sigma^2}{2} \tilde{\mathbf{S}} \tilde{\mathbf{S}}^T \right)^+ \left(\tilde{\mathbf{R}}_i^T\right)^T A_i \end{aligned} \tag{3.27}$$

$$I_{\mathrm{MMSE}_k} = \sum_{\substack{i=1 \\ i \neq k}}^{K} \beta_{k,i} b_i \tag{3.28}$$

$$N_{\mathrm{MMSE}_k} = \mathbf{w}_k \tilde{\mathbf{S}} \tilde{\mathbf{n}} \tag{3.29}$$

The log likelihood ratio can then be computed and from there, the probabilities of each bit to be used by the PIC detector. Unfortunately, the noise between each user's decision variables are correlated, and MAI also remains in the MMSE decision variables. To simplify the probabilities, it is assumed the residual MAI after the MMSE detector is modelled as a Gaussian random variable that is independent of the noise. This leads to the estimated mean and variance of each decision variable conditioned on b_k to be:

$$\mu_{\mathrm{MMSE}_k} = \beta_{k,k} b_k \tag{3.30}$$

$$\begin{aligned} \sigma^2_{\mathrm{MMSE}_k} &= E\left[\left(I_{\mathrm{MMSE}_k} + N_{\mathrm{MMSE}_k}\right)^2\right] \\ &= E\left[I^2_{\mathrm{MMSE}_k}\right] + 2E\left[I_{\mathrm{MMSE}_k} N_{\mathrm{MMSE}_k}\right] + E\left[N^2_{\mathrm{MMSE}_k}\right] \end{aligned} \tag{3.31}$$

The cross correlation between the interference and the noise is 0 as they are independent:

$$\begin{aligned}\sigma^2_{\mathrm{MMSE}_k} &= E\left[I^2_{\mathrm{MMSE}_k}\right] + E\left[N^2_{\mathrm{MMSE}_k}\right] \\ &= E\left[\left(\sum_{\substack{i=1 \\ i\neq k}}^{K} \beta_{k,i} b_i\right)^2\right] + E\left[\left(\mathbf{w}_k \tilde{\mathbf{S}} \tilde{\mathbf{n}}\right)^2\right]\end{aligned} \tag{3.32}$$

Each users bit is independent of one other, and to the noise, that is $E\left[b_i b_j\right] = 0, i \neq j$ and $E[b_i \tilde{\mathbf{n}}] = 0$. Utilizing the fact that $E[b_i^2] = 1$ and $E[\tilde{\mathbf{n}}\tilde{\mathbf{n}}^T] = \frac{\sigma^2}{2}\mathbf{I}$, the variance becomes:

$$\begin{aligned}\sigma^2_{\mathrm{MMSE}_k} &= \sum_{\substack{i=1 \\ i\neq k}}^{K} \beta_{k,i}^2 E[b_i^2] + \mathbf{w}_k \tilde{\mathbf{S}} E[\tilde{\mathbf{n}}\tilde{\mathbf{n}}^T] \tilde{\mathbf{S}}^T \mathbf{w}_k^T \\ &= \sum_{\substack{i=1 \\ i\neq k}}^{K} \left|\beta_{k,i}\right|^2 + \frac{\sigma^2}{2} \mathbf{w}_k \tilde{\mathbf{S}} \tilde{\mathbf{S}}^T \mathbf{w}_k^T\end{aligned} \tag{3.33}$$

This assumption is valid as can be seen by the simulation results. This leads to the log likelihood ratio of U_{MMSE_k} to be:

$$\begin{aligned}LLR\left(U_{\mathrm{MMSE}_k}\right) &= \log\left(\frac{p\left(U_{\mathrm{MMSE}_k} \middle| b_k = +1\right)}{p\left(U_{\mathrm{MMSE}_k} \middle| b_k = -1\right)}\right) \\ &= \log\left(\frac{\frac{1}{\sqrt{2\pi\sigma^2_{\mathrm{MMSE}_k}}} \exp\left[-\frac{\left(U_{MMSE_k} - \mu_{\mathrm{MMSE}_k}\right)^2}{2\sigma^2_{\mathrm{MMSE}_k}}\right]}{\frac{1}{\sqrt{2\pi\sigma^2_{\mathrm{MMSE}_k}}} \exp\left[-\frac{\left(U_{MMSE_k} + \mu_{\mathrm{MMSE}_k}\right)^2}{2\sigma^2_{\mathrm{MMSE}_k}}\right]}\right) \\ &= -\frac{\left(U_{MMSE_k} - \beta_{k,k}\right)^2}{2\sigma^2_{\mathrm{MMSE}_k}} + \frac{\left(U_{MMSE_k} + \beta_{k,k}\right)^2}{2\sigma^2_{\mathrm{MMSE}_k}} \\ &= \frac{2\beta_{k,k} U_{MMSE_k}}{\sigma^2_{\mathrm{MMSE}_k}} \\ &= \alpha_k U_{\mathrm{MMSE}_k}\end{aligned} \tag{3.34}$$

where:

$$\begin{aligned}\alpha_k &= \frac{2\beta_{k,k}}{\hat{\sigma}_k^2} \\ &= \frac{4\beta_{k,k}}{2\sum_{\substack{i=1 \\ i\neq k}}^{K}\left|\beta_{k,i}\right|^2 + \sigma^2 \mathbf{w}_k \tilde{\mathbf{S}}\tilde{\mathbf{S}}^T \mathbf{w}_k^T}\end{aligned} \tag{3.35}$$

The probability that $b_k = +1$ is:

$$\begin{aligned}p_k &= \frac{\exp\left(LLR\left(U_{\mathrm{MMSE}_k}\right)\right)}{1 + \exp\left(LLR\left(U_{\mathrm{MMSE}_k}\right)\right)} \\ &= \frac{\exp\left(\alpha_k U_{\mathrm{MMSE}_k}\right)}{1 + \exp\left(\alpha_k U_{\mathrm{MMSE}_k}\right)}\end{aligned} \tag{3.36}$$

With the probabilities computed, the soft bits are given by:

$$b_{\mathrm{soft}_k} = 2p_k - 1 \tag{3.37}$$

Or in vector notation:

$$\mathbf{b}_{\mathrm{soft}} = 2\mathbf{p} - \mathbf{1} \tag{3.38}$$

where $\mathbf{p} = [p_1, p_2, \ldots p_K]^T$ and $\mathbf{1}$ is a column vector that is all ones with size $K \times 1$. The soft bits in (3.38) can be rewritten as:

$$\begin{aligned}b_{\mathrm{soft}_k} &= 2\left(\frac{\exp\left(\alpha_k U_{\mathrm{MMSE}_k}\right)}{1 + \exp\left(\alpha_k U_{\mathrm{MMSE}_k}\right)}\right) - 1 \\ &= \frac{\exp\left(\alpha_k U_{\mathrm{MMSE}_k}\right) - 1}{\exp\left(\alpha_k U_{\mathrm{MMSE}_k}\right) + 1} \\ &= \tanh\left(\frac{\alpha_k U_{MMSE_k}}{2}\right)\end{aligned} \tag{3.39}$$

This result can be seen as taking the decision variables from the MMSE detector and applying a scaled sigmoid function, which in this case, is the hyperbolic tangent operator. The nonlinearity of the hyperbolic tangent operator offers partial interference cancellation depending how accurate the outputs of the MMSE detector are. When the decision variables after the MMSE detector are strong, the hyperbolic tangent operator will approach ± 1 and most of the MAI is cancelled. On the other hand, if the decision variables after the MMSE detector

are weak, then only partial amounts of MAI are cancelled. This is beneficial compared to hard PIC detectors. When the decision variables are weak for hard PIC detection, poor performance arises as likelihood of a wrong decision increases. Higher chances of wrong decisions results in the higher chances of doubling the MAI after the PIC detector.

The performance of this transformation also relies heavily on the values of α_k. The value of α_k shows how reliable the MMSE decision variables should be, relative to the channel conditions and multiple access interference. As α_k increases, the hyperbolic tangent operator approaches a sgn function, meaning the MMSE decision variables are expected to be accurate and will almost fully cancel the MAI for that respective user. On the other hand, if α_k is low, the decision variables from the MMSE detector are not expected to be accurate. This causes the hyperbolic tangent operator to have a lower slope at the origin and it requires the magnitude of the decision variables to be high to cancel more of the MAI for that user. To illustrate this, consider Figure 3.3 which shows the hyperbolic tangent operator for various values of SNR in an AWGN channel. As the SNR decreases, hyperbolic tangent operator's rate of change gets lower around the origin. On the other hand, as the SNR increases, the rate of change at the origin gets higher, and the detector starts to approach the hard decision detector. This means the decision variables after the MMSE detector are most likely to be correct and can be used to cancel more interference.

The PIC detector produces the final decision variables:

$$U_{\mathrm{PIC}_k} = U_k - \sum_{\substack{i=1 \\ i \neq k}}^{K} R_{i,k} A_i b_{\mathrm{soft}_i} \tag{3.40}$$

Finally, a final hard estimate of the bits is made. This is shown for user k and in vector noatation:

$$\hat{b}_k = \mathrm{sgn}\left(\Re\left(U_{\mathrm{PIC}_k}\right)\right) \tag{3.41}$$

$$\hat{\mathbf{b}} = \mathrm{sgn}\left(\Re\left(\mathbf{U}_{PIC}\right)\right) \tag{3.42}$$

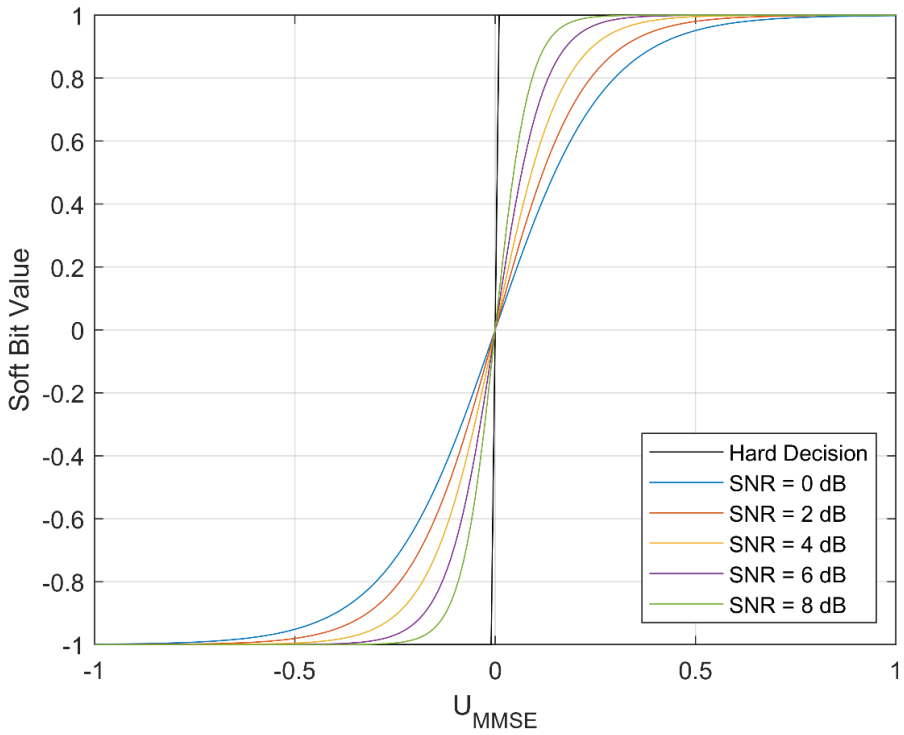

Figure 3.3: Plot of the nonlinear decision device used after the MMSE detector for various SNR

3.4.2 Frequency-Nonselective Fading Channel

The PIC-MMSE detector for the frequency-nonselective fading channel is very similar to that of the AWGN channel, except the received signals now have complex gains associated with them, which alters the derivation slightly. The major difference is the frequency-nonselective fading channel uses the correlation matrix $\widetilde{\mathbf{R}}'$ defined in (3.13) as opposed to the $\widetilde{\mathbf{R}}$ correlation matrix used for the AWGN channel. The MMSE filter for the frequency-nonselective fading channel is derived following the same procedure as before and is given as:

$$\mathbf{W'}_{\text{MMSE}} = \mathbf{P}\widetilde{\mathbf{R}}'^{T}\left(\widetilde{\mathbf{R}}'\mathbf{P}\widetilde{\mathbf{R}}'^{T} + \frac{\sigma^2}{2}\widetilde{\mathbf{S}}'\widetilde{\mathbf{S}}'^{T}\right)^{+} \tag{3.43}$$

and the MMSE filter for user k is:

$$\mathbf{w'}_{k} = P_k\widetilde{\mathbf{R}}'^{T}_{k}\left(\widetilde{\mathbf{R}}'\mathbf{P}\widetilde{\mathbf{R}}'^{T} + \frac{\sigma^2}{2}\widetilde{\mathbf{S}}'\widetilde{\mathbf{S}}'^{T}\right)^{+} \tag{3.44}$$

The decision variables after the MMSE detector are:

$$\begin{aligned}\mathbf{U'}_{\mathrm{MMSE}} &= \mathbf{W'}_{\mathrm{MMSE}}\widetilde{\mathbf{U}}' \\ &= \mathbf{P}\widetilde{\mathbf{R}}'^{T}\left(\widetilde{\mathbf{R}}'\mathbf{P}\widetilde{\mathbf{R}}'^{T}+\frac{\sigma^2}{2}\widetilde{\mathbf{S}}'\widetilde{\mathbf{S}}'^{T}\right)^{+}\widetilde{\mathbf{U}}' \\ &= \mathbf{P}\widetilde{\mathbf{R}}'^{T}\left(\widetilde{\mathbf{R}}'\mathbf{P}\widetilde{\mathbf{R}}'^{T}+\frac{\sigma^2}{2}\widetilde{\mathbf{S}}'\widetilde{\mathbf{S}}'^{T}\right)^{+}\left(\widetilde{\mathbf{R}}'\mathbf{A}\mathbf{b}+\widetilde{\mathbf{S}}'\widetilde{\mathbf{n}}\right) \\ &= \mathbf{P}\widetilde{\mathbf{R}}'^{T}\left(\widetilde{\mathbf{R}}'\mathbf{P}\widetilde{\mathbf{R}}'^{T}+\frac{\sigma^2}{2}\widetilde{\mathbf{S}}'\widetilde{\mathbf{S}}'^{T}\right)^{+}\widetilde{\mathbf{R}}'\mathbf{A}\mathbf{b}+\mathbf{P}\widetilde{\mathbf{R}}'^{T}\left(\widetilde{\mathbf{R}}'\mathbf{P}\widetilde{\mathbf{R}}'^{T}+\frac{\sigma^2}{2}\widetilde{\mathbf{S}}'\widetilde{\mathbf{S}}'^{T}\right)^{+}\widetilde{\mathbf{S}}'\widetilde{\mathbf{n}}\end{aligned} \tag{3.45}$$

The MMSE decision variable for user k can be written as:

$$\begin{aligned}U'_{\mathrm{MMSE}_k} &= \mathbf{w'}_k\widetilde{\mathbf{U}}' \\ &= \mathbf{w'}_k\left(\widetilde{\mathbf{R}}'^{T}_{k}\right)^{T}A_k b_k+\sum_{\substack{i=1\\ i\neq k}}^{K}\mathbf{w'}_k\left(\widetilde{\mathbf{R}}'^{T}_{\boldsymbol{i}}\right)^{T}A_i b_i+\mathbf{w}_k\widetilde{\mathbf{S}}'\widetilde{\mathbf{n}} \\ &= \beta'_{k,k}b_k+\sum_{\substack{i=1\\ i\neq k}}^{K}\beta'_{k,i}b_i+\mathbf{w'}_k\widetilde{\mathbf{S}}'\widetilde{\mathbf{n}} \\ &= \beta'_{k,k}b_k+I'_{\mathrm{MMSE}_k}+N'_{\mathrm{MMSE}_k}\end{aligned} \tag{3.46}$$

where:

$$\begin{aligned}\beta'_{k,i} &= \mathbf{w'}_k\left(\widetilde{\mathbf{R}}'^{T}_{\boldsymbol{i}}\right)^{T}A_i \\ &= P_k\widetilde{\mathbf{R}}'^{T}_{k}\left(\widetilde{\mathbf{R}}'\mathbf{P}\widetilde{\mathbf{R}}'^{T}+\frac{\sigma^2}{2}\widetilde{\mathbf{S}}'\widetilde{\mathbf{S}}'^{T}\right)^{+}\left(\widetilde{\mathbf{R}}'^{T}_{\boldsymbol{i}}\right)^{T}A_i\end{aligned} \tag{3.47}$$

$$I'_{\mathrm{MMSE}_k}=\sum_{\substack{i=1\\ i\neq k}}^{K}\beta'_{k,i}b_i \tag{3.48}$$

$$N'_{\mathrm{MMSE}_k}=\mathbf{w'}_k\widetilde{\mathbf{S}}'\widetilde{\mathbf{n}} \tag{3.49}$$

After the MMSE detector, the soft bits are computed and are of the form:

$$b'_{\mathrm{soft}_k}=\tanh\left(\frac{\alpha'_k U'_{\mathrm{MMSE}_k}}{2}\right) \tag{3.50}$$

where

$$\alpha'_k = \frac{4\beta'_{k,k}}{2\sum_{\substack{i=1 \\ i\neq k}}^{K}\left|\beta'_{k,i}\right|^2 + \sigma^2 \mathbf{w}'_k \tilde{\mathbf{S}}' \tilde{\mathbf{S}}'^T \mathbf{w}'^T_k} \tag{3.51}$$

The PIC detector produces the final decision variables using the soft bits:

$$U'_{\mathrm{PIC}_k} = U'_k - \sum_{\substack{i=1 \\ i\neq k}}^{K} R_{k,i} h_k^* h_i A_i b'_{\mathrm{soft}_i} \tag{3.52}$$

Finally, a final hard estimate of the bits is made:

$$\hat{b}'_k = \mathrm{sgn}\left(\Re\left(U'_{\mathrm{PIC}_k}\right)\right) \tag{3.53}$$

$$\hat{\mathbf{b}}' = \mathrm{sgn}\left(\Re\left(\mathbf{U}'_{PIC}\right)\right) \tag{3.54}$$

3.5 Approximate Bit Error Rate

In this section, the theoretical BER is presented. The exact BER of the proposed PIC-MMSE detector is very difficult to obtain because of the nonlinearity of the computations of the soft bits before the PIC detection from the hyperbolic tangent operator. In addition, the residual MAI is not Gaussian like the added noise. This combination of added Gaussian noise and MAI makes the exact BER expression difficult to obtain. Instead, various assumptions and approximations throughout the derivation are made to simplify some calculations. The biggest of which is assuming the residual MAI after the PIC detector is Gaussian distributed. This assumption is done by others for PIC detectors [40], [41], and the simulation results prove it to be accurate under certain conditions [42].

The analysis will be conducted under the AWGN channel, and with all users received power levels equal such that $A_k = A,\ k = 1, 2, \ldots K$. The decision variables after the PIC detector are:

$$
\begin{aligned}
U_{\mathrm{PIC}_k} &= \Re\left(Ab_k + \sum_{\substack{i=1 \\ i\neq k}}^{K} AR_{k,i}\left(b_i - b_{\mathrm{soft}_i}\right) + \mathbf{s}_k^H \mathbf{n} \right) \\
&= \Re\left(Ab_k + \sum_{\substack{i=1 \\ i\neq k}}^{K} AR_{k,i}\left[b_i - \tanh\left(\frac{\alpha_k U_{\mathrm{MMSE}_k}}{2}\right)\right] + \mathbf{s}_k^H \mathbf{n} \right) \\
&= Ab_k + \sum_{\substack{i=1 \\ i\neq k}}^{K} \lambda_{k,i}\left[b_i - \tanh\left(\frac{\alpha_k U_{\mathrm{MMSE}_k}}{2}\right)\right] + N_{\mathrm{PIC}_k} \\
&= Ab_k + I_{\mathrm{PIC}_k} + N_{\mathrm{PIC}_k}
\end{aligned}
\tag{3.55}
$$

where:

$$
\lambda_{k,i} = \Re\left(AR_{k,i}\right) \tag{3.56}
$$

$$
I_{\mathrm{PIC}_k} = \sum_{\substack{i=1 \\ i\neq k}}^{K} \lambda_{k,i}\left[b_i - \tanh\left(\frac{\alpha_k U_{\mathrm{MMSE}_k}}{2}\right)\right] \tag{3.57}
$$

$$
N_{\mathrm{PIC}_k} = \Re(\mathbf{s}_k^H \mathbf{n}) \tag{3.58}
$$

I_{PIC_k} is the residual MAI after cancellation and N_{PIC_k} is the noise seen by user k. The estimated bits after the PIC detector are:

$$
\begin{aligned}
\hat{b}_k &= \mathrm{sgn}\left(\Re\left(U_{\mathrm{PIC}_k}\right)\right) \\
&= \mathrm{sgn}\left[\Re\left(U_k - \sum_{\substack{i=1 \\ i\neq k}}^{K} R_{k,i} Ab_{\mathrm{soft}_i} \right)\right] \\
&= \mathrm{sgn}\left(Ab_k + I_{\mathrm{PIC}_k} + N_{\mathrm{PIC}_k}\right)
\end{aligned}
\tag{3.59}
$$

The probability of error assumes that the residual MAI is Gaussian distributed. The probability of error for user k is:

$$
P_{e,k} = P(b_k = -1)P\left(\hat{b}_k > 0 | b_k = -1\right) + P(b_k = 1)P\left(\hat{b}_k < 0 | b_k = 1\right) \tag{3.60}
$$

$$
\begin{aligned}
P_{e,k} &= \frac{1}{2}P\left(I_{\mathrm{PIC}_k} + N_{\mathrm{PIC}_k} > A\right) + \frac{1}{2}P\left(I_{\mathrm{PIC}_k} + N_{\mathrm{PIC}_k} < -A\right) \\
&= Q\left(\frac{A - E\left[I_{\mathrm{PIC}_k}\right]}{\sigma_{\mathrm{PIC}_k}}\right)
\end{aligned}
\tag{3.61}
$$

where $Q(\cdot)$ is the Q function defined as:

$$
Q(x) = \frac{1}{\sqrt{2\pi}}\int_x^{\infty} \exp\left(-\frac{u^2}{2}\right) du \tag{3.62}
$$

The effective variance $\sigma^2_{\mathrm{PIC}_k}$ is:

$$
\begin{aligned}
\sigma^2_{\mathrm{PIC}_k} &= \mathrm{Var}\left(I_{\mathrm{PIC}_k} + N_{\mathrm{PIC}_k}\right) \\
&= \mathrm{Var}\left(I_{\mathrm{PIC}_k}\right) + \mathrm{Var}\left(N_{\mathrm{PIC}_k}\right) + 2\mathrm{Cov}\left(I_{\mathrm{PIC}_k}, N_{\mathrm{PIC}_k}\right) \\
&= E\left[\left(I_{\mathrm{PIC}_k} - E\left[I_{\mathrm{PIC}_k}\right]\right)\left(I_{\mathrm{PIC}_k} - E\left[I_{\mathrm{PIC}_k}\right]\right)^T\right] + E\left[N_{\mathrm{PIC}_k}N^T_{\mathrm{PIC}_k}\right] \\
&\qquad + 2E\left[\left(I_{\mathrm{PIC}_k} - E\left[I_{\mathrm{PIC}_k}\right]\right)N^T_{\mathrm{PIC}_k}\right] \\
&= E\left[I^2_{\mathrm{PIC}_k}\right] + E\left[N_{\mathrm{PIC}_k}N^T_{\mathrm{PIC}_k}\right] + 2E\left[I_{\mathrm{PIC}_k}N^T_{\mathrm{PIC}_k}\right] - E\left[I_{\mathrm{PIC}_k}\right]^2
\end{aligned}
\tag{3.63}
$$

As can be seen from (3.63), the variance seen by user k depends on the MAI, the noise and the cross correlation between the noise and the MAI, as the noise affects decision variables from the MMSE detector. The following subsections go into detail determining the various expectations in (3.63). It is important to note that the expectations required in (3.63), are all computed with the condition $b_k = -1$, that is $E[\cdot] = E[\cdot\,|b_k = -1]$.

3.5.1 Computing $E\left[N_{\mathrm{PIC}_k}N^T_{\mathrm{PIC}_k}\right]$

Before computing$E\left[N_{\mathrm{PIC}_k}N^T_{\mathrm{PIC}_k}\right]$, N_{PIC_k} is reformatted:

$$
\begin{aligned}
N_{\mathrm{PIC}_k} &= \Re(\mathbf{s}_k^H\mathbf{n}) \\
&= \Re([\Re(\mathbf{s}_k^T)\Re(\mathbf{n}) + \Im(\mathbf{s}_k^T)\Im(\mathbf{n})] + j[-\Im(\mathbf{s}_k^T)\Re(\mathbf{n}) + \Re(\mathbf{s}_k^T)\Im(\mathbf{n})]) \\
&= \Re(\mathbf{s}_k^T)\Re(\mathbf{n}) + \Im(\mathbf{s}_k^T)\Im(\mathbf{n})
\end{aligned}
\tag{3.64}
$$

This result is just row k in $\tilde{\mathbf{S}}$ multiplied by the noise vector $\tilde{\mathbf{n}}$.

$$
N_{\mathrm{PIC}_k} = \tilde{\mathbf{S}}_k\tilde{\mathbf{n}} \tag{3.65}
$$

And the expectation is:

$$\begin{aligned} E\left[N_{\mathrm{PIC}_k} N_{\mathrm{PIC}_k}^T\right] &= E\left[\left(\tilde{\mathbf{S}}_k \tilde{\mathbf{n}}\right)\left(\tilde{\mathbf{S}}_k \tilde{\mathbf{n}}\right)^T\right] \\ &= E\left[\tilde{\mathbf{S}}_k \tilde{\mathbf{n}} \tilde{\mathbf{n}}^T \tilde{\mathbf{S}}_k^T\right] \\ &= \frac{\sigma^2}{2} \tilde{\mathbf{S}}_k \tilde{\mathbf{S}}_k^T \\ &= \frac{\sigma^2}{2} \end{aligned} \tag{3.66}$$

The multiplication of $\tilde{\mathbf{S}}_k$ and its transpose is just the energy of user k's spreading code which is normalized to be 1.

3.5.2 Computing $E\left[I_{\mathrm{PIC}_k}\right]$

Next the mean of the residual MAI, $E\left[I_{\mathrm{PIC}_k}\right]$ is computed.

$$\begin{aligned} E\left[I_{\mathrm{PIC}_k}\right] &= E\left\{\sum_{\substack{i=1 \\ i\neq k}}^{K} \lambda_{k,i}\left[b_i - \tanh\left(\frac{\alpha_i U_{\mathrm{MMSE}_i}}{2}\right)\right]\right\} \\ &= \sum_{\substack{i=1 \\ i\neq k}}^{K} \lambda_{k,i}\left\{\left(E[b_i] - E\left[\tanh\left(\frac{\alpha_i U_{\mathrm{MMSE}_i}}{2}\right)\right]\right)\right\} \end{aligned} \tag{3.67}$$

The expected value of b_i is zero due to it taking equal possible values of +/- 1 with equal probability.

$$\begin{aligned} E\left[I_{\mathrm{PIC}_k}\right] &= -\sum_{\substack{i=1 \\ i\neq k}}^{K} \lambda_{k,i} E\left[\tanh\left(\frac{\alpha_i U_{\mathrm{MMSE}_i}}{2}\right)\right] \\ &= -\sum_{\substack{i=1 \\ i\neq k}}^{K} \lambda_{k,i} E\left\{\tanh\left[\frac{\alpha_i}{2}\left(-\beta_{i,k} + \sum_{\substack{l=1 \\ l\neq k}}^{K} \beta_{i,l} b_l + N_{\mathrm{MMSE}_i}\right)\right]\right\} \end{aligned} \tag{3.68}$$

Note that the $-\beta_{i,k}$ term is present due to the conditional expectation including $b_k = -1$. The expectation required in (3.68) is taking the expectation of a Gaussian random variable transformed by the hyperbolic tangent operator. (3.68) can be rewritten as:

$$E\left[I_{\mathrm{PIC}_k}\right] = -\sum_{\substack{i=1 \\ i\neq k}}^{K} \lambda_{k,i}\, E\left[\tanh\left(-\frac{\alpha_i}{2}\beta_{i,k} + \Phi\right)\right] \tag{3.69}$$

where Φ is a Gaussian random variable with zero mean and variance:

$$\sigma_{\Phi}^2 = \frac{\alpha_i^2}{4}\left(\sum_{\substack{l=1 \\ l\neq k}}^{K} \left|\beta_{i,l}\right|^2 + \frac{\sigma^2}{2}\mathbf{w}_i\tilde{\mathbf{S}}\tilde{\mathbf{S}}^T\mathbf{w}_i^T\right) \tag{3.70}$$

The expectation in (3.69) can be written as:

$$E\left[\tanh\left(-\frac{\alpha_i}{2}\beta_{i,k} + \Phi\right)\right] = \int_{-\infty}^{\infty} \tanh\left(-\frac{\alpha_i}{2}\beta_{i,k} + \phi\right) f_{\Phi}(\phi)d\phi \tag{3.71}$$

where $f_{\Phi}(\phi)$ is the Gaussian probability density function which is:

$$f_{\Phi}(\phi)dx = \frac{1}{\sqrt{2\pi\sigma_{\Phi}^2}}\exp\left(-\frac{\phi^2}{2\sigma_{\Phi}^2}\right)d\phi \tag{3.72}$$

The $\tanh(\cdot)$ part of the integral makes it difficult to compute. To estimate the integral, the hyperbolic tangent operator with a scaled error function is substituted:

$$\tanh(x) \approx \mathrm{erf}\left(\frac{\sqrt{\pi}}{2}x\right) \tag{3.73}$$

where the error function is defined as:

$$\mathrm{erf}(x) = \frac{2}{\sqrt{\pi}}\int_0^x e^{-t^2}dt \tag{3.74}$$

This approximation is valid given the plot of both functions shown in Figure 3.4.

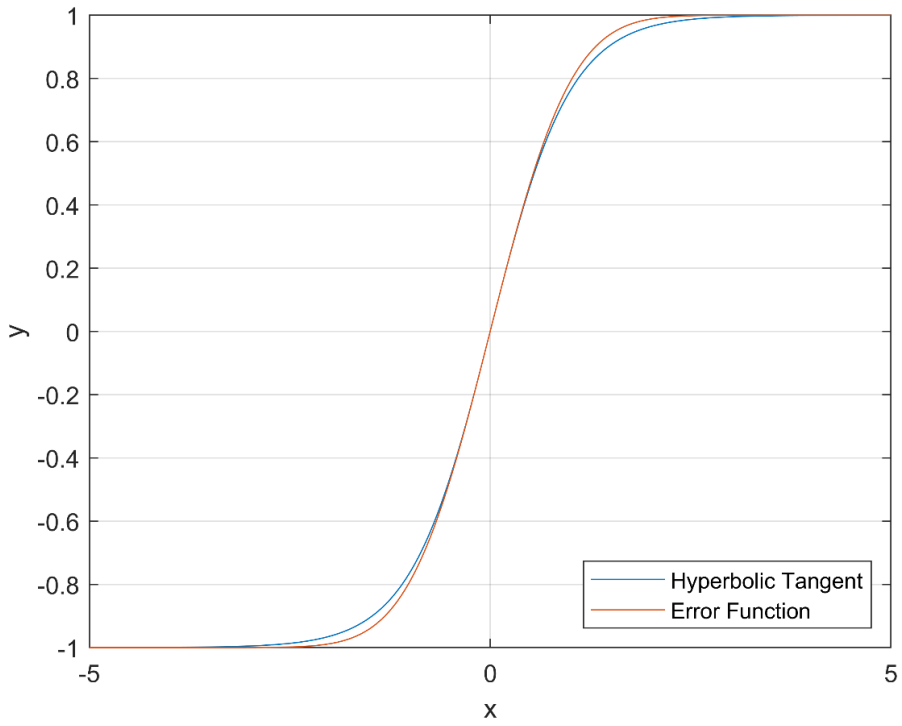

Figure 3.4: Plot of the hyperbolic tangent and scaled error function used for approximations

The expectation in (3.71) can be approximated as:

$$E\left[\tanh\left(-\frac{\alpha_i}{2}\beta_{i,k}+\Phi\right)\right] \approx \int_{-\infty}^{\infty}\operatorname{erf}\left[\frac{\sqrt{\pi}}{2}\left(-\frac{\alpha_i}{2}\beta_{i,k}+\phi\right)\right]\frac{1}{\sqrt{2\pi\sigma_\Phi^2}}\exp\left(-\frac{\phi^2}{2\sigma_\Phi^2}\right)d\phi \tag{3.75}$$

By using the following result from [43]:

$$\int_{-\infty}^{\infty}\operatorname{erf}[c_1x+c_2]\exp(-(c_3x+c_4)^2)\,dx=\frac{\sqrt{\pi}}{c_3}\operatorname{erf}\left[\frac{[c_3c_2-c_4c_1)}{\sqrt{{c_3}^2+{c_1}^2}}\right] \tag{3.76}$$

In this case:

$$c_1=\frac{\sqrt{\pi}}{2} \qquad c_2=-\frac{\sqrt{\pi}\alpha_i}{4}\beta_{i,k}$$

$$c_3=\frac{1}{\sqrt{2\sigma_\Phi^2}} \qquad c_4=0$$

Using this result, the integral in (3.75) is:

$$\int_{-\infty}^{\infty} \operatorname{erf}\left[\frac{\sqrt{\pi}}{2}\left(-\frac{\alpha_i}{2}\beta_{i,k}+\phi\right)\right]\frac{1}{\sqrt{2\pi\sigma_\Phi^2}}\exp\left(-\frac{\phi^2}{2\sigma_\Phi^2}\right)d\phi$$

$$=\frac{\sqrt{2\sigma_\Phi^2\pi}}{\sqrt{2\pi\sigma_\Phi^2}}\operatorname{erf}\left[\frac{-\frac{\sqrt{\pi}\alpha_i}{4\sqrt{2\sigma_\Phi^2}}\beta_{i,k}}{\sqrt{\frac{1}{2\sigma_\Phi^2}+\frac{\pi}{4}}}\right] \tag{3.77}$$

$$=\operatorname{erf}\left[\frac{-\sqrt{\pi}\alpha_i\beta_{i,k}}{4\sqrt{1+\frac{\pi\sigma_\Phi^2}{2}}}\right]$$

With this result, and the fact that $\operatorname{erf}(-a) = -\operatorname{erf}(a)$, $E[I_k]$ is:

$$E\left[I_{\mathrm{PIC}_k}\right] = -\sum_{\substack{i=1\\ i\neq k}}^{K}\lambda_{k,i}\operatorname{erf}\left[\frac{-\sqrt{\pi}\alpha_i\beta_{i,k}}{4\sqrt{1+\frac{\pi\sigma_\Phi^2}{2}}}\right]$$
$$=\sum_{\substack{i=1\\ i\neq k}}^{K}\lambda_{k,i}\operatorname{erf}\left[\frac{\sqrt{\pi}\alpha_i\beta_{i,k}}{4\sqrt{1+\frac{\pi\sigma_\Phi^2}{2}}}\right] \tag{3.78}$$

As can be seen from this result, there is importance on the value of $\beta_{i,k}$. When the MMSE detector does a good job mitigating the MAI, $\beta_{i,k}$ will be relatively small. When $\beta_{i,k}$ is small, the error function will approach 0, and so will $E\left[I_{PIC_k}\right]$.

3.5.3 Computing $E\left[I_{\mathrm{PIC}_k}^2\right]$:

Next, $E\left[I_{\mathrm{PIC}_k}^2\right]$ is computed, which is a bulk of the MAI variance added to the noise:

$$E\left[I_{\mathrm{PIC}_k}^2\right] = E\left[\left(\sum_{\substack{i=1 \\ i\neq k}}^{K} \alpha_{k,i}\left(b_i - \tanh\left(\frac{\alpha_i U_{\mathrm{MMSE}_i}}{2}\right)\right)\right)^2\right]$$

$$= \sum_{\substack{i=1 \\ i\neq k}}^{K} \lambda_{k,i}^2 \, E\left[\left(b_i - \tanh\left(\frac{\alpha_i U_{\mathrm{MMSE}_i}}{2}\right)\right)^2\right]$$

$$+ 2\sum_{\substack{i=2 \\ i\neq k}}^{K}\sum_{\substack{j=1 \\ j\neq k}}^{i-1} \lambda_{k,i}\lambda_{k,j} E\left[\left(b_i - \tanh\left(\frac{\alpha_i U_{\mathrm{MMSE}_i}}{2}\right)\right)\left(b_j - \tanh\left(\frac{\alpha_j U_{\mathrm{MMSE}_j}}{2}\right)\right)\right]$$

(3.79)

The variance of the MAI is broken down into 2 parts, the squared residual MAI and the cross correlation between residual MAI. Starting with the expectation in the first term:

$$E\left[\left(b_i - \tanh\left(\frac{\alpha_i U_{\mathrm{MMSE}_i}}{2}\right)\right)^2\right] = E[b_i^2 - 2b_i \tanh\left(\frac{\alpha_i U_{\mathrm{MMSE}_i}}{2}\right) + \tanh^2\left(\frac{\alpha_i U_{\mathrm{MMSE}_i}}{2}\right)$$

$$= 1 - 2E\left[b_i \tanh\left(\frac{\alpha_i U_{\mathrm{MMSE}_i}}{2}\right)\right] + E\left[\tanh^2\left(\frac{\alpha_i U_{\mathrm{MMSE}_i}}{2}\right)\right]$$

(3.80)

Finding $E\left[b_i \tanh\left(\frac{\alpha_i U_{\mathrm{MMSE}_i}}{2}\right)\right]$ first by expanding the expectation into conditional expectations:

$$
\begin{aligned}
&E\left[b_i \tanh\left(\frac{\alpha_i U_{\mathrm{MMSE}_i}}{2}\right)\right] \\
&\qquad = P(b_i = 1)E\left[\tanh\left(\frac{\alpha_i U_{\mathrm{MMSE}_i}}{2}\right)|b_i = 1\right] \\
&\qquad - \ P(b_i = -1)E\left[\tanh\left(\frac{\alpha_i U_{\mathrm{MMSE}_i}}{2}\right)|b_i = -1\right] \\
&= \frac{1}{2}E\left[\tanh\left(\frac{\alpha_i U_{\mathrm{MMSE}_i}}{2}\right)|b_i = 1\right] - \frac{1}{2}E\left[\tanh\left(\frac{\alpha_i U_{\mathrm{MMSE}_i}}{2}\right)|b_i = -1\right] \\
&= \frac{1}{2}E\left\{\tanh\left[\frac{\alpha_i}{2}\left(-\beta_{i,k} + \beta_{i,i} + \sum_{\substack{l=1 \\ l\neq k \\ l\neq i}}^{K} \beta_{k,l} b_l + N_{\mathrm{MMSE}_i}\right)\right]\right\} \\
&\qquad - \frac{1}{2}E\left\{\tanh\left[\frac{\alpha_i}{2}\left(-\beta_{i,k} - \beta_{i,i} + \sum_{\substack{l=1 \\ l\neq k \\ l\neq i}}^{K} \beta_{k,l} b_l + N_{\mathrm{MMSE}_i}\right)\right]\right\}
\end{aligned}
\tag{3.81}
$$

In both terms of (3.81), the residual MAI and the noise can be grouped together and be approximated as Gaussian noise. This results in:

$$
\begin{aligned}
&E\left[b_i \tanh\left(\frac{\alpha_i U_{\mathrm{MMSE}_i}}{2}\right)\right] \\
&\qquad = \frac{1}{2}E\left[\tanh\left(\frac{\alpha_i}{2}\left(-\beta_{i,k} + \beta_{i,i}\right) + \Phi\right)\right] \\
&\qquad - \frac{1}{2}E\left[\tanh\left(\frac{\alpha_i}{2}\left(-\beta_{i,k} - \beta_{i,i}\right) + \Phi\right)\right]
\end{aligned}
\tag{3.82}
$$

where Φ is a Gaussian random variable with zero mean and variance:

$$
\sigma_\Phi^2 = \frac{\alpha_i^2}{4}\left(\sum_{\substack{l=1 \\ l\neq i \\ l\neq k}}^{K} \left|\beta_{i,l}\right|^2 + \frac{\sigma^2}{2}\mathbf{w_i}\tilde{\mathbf{S}}\tilde{\mathbf{S}}^T\mathbf{w_i}^T\right) \tag{3.83}
$$

The expectation $E\left[b_i \tanh\left(\frac{\alpha_i U_{\mathrm{MMSE}_i}}{2}\right)\right]$ can be written in integral notation:

$$E\left[b_i \tanh\left(\frac{\alpha_i U_{\mathrm{MMSE}_i}}{2}\right)\right]$$
$$= \frac{1}{2}\int_{-\infty}^{\infty} \tanh\left(\frac{\alpha_i}{2}\left(-\beta_{i,k} + \beta_{i,i}\right) + \phi\right) f_\Phi(\phi) d\phi \tag{3.84}$$
$$-\frac{1}{2}\int_{-\infty}^{\infty} \tanh\left(\frac{\alpha_i}{2}\left(-\beta_{i,k} - \beta_{i,i}\right) + \phi\right) f_\Phi(\phi) d\phi$$

By taking the error function approximation as done when computing $E[I_k]$ in (3.73):

$$E\left[b_i \tanh\left(\frac{\alpha_i U_{\mathrm{MMSE}_i}}{2}\right)\right]$$
$$\approx \frac{1}{2}\int_{-\infty}^{\infty} \mathrm{erf}\left[\frac{\sqrt{\pi}}{2}\left(\frac{\alpha_i}{2}\left(-\beta_{i,k} + \beta_{i,i}\right) + \phi\right)\right] \frac{1}{\sqrt{2\pi\sigma_\Phi^2}} \exp\left(-\frac{\phi^2}{2\sigma_\Phi^2}\right) d\phi$$
$$-\frac{1}{2}\int_{-\infty}^{\infty} \mathrm{erf}\left[\frac{\sqrt{\pi}}{2}\left(\frac{\alpha_i}{2}\left(-\beta_{i,k} - \beta_{i,i}\right) + \phi\right)\right] \frac{1}{\sqrt{2\pi\sigma_\Phi^2}} \exp\left(-\frac{\phi^2}{2\sigma_\Phi^2}\right) d\phi \tag{3.85}$$

And following the result from (3.76), the integral $E\left[b_i \tanh\left(\frac{\alpha_i U_{\mathrm{MMSE}_i}}{2}\right)\right]$ results in:

$$E\left[b_i \tanh\left(\frac{\alpha_i U_{\mathrm{MMSE}_i}}{2}\right)\right]$$
$$\approx \frac{1}{2}\mathrm{erf}\left[\frac{\sqrt{\pi}\alpha_k\left(-\beta_{i,k} + \beta_{i,i}\right)}{4\sqrt{1 + \frac{\pi\sigma_\Phi^2}{2}}}\right] - \frac{1}{2}\mathrm{erf}\left[\frac{\sqrt{\pi}\alpha_k\left(-\beta_{i,k} - \beta_{i,i}\right)}{4\sqrt{1 + \frac{\pi\sigma_\Phi^2}{2}}}\right] \tag{3.86}$$

Now for the second expectation in (3.80), $E\left[\tanh^2\left(\frac{\alpha_i U_{\mathrm{MMSE}_i}}{2}\right)\right]$:

$$E\left[\tanh^2\left(\frac{\alpha_i U_{\mathrm{MMSE}_i}}{2}\right)\right] = E\left[\tanh^2\left(\frac{\alpha_i}{2}\left(-\beta_{i,k} + \sum_{\substack{l=1 \\ l\neq k}}^{K} \beta_{i,l} b_l + N_{\mathrm{MMSE}_i}\right)\right)\right] \tag{3.87}$$

Again, by taking the residual MAI and noise and grouping it together as Gaussian noise:

$$E\left[\tanh^2\left(\frac{\alpha_i U_{\mathrm{MMSE}_i}}{2}\right)\right] = E\left[\tanh^2\left(-\frac{\alpha_i}{2}\beta_{i,k} + \Phi\right)\right] \tag{3.88}$$

The variance of Φ is:

$$\sigma_{\Phi}^{2} = \frac{\alpha_i^2}{4}\left(\sum_{\substack{l=1 \\ l\neq k}}^{K}\left|\beta_{i,l}\right|^2 + \frac{\sigma^2}{2}\mathbf{w}_i\tilde{\mathbf{S}}\tilde{\mathbf{S}}^T\mathbf{w}_i^T\right) \tag{3.89}$$

The expectation in integral form:

$$E\left[\tanh^2\left(\frac{\alpha_i U_{\mathrm{MMSE}_i}}{2}\right)\right] = \int_{-\infty}^{\infty}\tanh^2\left(-\frac{\alpha_i}{2}\beta_{i,k} + \phi\right) f_{\Phi}(\phi)d\phi \tag{3.90}$$

The integral required does not have a closed form solution. Even if the error function approximation as done in (3.73), the result still does not have a closed form solution. For the sake of this approximation, (3.90) is computed numerically. The result of this integral/expectation is left as:

$$E\left[\tanh^2\left(\frac{\alpha_i U_{\mathrm{MMSE}_i}}{2}\right)\right] = \Lambda_1(k,i) \tag{3.91}$$

The result for $E\left[\left(b_i - \tanh\left(\frac{\alpha_i U_{\mathrm{MMSE}_i}}{2}\right)\right)^2\right]$ is:

$$E\left[\left(b_i - \tanh\left(\frac{\alpha_i U_{\mathrm{MMSE}_i}}{2}\right)\right)^2\right]$$
$$= 1 - \left(\mathrm{erf}\left[\frac{\sqrt{\pi}\alpha_k\left(-\beta_{i,k} + \beta_{i,i}\right)}{4\sqrt{1 + \frac{\pi\sigma_{\Phi}^2}{2}}}\right] - \mathrm{erf}\left[\frac{\sqrt{\pi}\alpha_k\left(-\beta_{i,k} - \beta_{i,i}\right)}{4\sqrt{1 + \frac{\pi\sigma_{\Phi}^2}{2}}}\right]\right) + \Lambda_1(k,i) \tag{3.92}$$

Next is to compute the cross terms in (3.79):

$$E\left[\left(b_i-\tanh\left(\frac{\alpha_i U_{\mathrm{MMSE}_i}}{2}\right)\right)\left(b_j-\tanh\left(\frac{\alpha_j U_{\mathrm{MMSE}_j}}{2}\right)\right)\right]$$
$$=E\left[\tanh\left(\frac{\alpha_i U_{\mathrm{MMSE}_i}}{2}\right)\tanh\left(\frac{\alpha_j U_{\mathrm{MMSE}_j}}{2}\right)\right]-E\left[b_i\tanh\left(\frac{\alpha_j U_{\mathrm{MMSE}_j}}{2}\right)\right]$$
$$-E\left[b_j\tanh\left(\frac{\alpha_i U_{\mathrm{MMSE}_i}}{2}\right)\right] \tag{3.93}$$

Computing $E\left[\tanh\left(U_{\mathrm{MMSE}_i}\right)\tanh\left(\frac{\alpha_j U_{\mathrm{MMSE}_j}}{2}\right)\right]$ first, and assuming the interference in the MMSE decision variables is Gaussian:

$$E\left[\tanh\left(\frac{\alpha_i U_{\mathrm{MMSE}_i}}{2}\right)\tanh\left(\frac{\alpha_j U_{\mathrm{MMSE}_j}}{2}\right)\right]$$
$$=E\left[\tanh\left(-\frac{\alpha_i}{2}\beta_{i,k}+\Phi_i\right)\tanh\left(-\frac{\alpha_j}{2}\beta_{j,k}+\Phi_j\right)\right] \tag{3.94}$$

where the variance of Φ_i and Φ_j and correlation coefficient ρ_{Φ_i,Φ_i} are:

$$\sigma_{\Phi_i}^2=\frac{\alpha_i^2}{4}\left(\sum_{\substack{l=1\\l\neq k}}^{K}\left|\beta_{i,l}\right|^2+\frac{\sigma^2}{2}\mathbf{w}_i\tilde{\mathbf{S}}\tilde{\mathbf{S}}^T\mathbf{w}_i^T\right) \tag{3.95}$$

$$\sigma_{\Phi_j}^2=\frac{\alpha_j^2}{4}\left(\sum_{\substack{l=1\\l\neq k}}^{K}\left|\beta_{j,l}\right|^2+\frac{\sigma^2}{2}\mathbf{w}_j\tilde{\mathbf{S}}\tilde{\mathbf{S}}^T\mathbf{w}_j^T\right) \tag{3.96}$$

$$\rho_{\Phi_i,\Phi_i}=\frac{\mathrm{Cov}\left(\Phi_i,\Phi_j\right)}{\sigma_{\Phi_i}\sigma_{\Phi_j}}$$
$$=\frac{\alpha_i\alpha_j}{4\sigma_{\Phi_i}\sigma_{\Phi_j}}\left(\sum_{\substack{l=1\\l\neq k}}^{K}\beta_{i,l}\beta_{j,l}+\frac{\sigma^2}{2}\mathbf{w}_i\tilde{\mathbf{S}}\tilde{\mathbf{S}}^T\mathbf{w}_j^T\right) \tag{3.97}$$

This integral form of $E\left[\tanh\left(-\frac{\alpha_i}{2}\beta_{i,k}+\Phi_i\right)\tanh\left(-\frac{\alpha_j}{2}\beta_{j,k}+\Phi_j\right)\right]$ is:

$$E\left[\tanh\left(-\frac{\alpha_i}{2}\beta_{i,k}+\Phi_i\right)\tanh\left(-\frac{\alpha_j}{2}\beta_{j,k}+\Phi_j\right)\right]$$
$$=\iint_{-\infty}^{\infty}\tanh\left(-\frac{\alpha_i}{2}\beta_{i,k}+\Phi_i\right)\tanh\left(-\frac{\alpha_j}{2}\beta_{j,k}+\Phi_j\right)f_{\Phi_i,\Phi_j}(\phi_i,\phi_j)d\phi_i d\phi_j \tag{3.98}$$

where the joint distribution $f_{\Phi_i,\Phi_j}(\phi_i,\phi_j)$ is:

$$f_{\Phi_i,\Phi_j}(\phi_i,\phi_j)=\frac{1}{2\pi\sigma_{\Phi_i}\sigma_{\Phi_j}\sqrt{1-\rho_{\Phi_i,\Phi_i}^2}}\exp\left(-\frac{1}{2\left(1-\rho_{\Phi_i,\Phi_i}^2\right)}\left[\frac{\phi_i^2}{2\sigma_{\Phi_i}^2}+\frac{\phi_j^2}{2\sigma_{\Phi_j}^2}-\frac{2\rho_{\Phi_i,\Phi_i}\phi_i\phi_j}{\sigma_{\Phi_i}\sigma_{\Phi_j}}\right]\right) \tag{3.99}$$

The double integral in (3.98) does not have a closed form solution and is computed numerically. It is given the notation:

$$E\left[\tanh\left(-\frac{\alpha_i}{2}\beta_{i,k}+\Phi_i\right)\tanh\left(-\frac{\alpha_j}{2}\beta_{j,k}+\Phi_j\right)\right]=\Lambda_2(k,i) \tag{3.100}$$

The 2 cross terms in (3.93) involving b_i and $\tanh\left(\frac{\alpha_j U_{\mathrm{MMSE}_j}}{2}\right)$ or b_j and $\tanh\left(\frac{\alpha_i U_{\mathrm{MMSE}_i}}{2}\right)$ can be derived from the same result from (3.73), except adjusting which βs are in the numerator.

$$E\left[b_i\tanh\left(\frac{\alpha_j U_{\mathrm{MMSE}_j}}{2}\right)\right]$$
$$=\frac{1}{2}\operatorname{erf}\left[\frac{\sqrt{\pi}\alpha_j\left(-\beta_{j,k}+\beta_{j,i}\right)}{4\sqrt{1+\frac{\pi\sigma_{\Phi_j}^2}{2}}}\right]-\frac{1}{2}\operatorname{erf}\left[\frac{\sqrt{\pi}\alpha_j\left(-\beta_{j,k}-\beta_{j,i}\right)}{4\sqrt{1+\frac{\pi\sigma_{\Phi_j}^2}{2}}}\right] \tag{3.101}$$

$$E\left[b_j \tanh\left(\frac{\alpha_i U_{\mathrm{MMSE}_i}}{2}\right)\right]$$
$$= \frac{1}{2}\operatorname{erf}\left[\frac{\sqrt{\pi}\alpha_i(-\beta_{i,k}+\beta_{i,j})}{4\sqrt{1+\frac{\pi\sigma_{\Phi_i}^2}{2}}}\right] - \frac{1}{2}\operatorname{erf}\left[\frac{\sqrt{\pi}\alpha_i(-\beta_{i,k}-\beta_{i,j})}{4\sqrt{1+\frac{\pi\sigma_{\Phi_i}^2}{2}}}\right] \tag{3.102}$$

3.5.4 Computing $E\left[I_{\mathrm{PIC}_k} N_{\mathrm{PIC}_k}\right]$:

Lastly, the cross correlation between the residual MAI and the noise are computed.

$$E\left[N_{\mathrm{PIC}_k} I_{\mathrm{PIC}_k}\right] = E\left\{N_{\mathrm{PIC}_k}\left[\sum_{\substack{i=1\\ i\neq k}}^{K} \lambda_{k,i}\left(b_i - \tanh\left(\frac{\alpha_i U_{\mathrm{MMSE}_i}}{2}\right)\right)\right]\right\} \tag{3.103}$$
$$= \sum_{\substack{i=1\\ i\neq k}}^{K} \alpha_{k,i}\left\{E\left[N_{\mathrm{PIC}_k} b_i\right] - E\left[N_{\mathrm{PIC}_k}\tanh\left(\frac{\alpha_i U_{\mathrm{MMSE}_i}}{2}\right)\right]\right\}$$

The noise and b_i are uncorrelated, and (3.103) simplifies to:

$$E\left[N_{\mathrm{PIC}_k} I_{\mathrm{PIC}_k}\right] = -\sum_{\substack{i=1\\ i\neq k}}^{K} \lambda_{k,i}\, E\left[N_{\mathrm{PIC}_k}\tanh\left(\frac{\alpha_i U_{\mathrm{MMSE}_i}}{2}\right)\right] \tag{3.104}$$

Taking the expectation:

$$E\left[N_{\mathrm{PIC}_k}\tanh\left(\frac{\alpha_i U_{\mathrm{MMSE}_i}}{2}\right)\right]$$
$$= E\left\{N_{\mathrm{PIC}_k}\tanh\left[\frac{\alpha_i}{2}\left(-\beta_{i,k} + \sum_{\substack{l=1\\ l\neq k}}^{K}\beta_{i,l} b_l + N_{\mathrm{MMSE}_i}\right)\right]\right\} \tag{3.105}$$

By grouping the interference and noise inside the hyperbolic tangent:

$$E\left[N_{\mathrm{PIC}_k}\tanh\left(\frac{\alpha_i U_{\mathrm{MMSE}_i}}{2}\right)\right] = E\left[N_{\mathrm{PIC}_k}\tanh\left(-\frac{\alpha_i}{2}\beta_{i,k} + \Phi\right)\right] \tag{3.106}$$

where the variance of Φ is:

$$\sigma_{\Phi}^{2} = \frac{\alpha_i}{2}\left(\sum_{\substack{l=1 \\ l\neq k}}^{K}\left|\beta_{i,l}\right|^2 + \frac{\sigma^2}{2}\mathbf{w}_i\tilde{\mathbf{S}}\tilde{\mathbf{S}}^T\mathbf{w}_i^T\right) \tag{3.107}$$

The noise N_{PIC_k}, and Φ are correlated, as Φ contains the noise term $N_{\mathrm{MMSE}_i} = \mathbf{w}_i\tilde{\mathbf{S}}\tilde{\mathbf{n}}$ and $N_{\mathrm{PIC}_k} = \tilde{\mathbf{S}}_k\tilde{\mathbf{n}}$. Their cross-correlation coefficient is:

$$\begin{aligned}\rho_{N_{\mathrm{PIC}_k},\Phi} &= \frac{\mathrm{Cov}\left(N_{\mathrm{PIC}_k},\Phi\right)}{\sigma_{N_{\mathrm{PIC}_k}}\sigma_{\Phi}} \\ &= \frac{\tilde{\mathbf{S}}_k\tilde{\mathbf{S}}^T\mathbf{w}_i^T\sigma}{\sqrt{2\sigma_{\Phi}^2}}\end{aligned} \tag{3.108}$$

The joint distribution between N_{PIC_k} and Φ is:

$$\begin{aligned}&f_{N_{\mathrm{PIC}_k},\Phi}\left(n_{\mathrm{PIC}_k},\phi\right) \\ &\quad= \frac{1}{2\pi\sigma_{N_{\mathrm{PIC}_k}}\sigma_{\Phi}\sqrt{1-\rho_{N_{\mathrm{PIC}_k},\Phi}{}^2}}\exp\left(-\frac{1}{2\left(1-\rho_{N_{\mathrm{PIC}_k},\Phi}{}^2\right)}\left[\frac{n_k^2}{2\sigma_{N_{\mathrm{PIC}_k}}^2}+\frac{\phi^2}{2\sigma_{\Phi}^2}\right.\right. \\ &\quad\left.\left.-\frac{2\rho_{N_{\mathrm{PIC}_k},\Phi}n_k\phi}{\sigma_{\Phi}\sigma_{N_{\mathrm{PIC}_k}}}\right]\right)\end{aligned} \tag{3.109}$$

Therefore, $E\left[N_{\mathrm{PIC}_k}\tanh\left(-\frac{\alpha_i}{2}\beta_{i,k}+\Phi\right)\right]$ can be written in integral notation as:

$$\begin{aligned}&E\left[N_{\mathrm{PIC}_k}\tanh\left(\frac{\alpha_i U_{\mathrm{MMSE}_i}}{2}\right)\right] \\ &\quad= \int_{-\infty}^{\infty}\!\!\int n_{\mathrm{PIC}_k}\tanh\left(-\frac{\alpha_k}{2}\beta_{i,k}+\phi\right)f_{N_{\mathrm{PIC}_k},\Phi}\left(n_{\mathrm{PIC}_k},\phi\right)dn_{\mathrm{PIC}_k}d\phi\end{aligned} \tag{3.110}$$

Again, this integral does not have a closed form solution and will be computed numerically. It is represented by:

$$E\left[N_{\mathrm{PIC}_k}\tanh\left(\frac{\alpha_i U_{\mathrm{MMSE}_i}}{2}\right)\right] = \Lambda_3(k,i) \tag{3.111}$$

3.6 Complexity Analysis

Table 3.1 highlights the computational complexity of the proposed PIC-MMSE detector as well as the MPA detector. The complexity analysis for the MPA detector was taken from the work done in [44]. In addition, the complexity analysis for the PIC-MMSE and the MPA detectors are done in the AWGN channel and with equal received power from each user. It is assumed in the computational analysis that each complex multiplication requires 4 real multiplications and 2 real additions, while a complex addition requires 2 real additions.

The complexity of the PIC-MMSE detector can be broken down into each stage of processing:

1. The first stage involves the received chips being despread to the initial decision variables in (3.2). This despreading is a matrix multiplication between the spreading codes and the received signal. The spreading codes used to despread only contain d_v nonzero chips, and thus each dot product in the matrix multiplication will only contain d_v terms. This results in Kd_v complex multiplications and $K(d_v - 1)$ complex additions, or $4Kd_v$ real multiplications and $2Kd_v + 2K(d_v - 1)$ real additions.
2. The second stage is the splitting of the real and complex parts, which is does not use any computations.
3. The third stage is applying the MMSE filter. Note, the PIC-MMSE detector does not need to compute $\mathbf{W}_{\mathrm{MMSE}}$ every signaling interval, as it can be computed beforehand with prior knowledge of the spreading sequences of each user and the SNR. The MMSE filter is simply a matrix multiplication to the split decision variables. The size of $\mathbf{W}_{\mathrm{MMSE}}$ is $K \times 2K$ and $\tilde{\mathbf{U}}$ is $2K \times 1$. This results in $2K^2$ real multiplications and $K(2K - 1)$ real additions.
4. The fourth stage is computing the probabilities of the MMSE decision variables as is done in (3.36). The quantity α_k in the exponential terms again can be precomputed for the same reasons as the MMSE filter in stage 3. There is a multiplication between α_k and U_{MMSE_k}, and the division of exponentials is counted as another multiplication. There is a single addition that occurs in the denominator. Thus, the total number of real multiplications is equal to $2K$, the total number of real additions is K and the number of exponentials is also K.

5. The fifth stage is the conversion of probabilities to soft bits as is done in (3.38). This requires K real multiplications and K real additions.
6. The sixth and final stage is the PIC detector as is done in (3.40). For each user, the sum contains $K-1$ complex terms, each with one complex multiplication. The sum is then subtracted from the initial decision variable, which is counted as a single complex addition. In total, there are $4K(K-1)$ real multiplications, and $2K(K-1)+2K^2$ real additions.

Table 3.1: Complexity Analysis between the proposed PIC-MMSE and MPA detectors

	PIC-MMSE	MPA
Real Multiplications	$6K^2+4Kd_v-K$	$t_{max}Nd_fM^{d_f}(2d_f+1)$ $+t_{max}Kd_vM(d_v-2)$
Real Additions	$6K^2+4Kd_v-4K$	$t_{max}Nd_f\left[(d_f+1)M^{d_f}-M\right]$
Exponentials	K	$t_{max}Nd_fM^{d_f}$

The total number of multiplications, additions and exponentials for both MPA and the proposed PIC-MMSE detectors are listed in Table 3.1. As can be seen, the complexity of the proposed algorithm is $\mathcal{O}(K^2)$, compared to the complexity of $\mathcal{O}\left(M^{d_f}\right)$ with the MPA detector. The PIC-MMSE detector limits its complexity to the fact that it only performs linear filtering on the received signal. It does not require any search computations like MPA detection, which brings exponential complexity.

It may appear that as K increases, the computational complexity of the PIC-MMSE detector becomes greater than that of the MPA detector. But, as K increases, the number of required iterations also increases, as well as d_f which in turn, increases the number of computations required per iteration. Even if d_f is kept relatively low, such that the number of computations per iteration are relatively low, more iterations will have to be performed to share the inferences of each user's symbol with every function and variable node. The proposed PIC-MMSE detector does not have this trade-off between the number of iterations and d_f.

When dealing with the frequency-nonselective fading channel, the analysis gets a little more complicated due to the updated correlation matrix $\widetilde{\mathbf{R}}'$ which contains the complex channel gains. With the AWGN channel, the pseudoinverse required for the MMSE filter was needed to be computed once, due to no changes in the channel conditions. In the frequency-nonselective fading channel, this inverse will need to be recomputed as the channel gains change, which depends how often the channel is changing. One alternative to this is to use an adaptive algorithm to obtain the pseudoinverse. If the channel is not changing drastically, a method such as recursive least squares, or least means squares can be used to update the inverse. In addition, the MPA will also require some additional processing to adjust for the changing channel conditions.

3.7 Simulation Results

In this section, the performance of the PIC-MMSE detector is presented. BER plots as well as tables indicating the number of computations required are included. The assumptions made for the simulations are the same assumptions in Chapter 2. In addition, both the 6x9 and 12x16 spreading matrices given in (2.23) and (2.24) respectively are used.

Figure 3.5 and Figure 3.6 show the BER performance of the MPA detector using 3 iterations, and other conventional detectors, including the proposed PIC-MMSE detector. The conventional detectors include the single user detector, MMSE, ZF and PIC detectors. The PIC detector uses the decision variables after the single user detector. The MPA and PIC-MMSE detectors perform best, as expected. The other conventional detectors are not enough to handle the overloading that is present in these systems.

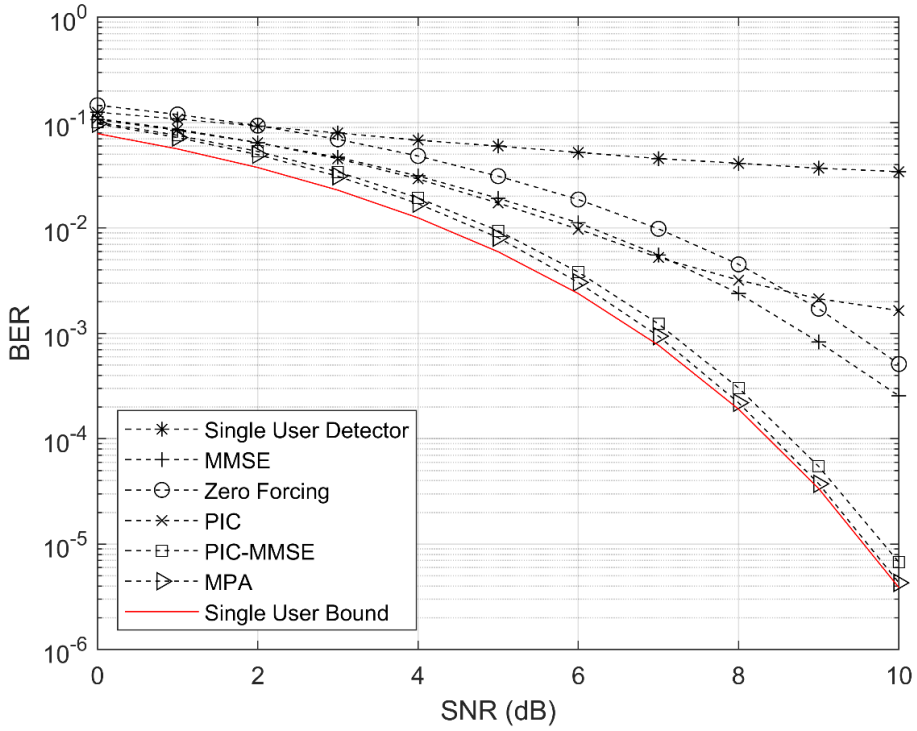

Figure 3.5: BER plot of the various conventional detection schemes for a system load of 9 users and 6 chips

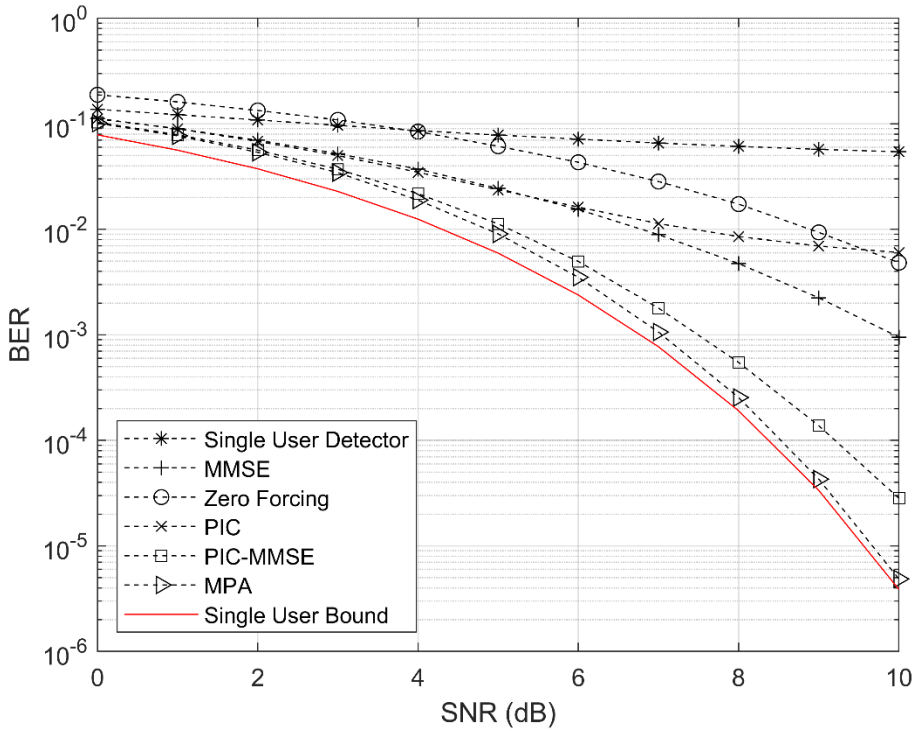

Figure 3.6: BER plot of the various conventional detection schemes for a system load of 16 users and 12 chips

Figure 3.7 and Figure 3.8 show the PIC-MMSE detector BER performance with various decision functions after the MMSE detector. This includes the linear, hard, and hyperbolic tangent decision devices that were presented in Figure 3.1. The nonlinear hyperbolic tangent operator proposed outperforms both the linear and hard decision devices which are used in typical PIC detectors. But as the SNR increases, the gap between the hard decision function and the hyperbolic tangent function, especially for the 9 user 6 chip system, decreases. This can be attributed to the hyperbolic tangent function approaching the hard detector as the SNR increases, due to the scaling factor α_k also increasing, as can be seen in Figure 3.3.

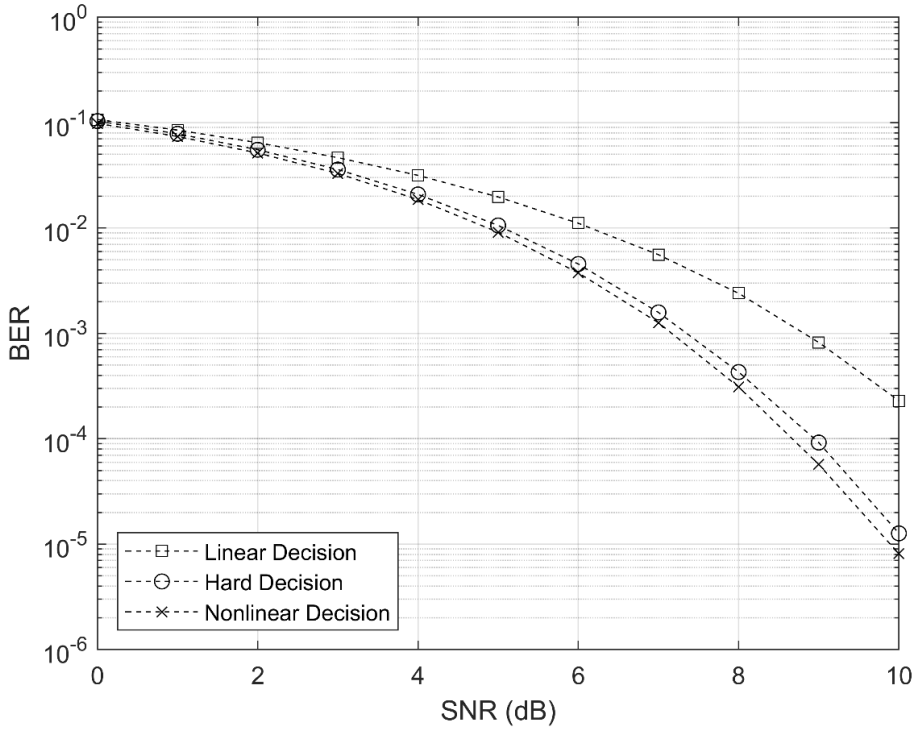

Figure 3.7: BER performance for different decision functions after the MMSE detector with the proposed PIC-MMSE detector for the 6 chips 9 user system

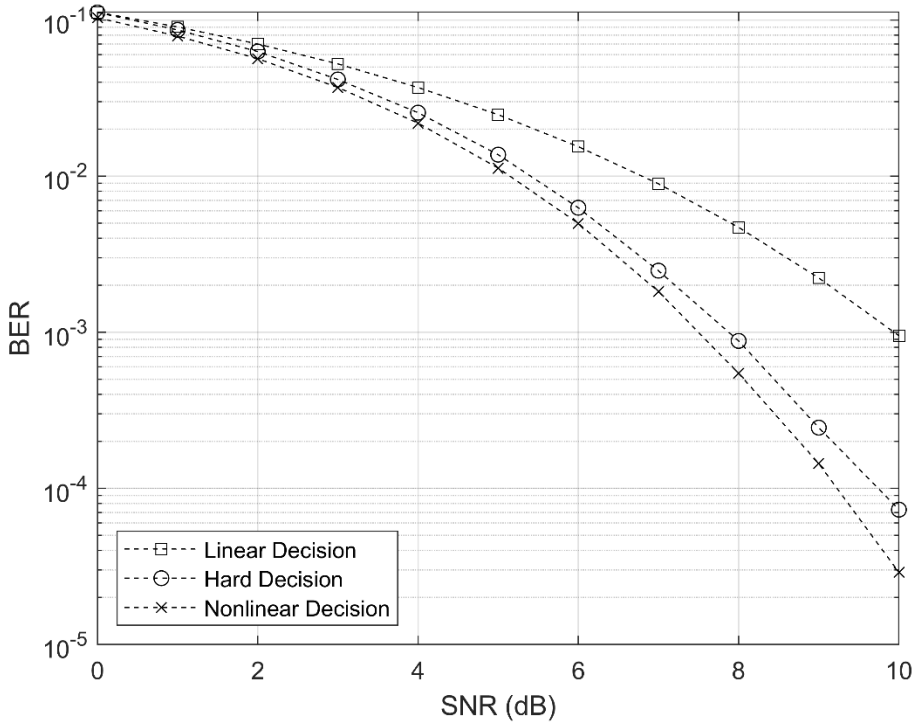

Figure 3.8: BER performance for different decision functions after the MMSE detector with the proposed PIC-MMSE detector for the 12 chips 16 user system

Figure 3.9 and Figure 3.10 show the approximate BER derived in the previous section with the simulation results for the 6 chip 9 user and 12 chip 16 user systems, respectively. The approximation is not perfect, as can be seen by the overshooting in the low SNR region. The various Gaussian assumptions made during the derivation are the main cause of this overshoot with both systems. But, the approximation gets tighter as the SNR increases. This is because of the multiple access interference decreasing, and the approximation is having less effect on the BER performance.

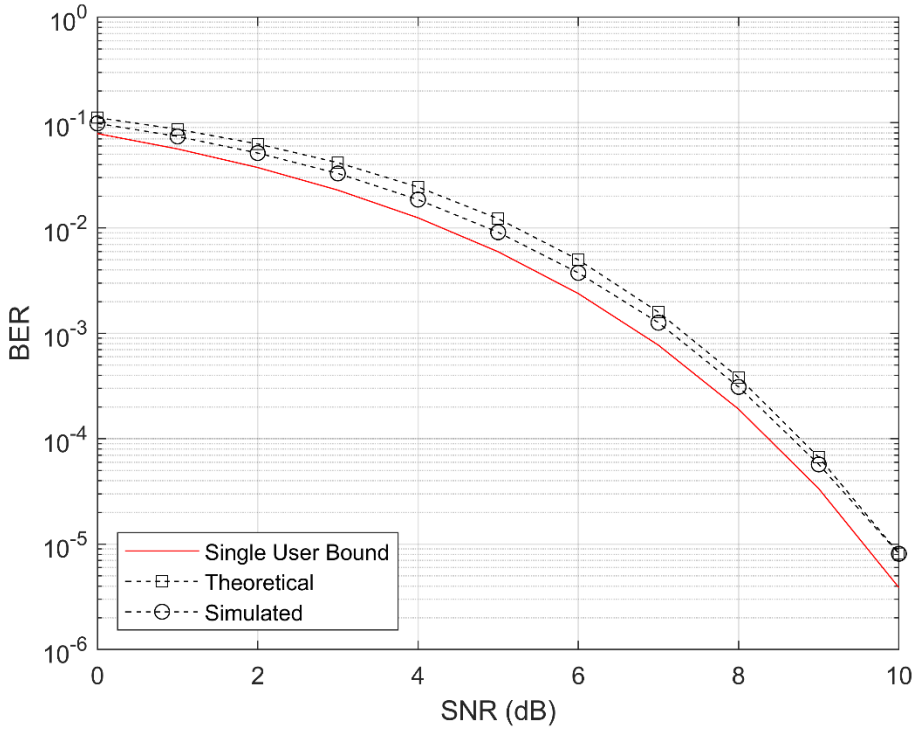

Figure 3.9: Approximate BER performance for the 6 chips 9 user system

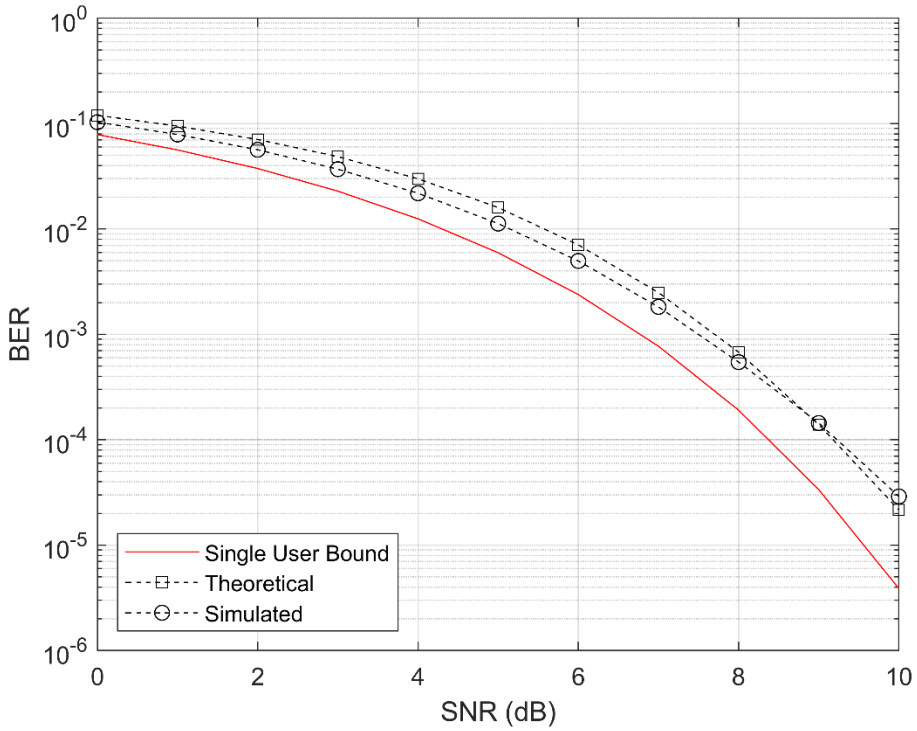

Figure 3.10: Approximate BER performance for the 12 chips 16 user system

Figure 3.11 and Figure 3.12 compare the number of computations used by both detectors. Table 3.2 and Table 3.3 give the complexity analysis as well as required SNR to achieve a BER of 10^{-3}. The number of multiplications, additions and exponentials are computed by substituting the system parameters into the expressions given in Table 3.1. The reduction in computations is drastically reduced compared to the MPA detector. The difference in computational complexity between both LDS systems shows how heavily the MPA detector relies on the number of interfering users per chip, d_f. The 9 user 6 chip system has $d_f = 3$ and the 16 user 12 chip system has $d_f = 4$. Due to the MPA detector having complexity that is exponential to d_f, even slight increases in d_f cause the number of computations required increase quickly, as can be seen in these simulations.

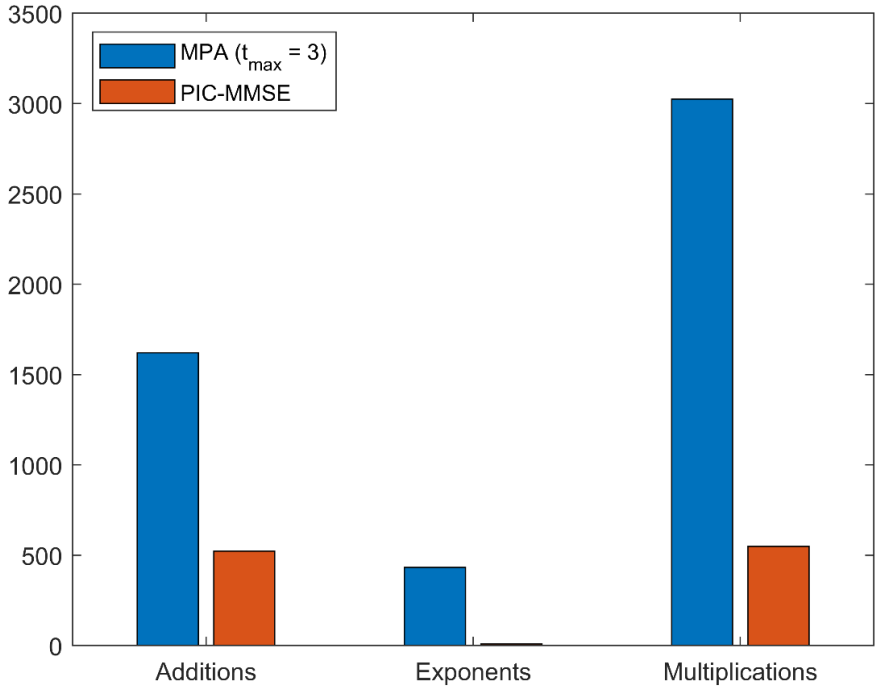

Figure 3.11: Computational complexity of the PIC-MMSE and MPA detectors for the 9 users 6 chips system.

Table 3.2: Required SNR to achieve BER of 10^{-3} and the number of computations required for the 6 chip 9 user system

	PIC-MMSE	MPA (3 iterations)	Difference
SNR	7.25 dB	6.97 dB	-0.28 dB
Real Multiplications	549	3024	-81.84%
Real Additions	522	1620	-67.87%
Exponentials	9	432	-97.92%

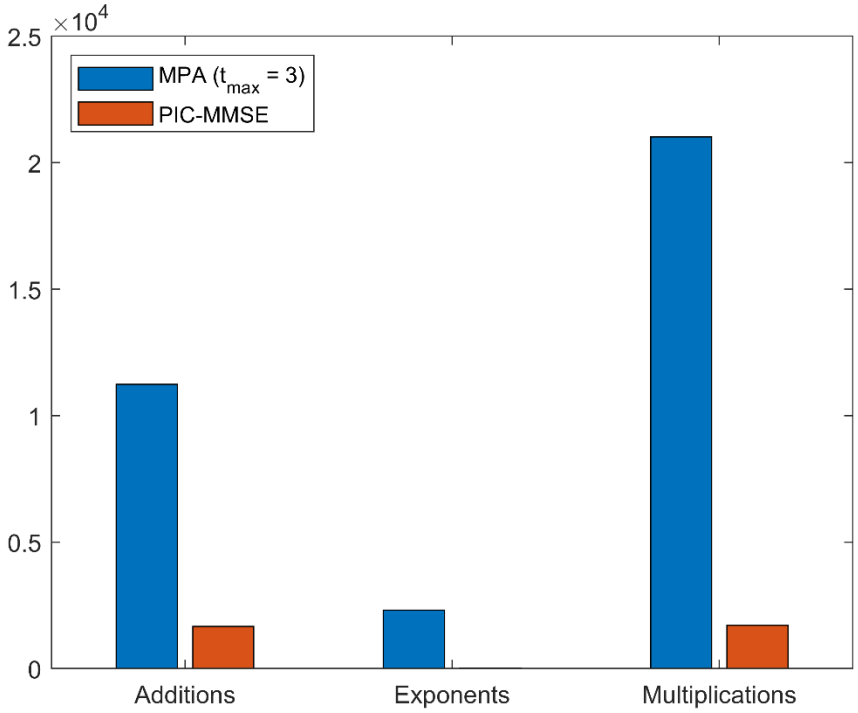

Figure 3.12: Computational complexity of the PIC-MMSE and MPA detectors for the 16 user 12 chips system

Table 3.3: Required SNR to achieve BER of 10^{-3} and the number of computations required for the 12 chip 16 user system

	PIC-MMSE	MPA (3 iterations)	Difference
SNR (dB)	7.63	7.07 dB	-0.56 dB
Real Multiplications	1712	21024	-91.86%
Real Additions	1664	11232	-85.19%
Exponentials	16	2304	-99.31%

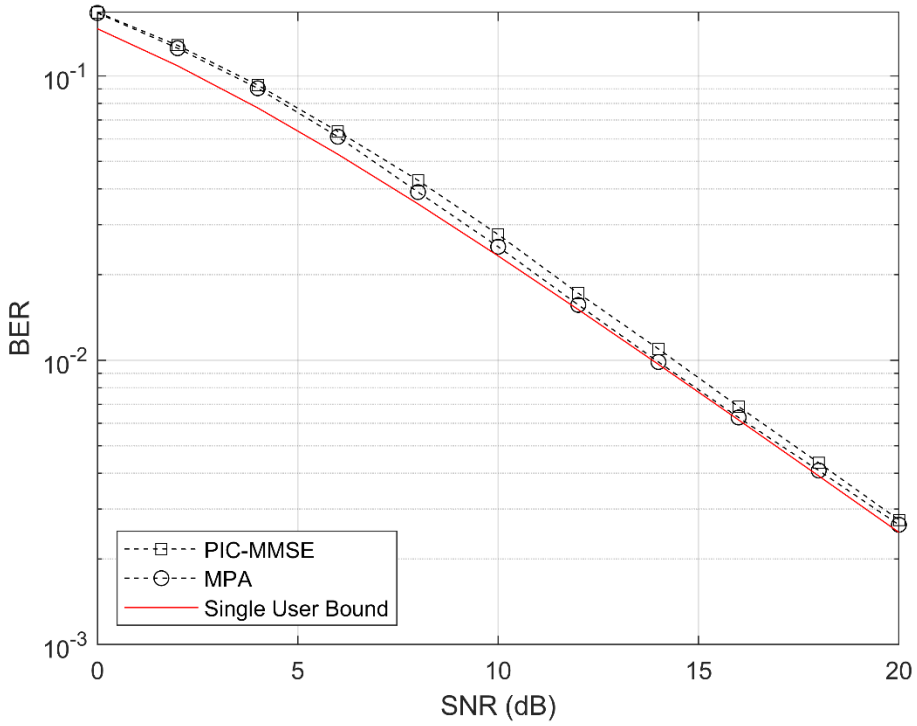

Figure 3.13: BER plot of the PIC-MMSE and MPA detectors for a system load of 9 users and 6 chips

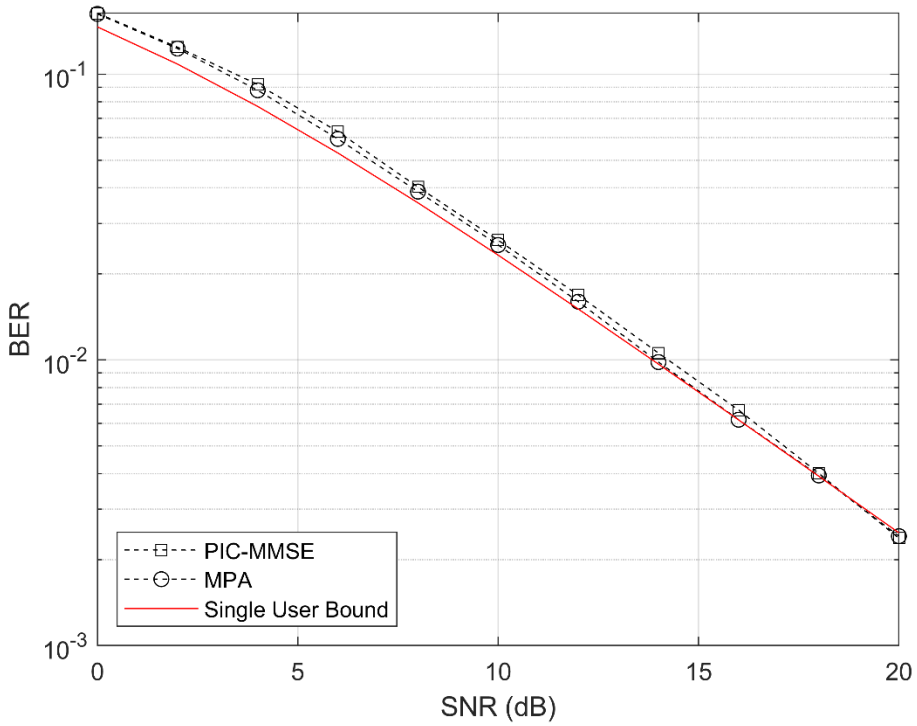

Figure 3.14: BER plot of the PIC-MMSE and MPA detectors for a system load of 16 users and 12 chips

Figure 3.13 and Figure 3.14 show the BER performance of both the PIC-MMSE and MPA detectors in the frequency-nonselective fading channel. As can be seen, both detectors perform well in the frequency-nonselective fading channel and approach the single user bound. The independent channel gains create additional diversity, and this helps separate the symbols with the PIC detector.

3.8 Summary

This chapter presented the proposed PIC-MMSE detector as well as analyzed other conventional detectors that are typically used in CDMA systems and applied them to LDS systems. An approximate expression for the BER of the PIC-MMSE detector was also presented. The approximate BER expression was compared to simulation results, and was shown to be valid, especially at high SNR. In addition, the complexity analysis of the proposed PIC-MMSE detector was presented and compared to the complexity of the MPA detector. It was shown that the proposed detector has complexity of $O(K^2)$ compared to $O\left(M^{d_f}\right)$ of the MPA detector.

Simulation results of the BER performance were presented between conventional detection techniques, the proposed PIC-MMSE and MPA detectors for various system loads and sizes. It was shown the PIC-MMSE detector had massive reductions in computations compared to the MPA detector, with losses of about a fraction of a dB.

Chapter 4
Precoding Scheme for LDS Systems in Frequency-Selective Channels

4.1 Introduction

Most of the research on LDS or SCMA systems has been done under the simple AWGN channel, or the frequency-nonselective fading channel. This is important especially for channels using mmWaves. When research is extended to the frequency selective channel, the spreading sequences are implemented on orthogonal subcarriers, like OFDM or multicarrier CDMA (MC-CDMA) [45]. OFDM or MC-CDMA systems can handle the frequency-selectivity due to their subcarriers having bandwidth that is smaller than the coherence bandwidth [46]. This allows for each subcarrier to experience flat fading, which makes detection easier. The downside to using OFDM over CDMA is OFDM has a relatively high peak to average power ratio (PAPR) which may cause saturation in the power amplifiers [47]. Unfortunately, LDS-CDMA is unable, without the help of external processing, to overcome the multipath channel. Due to the requirement of synchronous chip level processing, multipath channels will spread the chips across each other, destroying the low-density structure. Standard CDMA can overcome multipath channels with the use of a RAKE receiver, which uses diversity combining to sum the delayed components produced from the multipath channel coherently [48]. Other equalization methods that were applied to standard CDMA that can be extended to LDS systems include FDE [49], and blind equalization methods [50].

In this chapter, a precoding scheme for LDS systems that is designed to overcome the multipath channel is proposed. This precoding applies the inverse channel frequency response to the transmitted signal before transmission, such that the multipath degradation is reduced. The precoding scheme can be applied to mmWave channels as well. Simulation results show this precoding scheme results in better performance for both the MPA and the proposed PIC-

MMSE detector in the multipath channel. Simulations where channel errors are present are also included.

4.2 System Model

The system model for LDS systems in the presence of frequency-selective fading is introduced in this section. The system model assumes a CDMA system with K users and the spreading sequences are complex with a length of N chips. The discrete time system model for the system is shown in (4.1), where $\mathbf{r} = [r_1, r_2, \dots r_N]^T \in \mathbb{C}^N$ is the received signal, $\mathbf{s}_k = \left[\mathrm{s}_{1,k}, \mathrm{s}_{2,k} \dots \mathrm{s}_{N,k}\right]^T \in \mathbb{C}^N$ is user k's spreading code, $\mathrm{x}_k \in \mathcal{X}$ is the symbol user k is transmitting and $\mathbf{n} = [n_1, n_2 \dots n_N]^T \in \mathbb{C}^N$ is the complex additive white Gaussian noise with covariance matrix $\sigma^2\mathbf{I}$.

The multipath channel is modelled by a tap delay line finite impulse response (FIR) filter of length L chips. The signal generated from each user is convolved through the multipath channel, where $\mathbf{h}_k = \frac{1}{\sqrt{L}}\left[h_{1,k}, h_{2,k}, \dots h_{L,k}\right]^T$ is the impulse response of the multipath channel for user k. Each element in $\mathbf{h}_k$ is a Gaussian random variable with zero mean and unit variance. The $\frac{1}{\sqrt{L}}$ factor is added to keep the energy the channel applies to the transmitted signal on average at unity. The channel impulse responses between users are assumed to be independent from one another. The system model is:

$$\mathbf{r} = \sum_{k=1}^{K} \mathbf{h}_k * (\mathbf{s}_k x_k) + \mathbf{n} \tag{4.1}$$

where $*$ is the convolution operator.

4.3 Precoding Scheme

The block diagram for the proposed precoding scheme is given in Figure 4.1. Initially, each user spreads N_{syms} symbols with their spreading code, which results in NN_{syms} chips. The NN_{syms} chips are passed to a serial to parallel converter and a Discrete Fourier Transform (DFT) is applied. After the DFT, the inverse channel frequency response is applied, and this frequency response is normalized such that the power transmitted from each user is constant

and does not fluctuate. Fluctuating transmit power is undesirable as it reduces amplifier efficiency. This is a common problem with OFDM, and applying a normalized channel frequency response keeps the transmit power constant. Next, an Inverse Discrete Fourier Transform (IDFT) is applied to get the sequence back to the time domain. A cyclic prefix (CP) is added such that the convolution between the transmitted signal and the channel impulse response appears as circular convolution after the removal of the cyclic prefix, similar to OFDM transmission.

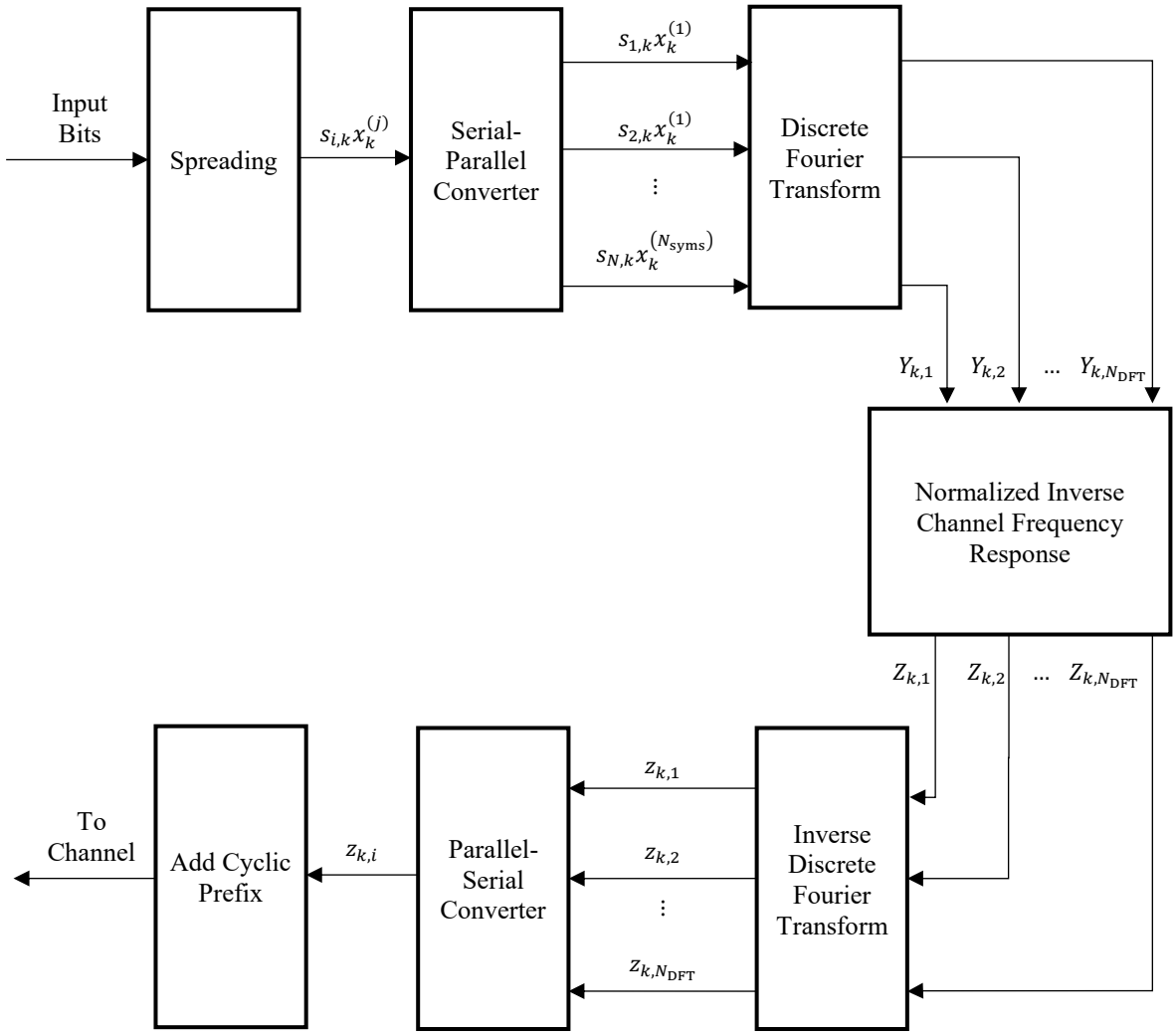

Figure 4.1: Block diagram of the proposed precoding scheme for LDS systems in multipath channels

The precoding for user k begins with spreading N_{syms} bits and running them through a serial to parallel converter. This signal is represented by $\mathbf{y}_k$ and is:

$$\mathbf{y}_k = \left[s_{1,k}x_k^{(1)}, s_{2,k}x_k^{(1)}, \ldots\ s_{N,k}x_k^{(1)}, s_{1,k}x_k^{(2)}, s_{2,k}x_k^{(2)}, \ldots s_{N,k}x_k^{(N_{\text{syms}})}\right]^T \tag{4.2}$$

where $x_k^{(i)}$ represents the ith symbol for user k. Next, a DFT is applied to $\mathbf{y}_k$ where $\text{DFT}_{N_{\text{DFT}}}\{\cdot\}$ is the DFT operation with length $N_{\text{DFT}} = NN_{\text{syms}}$. The result after taking the DFT of the spread bits is:

$$\begin{aligned} \mathbf{Y}_k &= \text{DFT}_{N_{\text{DFT}}}\{\mathbf{y}_k\} \\ &= \mathbf{F}^{(N_{\text{DFT}})}\mathbf{y}_k \end{aligned} \tag{4.3}$$

where $\mathbf{Y}_k$ is of size NN_{syms} and is the frequency domain signal of the spread symbols. $\mathbf{F}_{N_{\text{DFT}}}$ is the DFT matrix which is defined as:

$$\mathbf{F}^{(N_{\text{DFT}})} = \frac{1}{\sqrt{N_{\text{DFT}}}}\begin{bmatrix} 1 & 1 & 1 & \cdots & 1 \\ 1 & \omega & \omega^2 & \cdots & \omega^{(N_{\text{DFT}}-1)} \\ 1 & \omega^2 & \omega^4 & \cdots & \omega^{2(N_{\text{DFT}}-1)} \\ \vdots & \vdots & \vdots & \ddots & \vdots \\ 1 & \omega^{(N_{\text{DFT}}-1)} & \omega^{2(N_{\text{DFT}}-1)} & \cdots & \omega^{(N_{\text{DFT}}-1)(N_{\text{DFT}}-1)} \end{bmatrix} \tag{4.4}$$

where $\omega = \exp\left(-\frac{j2\pi}{N_{DFT}}\right)$. The ith frequency bin of $\mathbf{Y}_k$ is row i in $\mathbf{F}_{N_{\text{DFT}}}$ multiplied by the time domain signal $\mathbf{y}_k$.

$$Y_{k,i} = \mathbf{F}_i^{(N_{\text{DFT}})}\mathbf{y}_k \tag{4.5}$$

At frequency bin i, the normalized channel impulse response frequency bin is multiplied to $Y_{k,i}$

$$Z_{k,i} = \widetilde{H}_{\text{inv}_{k,i}} Y_{k,i} \tag{4.6}$$

where the normalized channel frequency response at bin i is:

$$\begin{aligned} \widetilde{H}_{\text{inv}_{k,i}} &= \frac{H_{\text{inv}_{k,i}}}{\sqrt{E_{\mathbf{H}_{\text{inv}_k}}}} \\ &= \frac{1}{\sqrt{E_{\mathbf{H}_{\text{inv}_k}} H_{k,i}}} \end{aligned} \tag{4.7}$$

where $H_{k,i}$ is the ith frequency bin of $\mathbf{H}_k$ which is the DFT of the channel impulse response:

$$\mathbf{H}_k = \mathrm{DFT}_{N_{\mathrm{DFT}}}\{\mathbf{h}_k\} \tag{4.8}$$

and $E_{\mathbf{H}_{\mathrm{inv}_k}}$ is the energy of the inverse channel frequency response and is given by:

$$E_{\mathbf{H}_{\mathrm{inv}_k}} = \frac{1}{N_{\mathrm{DFT}}} \sum_{i=1}^{N_{\mathrm{DFT}}} \frac{1}{\left|H_{k,i}\right|^2} \tag{4.9}$$

The vector notation of (4.6) can be represented by:

$$\mathbf{Z}_k = \widetilde{\mathbf{H}}_{\mathrm{inv}_k} \odot \mathbf{Y}_k \tag{4.10}$$

where $\odot$ represents element-wise multiplication. After applying the inverse channel response, the IDFT is applied to get the signal back to the time domain:

$$\begin{aligned} \mathbf{z}_k &= \mathrm{IDFT}\{\mathbf{Z}_k\} \\ &= \mathbf{F}^{(N_{\mathrm{DFT}})^{-1}}\mathbf{Z}_k \end{aligned} \tag{4.11}$$

where $\mathrm{IDFT}\{\cdot\}$ is the inverse DFT operation, $\boldsymbol{z}_k$ is the precoded signal in the time domain, and $\mathbf{F}^{(N_{\mathrm{DFT}})^{-1}}$ is the inverse DFT matrix which is also the Hermitian transpose of $\mathbf{F}^{(N_{\mathrm{DFT}})}$:

$$\mathbf{F}^{(N_{\mathrm{DFT}})^{-1}} = \mathbf{F}^{(N_{\mathrm{DFT}})^H} \tag{4.12}$$

The last step of the precoding procedure is to add a cyclic prefix like in OFDM and SC-FDMA systems. This is to ensure that the output of the convolution with the channel impulse response results in circular convolution. The transmitted symbol for user k becomes:

$$\tilde{\mathbf{z}}_k = \left[z_{k,N_{\mathrm{DFT}}-N_{\mathrm{CP}}+1}, z_{k,N_{\mathrm{DFT}}-N_{\mathrm{CP}}}, \ldots\ z_{k,N_{\mathrm{DFT}}}, z_{k,1}, z_{k,2}, \ldots\ z_{k,N_{\mathrm{DFT}}}\right]^T \tag{4.13}$$

where N_{CP} is the length of the cyclic prefix, which must be larger than $L-1$. The following transmission precoding and reception after the channel can now be represented by circular convolution:

$$\mathbf{r} = \sum^{K} \mathbf{h}_k * \tilde{\mathbf{z}}_k \tag{4.14}$$

$$= \sum_{k=1}^{K} \mathbf{h}_k \circledast \mathbf{z}_k$$

where $\circledast$ is the circular convolution operator. Circular convolution results in multiplication in the discrete frequency domain., and (4.14) can be rewritten as:

$$\begin{aligned}
\mathbf{r} &= \sum_{k=1}^{K} \mathbf{h}_k \circledast \mathbf{z}_k \\
&= \sum_{k=1}^{K} \mathbf{F}^{(N_{\mathrm{DFT}})^{-1}} (\mathbf{H}_k \odot \mathbf{Z}_k) \\
&= \sum_{k=1}^{K} \mathbf{F}^{(N_{\mathrm{DFT}})^{-1}} \left(\mathbf{H}_k \odot \widetilde{\mathbf{H}}_{\mathrm{inv}_k} \odot \mathbf{Y}_k\right) \\
&= \sum_{k=1}^{K} \mathbf{F}^{(N_{\mathrm{DFT}})^{-1}} \left[\left(\mathbf{H}_k \odot \widetilde{\mathbf{H}}_{\mathrm{inv}_k}\right) \odot \left(\mathbf{F}_i^{(N_{\mathrm{DFT}})} \mathbf{y}_k\right)\right] \\
&= \sum_{k=1}^{K} \frac{1}{\sqrt{E_{\mathbf{H}_{\mathrm{inv}_k}}}} \mathbf{y}_k \\
&= \sum_{k=1}^{K} \gamma_k \mathbf{y}_k
\end{aligned} \tag{4.15}$$

The transmitter precoding has transformed the multipath channel into a single path channel. The equivalent single path channel for user k has a gain $\gamma_k = \frac{1}{\sqrt{E_{\mathbf{H}_{\mathrm{inv}_k}}}}$ which is a random variable that is dependent on the tapped delay line channel, $\mathbf{h}_k$. The exact distribution of γ_k is very difficult to determine theoretically due to the various operations performed. For this thesis, $\mathbf{h}_k$ is a tapped delay line where each tap is a complex Gaussian random variable, but other channel models could be used, such as each channel tap having exponentially decaying amplitudes.

$\mathbf{y}_k$ is a block of N_{syms} of spread symbols for user k. The complete received signal for just one symbol in this block is:

$$\mathbf{r} = \sum_{k=1}^{K} \gamma_k \mathbf{s}_k \mathrm{x}_k + \mathbf{n} \tag{4.16}$$

$$\mathbf{r} = \mathbf{S\Gamma x} + \mathbf{n} \tag{4.17}$$

where $\mathbf{\Gamma}$ is a diagonal matrix with elements:

$$\mathbf{\Gamma} = \begin{bmatrix} \gamma_1 & 0 & \cdots & 0 \\ 0 & \gamma_2 & 0 & \vdots \\ \vdots & 0 & \ddots & 0 \\ 0 & \cdots & 0 & \gamma_K \end{bmatrix} \tag{4.18}$$

To view the properties of γ_k, simulations with 100,000 random generations of a channel vector with length L taps and a single Rayleigh random variable are done. Histograms of γ_k with varying L, and a Rayleigh random variable as a refeence are plotted to see their approximate distributions. These results are shown in Figure 4.2, Figure 4.3 and Figure 4.4. As the channel length increases, the mean and variance of the distribution of γ_k both decreases. This is due to the precoding essentially averaging the channel taps. This causes the randomness of γ_k to decrease. The downfall of this is that γ_k has a mean that is approximately 0.5.

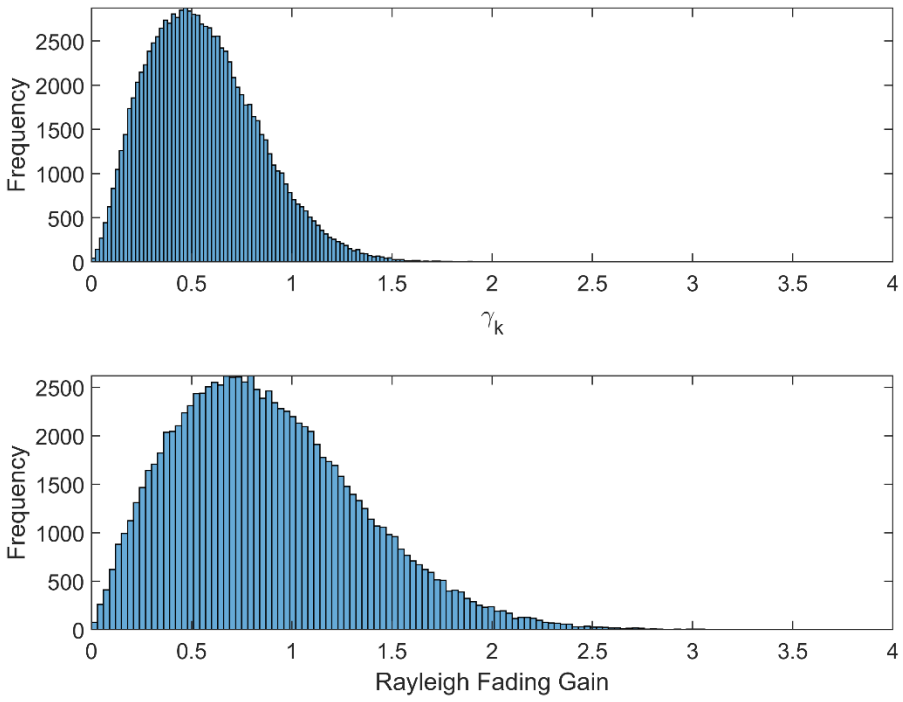

Figure 4.2: Histogram of γ_k and a Rayleigh random variable with $L = 3$ channel taps

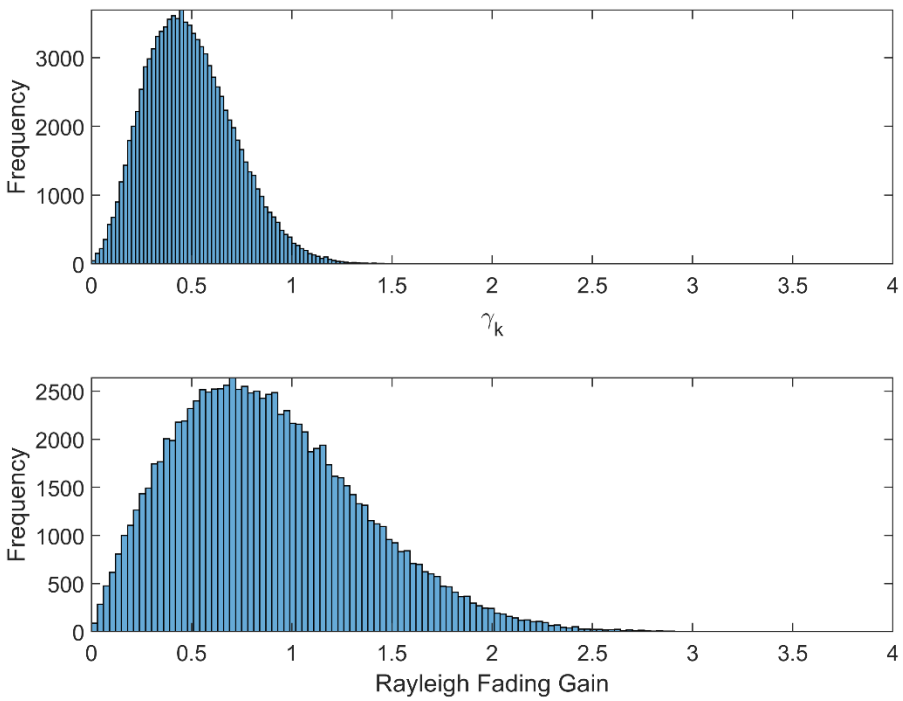

Figure 4.3: Histogram of γ_k and a Rayleigh random variable with $L = 5$ channel taps

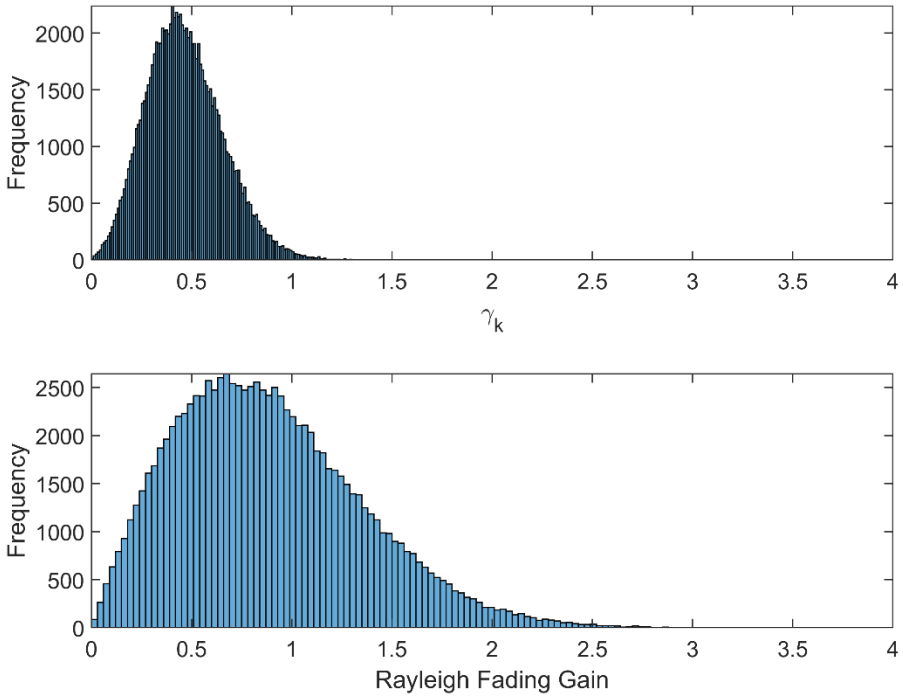

Figure 4.4: Histogram of γ_k and a Rayleigh random variable with $L = 7$ channel taps

4.3.1 The Example of a Single Tap Multipath Channel (Frequency-Nonselective Fading)

When the channel is frequency-nonselective, the tapped delay line channel model simplifies to a single tap complex Gaussian random variable. The system model is now:

$$\begin{aligned}\mathbf{h}_k &= h_k \\ &= |h_k| \exp(j\theta_k)\end{aligned} \tag{4.19}$$

where $|h_k|$ is the magnitude of h_k which has a Rayleigh distribution and θ_k is the phase of the single tap channel and has a uniform distribution between $[0,2\pi]$. Assuming $N_{\text{syms}} = 1$, the received signal becomes:

$$\begin{aligned}\mathbf{r} &= \sum_{k=1}^{K} \mathbf{h}_k * (\mathbf{s}_k \mathrm{x}_k) + \mathbf{n} \\ &= \sum_{k=1}^{K} \mathbf{s}_k h_k \mathrm{x}_k + \mathbf{n}\end{aligned} \tag{4.20}$$

When the precoding is applied to this type of channel, the discrete frequency spectrum will be flat with a gain that is Rayleigh distributed. The DFT of the channel response is:

$$\begin{aligned}\mathbf{H}_k &= \mathrm{DFT}_{N_{\mathrm{DFT}}}\{\mathbf{h}_k\} \\ &= h_k \mathbf{1}_{N_{\mathrm{DFT}}}\end{aligned} \tag{4.21}$$

where $\mathbf{1}_{N_{\mathrm{DFT}}}$ is a vector of all 1's. The inverse of the channel at bin i is:

$$H_{\mathrm{inv}_{k,i}} = \frac{1}{h_k} \tag{4.22}$$

The energy of the inverse channel frequency response:

$$\begin{aligned}E_{\mathbf{H}_{\mathrm{inv}_k}} &= \frac{1}{N_{\mathrm{DFT}}} \sum_{i=1}^{N_{\mathrm{DFT}}} \frac{1}{\left|H_{k,i}\right|^2} \\ &= \frac{1}{|h_k|^2}\end{aligned} \tag{4.23}$$

This leads to the normalized channel response at bin i to be:

$$\begin{aligned}\widetilde{H}_{\mathrm{inv}_{k,i}} &= \frac{H_{\mathrm{inv}_{k,i}}}{\sqrt{E_{\mathbf{H}_{\mathrm{inv}_k}}}} \\ &= \frac{|h_k|}{h_k} \\ &= \exp(-j\theta_k)\end{aligned} \tag{4.24}$$

What this result shows is that with a single tap channel, the precoder will just apply the phase correction to the spread bits. After applying this phase correction, the received signal will now be a sum of each user's spread data with a varying real gain. As will be shown in the simulation results, this improves performance by giving some diversity between the users. More on the effects of the precoding scheme in the following section.

4.4 The Effects of Precoding on Multiuser Detectors

After each user transmits through the channel with precoding, the multipath fading is eliminated. The received signal is a sum of each user's signal, except each user is now attenuated. This will affect the performance of the various LDS detectors. The MPA and PIC-MMSE detectors are affected in a similar manner to how the frequency-nonselective fading channel affected the detectors. How the precoding affects these detectors is presented in this section.

4.4.1 MPA Detector

The alterations required for the MPA detector are minimal, and only change the metrics computed at the function nodes. The metrics in (2.18) are changed to include the effective channel gains:

$$M_n(\mathbf{x}) = \exp\left(-\frac{1}{2\sigma^2}\left|y_n - \sum_{k\in\xi_n} s_{n,k}A_k\gamma_k x_k\right|^2\right) \tag{4.25}$$

The messages passed between function nodes and variable nodes are the same, as shown in (2.19) and (2.20).

4.4.2 PIC-MMSE Detector

The PIC-MMSE detector also has minimal changes compared to the AWGN channel. The notation $(\cdot)''$ throughout this chapter identifies this variable is for the frequency-selective channel with precoding. The split decision variables after despreading become:

$$\begin{aligned} U''_k &= \mathbf{s}_k^H \mathbf{r} \\ &= \gamma_k A_k b_k + \sum_{\substack{i=1 \\ i \neq k}}^{K} R_{k,i} \gamma_i A_i b_i + \mathbf{s}_k^H \mathbf{n} \end{aligned} \tag{4.26}$$

And in vector notation:

$$\begin{aligned} \mathbf{U}'' &= \mathbf{S}^H \mathbf{r} \\ &= \mathbf{R A \Gamma b} + \mathbf{S}^H \mathbf{n} \end{aligned} \tag{4.27}$$

Then splitting real and imaginary parts:

$$\begin{aligned} \widetilde{\mathbf{U}}'' &= \begin{bmatrix} \Re(\mathbf{U}) \\ \Im(\mathbf{U}) \end{bmatrix} \\ &= \begin{bmatrix} \Re(\mathbf{R}) & -\Im(\mathbf{R}) \\ \Im(\mathbf{R}) & \Re(\mathbf{R}) \end{bmatrix} \begin{bmatrix} \Re(\mathbf{A\Gamma b}) \\ \Im(\mathbf{A\Gamma b}) \end{bmatrix} + \begin{bmatrix} \Re(\mathbf{S}^H) & -\Im(\mathbf{S}^H) \\ \Im(\mathbf{S}^H) & \Re(\mathbf{S}^H) \end{bmatrix} \begin{bmatrix} \Re(\mathbf{n}) \\ \Im(\mathbf{n}) \end{bmatrix} \\ &= \widetilde{\mathbf{R}} \mathbf{A \Gamma b} + \widetilde{\mathbf{S}} \widetilde{\mathbf{n}} \end{aligned} \tag{4.28}$$

The MMSE filter for the multipath channel with precoding is derived in a similar manner to that of the AWGN channel. The MMSE filter is:

$$\mathbf{W}''_{\text{MMSE}} = \boldsymbol{\Upsilon} \widetilde{\mathbf{R}}^T \left(\widetilde{\mathbf{R}} \boldsymbol{\Upsilon} \widetilde{\mathbf{R}}^T + \frac{\sigma^2}{2} \widetilde{\mathbf{S}} \widetilde{\mathbf{S}}^T \right)^+ \tag{4.29}$$

where the amplitudes and effective channel gains are grouped together to form:

$$\boldsymbol{\Upsilon} = \begin{bmatrix} \gamma_1^2 A_1^2 & 0 & \cdots & 0 \\ 0 & \gamma_2^2 A_2^2 & 0 & \vdots \\ \vdots & 0 & \ddots & 0 \\ 0 & \cdots & 0 & \gamma_K^2 A_K^2 \end{bmatrix} \tag{4.30}$$

The filter for user k is:

$$\mathbf{w''}_k = A_k^2 \gamma_k^2 \widetilde{\mathbf{R}}_k^T \left(\widetilde{\mathbf{R}} \boldsymbol{\Upsilon} \widetilde{\mathbf{R}}^T + \frac{\sigma^2}{2} \tilde{\mathbf{S}} \tilde{\mathbf{S}}^T \right)^+ \tag{4.31}$$

The decision variables in vector form after the MMSE detector are:

$$\begin{aligned} \mathbf{U''}_{\text{MMSE}} &= \mathbf{W''}_{\text{MMSE}} \widetilde{\mathbf{U}}'' \\ &= \boldsymbol{\Upsilon} \widetilde{\mathbf{R}}^T \left(\widetilde{\mathbf{R}} \boldsymbol{\Upsilon} \widetilde{\mathbf{R}}^T + \frac{\sigma^2}{2} \tilde{\mathbf{S}} \tilde{\mathbf{S}}^T \right)^+ \widetilde{\mathbf{U}}'' \\ &= \boldsymbol{\Upsilon} \widetilde{\mathbf{R}}^T \left(\widetilde{\mathbf{R}} \boldsymbol{\Upsilon} \widetilde{\mathbf{R}}^T + \frac{\sigma^2}{2} \tilde{\mathbf{S}} \tilde{\mathbf{S}}^T \right)^+ \left(\widetilde{\mathbf{R}} \mathbf{A} \boldsymbol{\Gamma} \mathbf{b} + \tilde{\mathbf{S}} \tilde{\mathbf{n}} \right) \\ &= \boldsymbol{\Upsilon} \widetilde{\mathbf{R}}^T \left(\widetilde{\mathbf{R}} \boldsymbol{\Upsilon} \widetilde{\mathbf{R}}^T + \frac{\sigma^2}{2} \tilde{\mathbf{S}} \tilde{\mathbf{S}}^T \right)^+ \widetilde{\mathbf{R}} \mathbf{A} \boldsymbol{\Gamma} \mathbf{b} + \boldsymbol{\Upsilon} \widetilde{\mathbf{R}}^T \left(\widetilde{\mathbf{R}} \boldsymbol{\Upsilon} \widetilde{\mathbf{R}}^T + \frac{\sigma^2}{2} \tilde{\mathbf{S}} \tilde{\mathbf{S}}^T \right)^+ \tilde{\mathbf{S}} \tilde{\mathbf{n}} \end{aligned} \tag{4.32}$$

The decision variable for user k after the MMSE detector can be written as:

$$\begin{aligned} U''_{\text{MMSE}_k} &= \mathbf{w''}_k \widetilde{\mathbf{U}}'' \\ &= \mathbf{w''}_k \left(\widetilde{\mathbf{R}}_k^T \right)^T \gamma_k A_k b_k + \sum_{\substack{i=1 \\ i \neq k}}^{K} \mathbf{w''}_k \left(\widetilde{\mathbf{R}}_i^T \right)^T \gamma_i A_i b_i + \mathbf{w''}_k \tilde{\mathbf{S}} \tilde{\mathbf{n}} \\ &= \beta''_{k,k} b_k + \sum_{\substack{i=1 \\ i \neq k}}^{K} \beta''_{k,i} b_i + \mathbf{w''}_k \tilde{\mathbf{S}} \tilde{\mathbf{n}} \\ &= \beta''_{k,k} b_k + I''_{\text{MMSE}_k} + N''_{\text{MMSE}_k} \end{aligned} \tag{4.33}$$

where:

$$\begin{aligned} \beta''_{k,i} &= \mathbf{w''}_k \left(\widetilde{\mathbf{R}}_i^T \right)^T \gamma_i A_i \\ &= P_k \gamma_k^2 \widetilde{\mathbf{R}}_k^T \left(\widetilde{\mathbf{R}} \boldsymbol{\Upsilon} \widetilde{\mathbf{R}}^T + \frac{\sigma^2}{2} \tilde{\mathbf{S}} \tilde{\mathbf{S}}^T \right)^+ \left(\widetilde{\mathbf{R}}_i^T \right)^T \gamma_i A_i \end{aligned} \tag{4.34}$$

$$I''_{\text{MMSE}_k} = \sum_{\substack{i=1 \\ i \neq k}}^{K} \beta''_{k,i} b_i \tag{4.35}$$

$$N''_{\text{MMSE}_k} = \mathbf{w''}_k \tilde{\mathbf{S}} \tilde{\mathbf{n}} \tag{4.36}$$

After the MMSE detector, the soft bits are computed and are of the form:

$$b''_{\text{soft}_k} = \tanh\left(\frac{\alpha''_k U''_{\text{MMSE}_k}}{2}\right) \tag{4.37}$$

where

$$\alpha''_k = \frac{4\beta''_{k,k}}{2\sum_{\substack{i=1 \\ i\neq k}}^{K}\left|\beta''_{k,i}\right|^2 + \sigma^2 \mathbf{w}''_k \tilde{\mathbf{S}}\tilde{\mathbf{S}}^T \mathbf{w}''^T_k} \tag{4.38}$$

The PIC detector produces the final decision variables using the soft bits:

$$U''_{\text{PIC}_k} = U''_k - \sum_{\substack{i=1 \\ i\neq k}}^{K} R_{i,k} A_i \gamma_i b''_{\text{soft}_i} \tag{4.39}$$

Finally, a final hard estimate of the bits is made:

$$\hat{b}''_k = \text{sgn}\left(\Re\left(U''_{\text{PIC}_k}\right)\right) \tag{4.40}$$

$$\hat{\mathbf{b}}'' = \text{sgn}\left(\Re\left(\mathbf{U}''_{PIC}\right)\right) \tag{4.41}$$

4.5 Channel Estimation Errors

The performance of the proposed precoding scheme directly relies on the channel state information. Multipath fading channels are constantly changing and can vary depending on the environment and application of the communication link. Depending how often the channel state information is updated, the channel state information may not be accurate relative to the actual channel conditions. The proposed precoding scheme also relies on the receiver communicating the channel state information back to the transmitter. This backwards communication will have to be done over a reliable channel. This also causes delays to the accuracy of the channel state information used and the actual channel. In addition, how the channel state information is obtained varies depending on the estimation scheme used. With all these variables affecting the quality of the channel state information, it is beneficial to view the performance of the precoding scheme in the presence of channel estimation errors.

The error added to the channel state information depends heavily on the method used to estimate the channel state information. In this thesis, the specific channel estimation methods

such as pilot insertion or blind schemes are not investigated. Instead, Gaussian noise is added to the channel state information to test this. In simulations, the variance of the noise will be varied to show the performance in the presence of inaccurate channel state information. The estimated channel vector at tap i for user k is:

$$\hat{h}_{i,k} = h_{i,k} + \epsilon_{i,k} \tag{4.42}$$

where $\epsilon_{i,k}$ is a Gaussian random variable with zero mean and variance $\sigma^2_{\epsilon_{i,k}}$.

4.6 Simulation Results

In this section, the BER performance of the precoding scheme will be examined. The performance of the precoding scheme is analyzed by varying different parameters which include the multipath channel length and decoding methods. In addition, the BER performance in the presence of estimation errors is examined. The simulation parameters are:

- The 6 chip 9 user system in (2.24) is used for all simulations.
- BPSK modulation is used.
- Each user transmits with unit energy per bit
- The number of symbols (bits) grouped together in parallel is $N_{\text{syms}} = 100$ for all simulations. This leads to $N_{\text{syms}}N = (6)(100) = 600$ chips used for the DFT and IDFT operation.
- The multipath channel is assumed to remain constant during each precoding instance.
- The multipath channel is zero padded to a length of 600 for the DFT operation.

In Figure 4.5, Figure 4.6, Figure 4.7, and Figure 4.8, the precoding scheme is applied to a multipath channel with varying channel lengths of $L = 1,3,5,7$. The MPA, and PIC-MMSE detector as well as the single user bound in the frequency-nonselective fading channel are presented. For the single tap channel, both the MPA and PIC-MMSE detectors approach the single user bound. As was shown in section 4.3.1, the precoding removes the phase of the complex channel gains. The effective channel gain for each user will be independent, which allows for additional diversity between them.

As the channel length increases, the performance of the precoding scheme starts to saturate for both the MPA and PIC-MMSE detectors. Longer channel vectors result in more multipath rich environments, which negatively impacts performance. But, the precoding scheme can handle these harsher channels which is very beneficial.

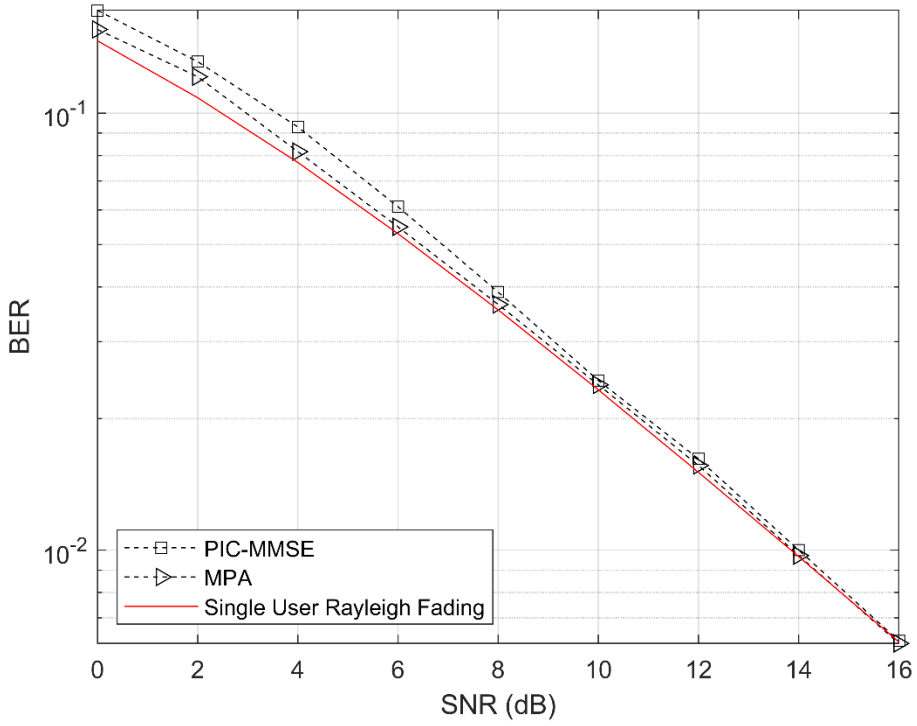

Figure 4.5: The MPA and PIC-MMSE detectors with precoding for a multipath channel with $L = 1$ number of taps

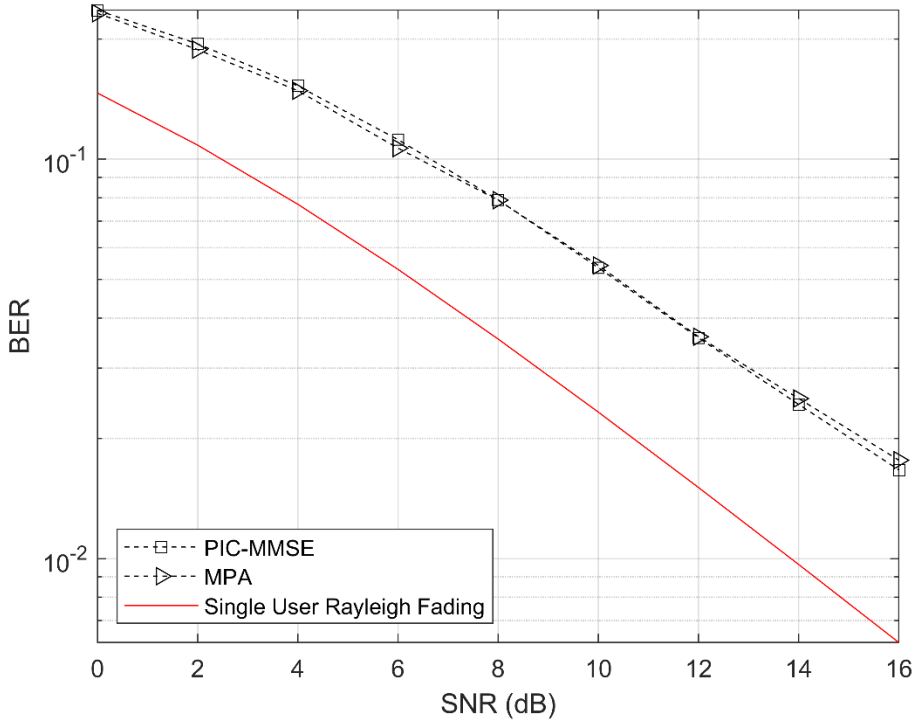

Figure 4.6: The MPA and PIC-MMSE detectors with precoding for a multipath channel with $L = 3$ number of taps

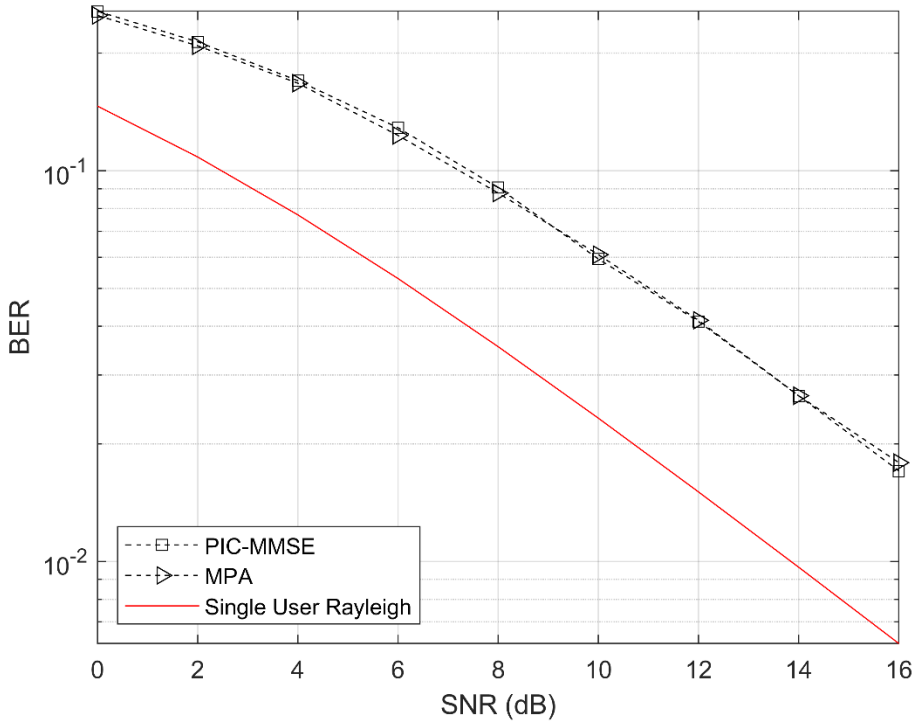

Figure 4.7: The MPA and PIC-MMSE detectors with precoding for a multipath channel with $L = 5$ number of taps

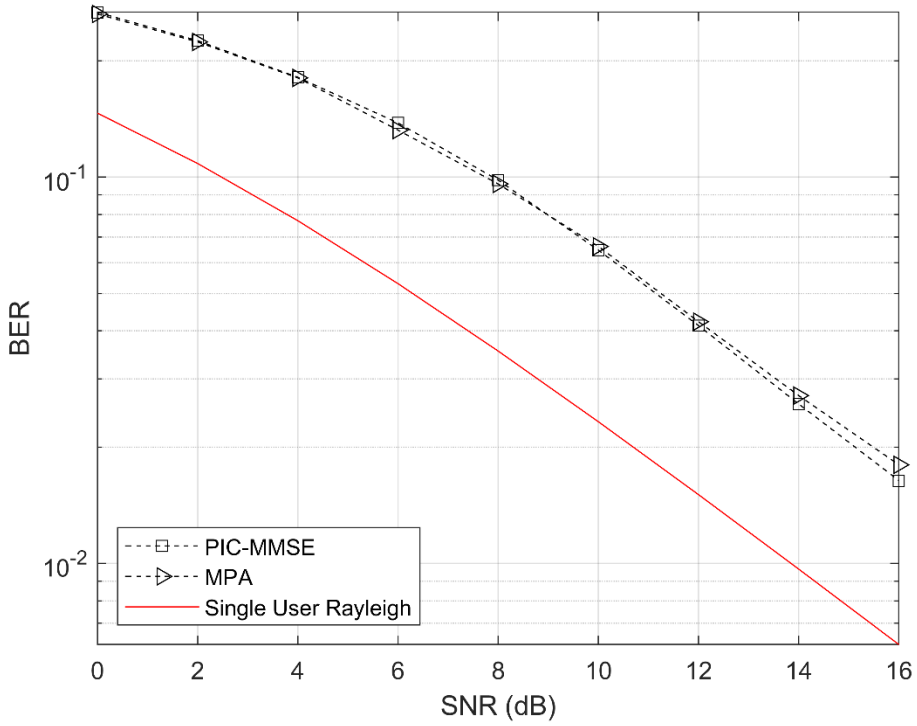

Figure 4.8: The MPA and PIC-MMSE detectors with precoding for a multipath channel with $L = 7$ number of taps

Next, the performance of the precoding scheme in the presence of channel estimation errors is examined, as discussed in section 4.5. To simulate this, zero mean Gaussian noise is added to the channel vector with varying variance. Figure 4.9, Figure 4.10 and Figure 4.11 show the BER performance with varying levels of noise added to the channel vector, and varying channel lengths. As the channel length increases, it is evident that the effect of the estimation errors becomes more severe, as expected.

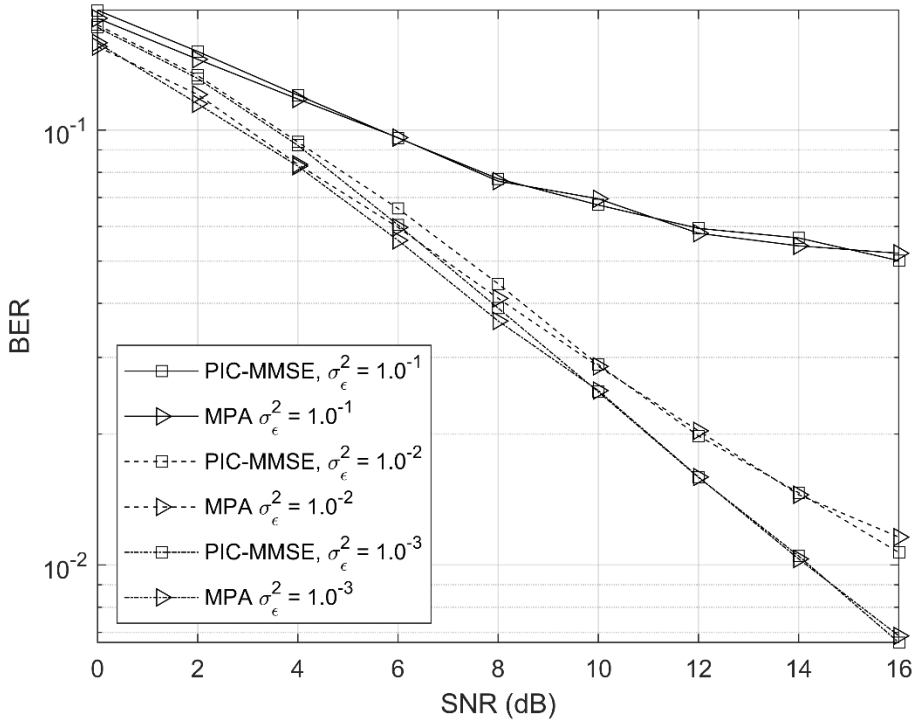

Figure 4.9: BER performance in the presence of channel estimation errors to the MPA and PIC-MMSE detectors with a multipath channel of $L = 1$ taps

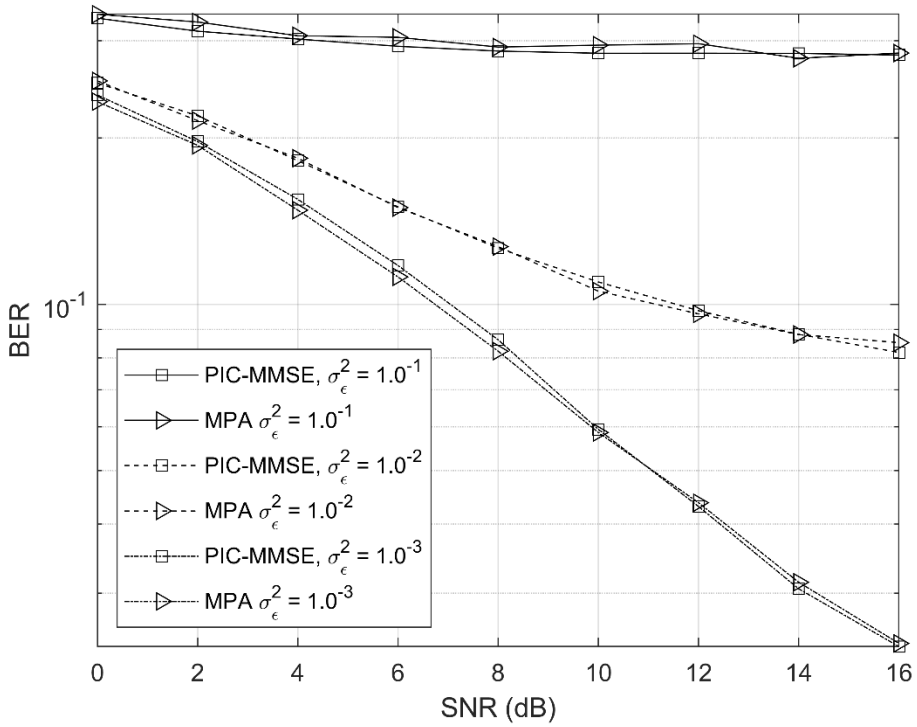

Figure 4.10: BER performance in the presence of channel estimation errors to the MPA and PIC-MMSE detectors with a multipath channel of $L = 3$ taps

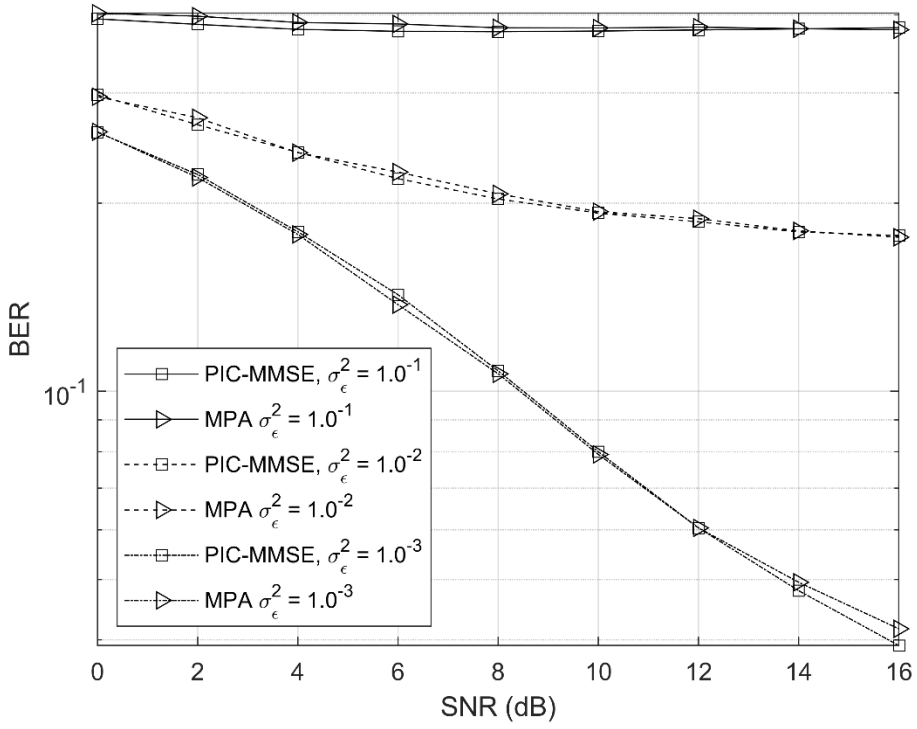

Figure 4.11: BER performance in the presence of channel estimation errors to the MPA and PIC-MMSE detectors with a multipath channel of $L = 5$ taps

4.7 Summary

In this chapter, a precoding scheme designed for multipath channels was presented. The low-density structure of LDS systems makes them even more susceptible to the effects of multipath fading compared to regular spread spectrum systems. The proposed precoding scheme applies a normalized inverse channel frequency response to the spread chips. When this precoded signal passes through the multipath channel, the delayed components of the multipath channel are eliminated. This effectively transforms the multipath channel into a single path channel.

In addition, the MPA and PIC-MMSE detectors were altered to improve their performance in the presence of precoding and multipath fading. Simulation results were presented to test the BER performance of the precoding scheme for both the MPA and PIC-MMSE detectors. It was shown that as the number of channel taps increased, the BER performance saturated, which shows the precoding scheme to be effective even in harsh multipath conditions.

Chapter 5
Conclusions and Potential Future Work

5.1 Conclusion

NOMA schemes have become a popular alternative for future wireless networks, including 5G, compared to typical OMA schemes due to the high spectral efficiencies they offer. Code-domain NOMA is among this popular group and include schemes like LDS and SCMA. LDS systems use MPA detection for MUD, which has complexity exponential to the number of interfering users per chip. In addition, LDS systems require full synchronization as MPA detection is a chip-level iterative algorithm. A multipath environment will destroy the LDS structure and MUD is difficult. These two inherent issues of high computational complexity and multipath channels are addressed in this thesis.

In chapter 2, LDS systems were discussed and examined in detail. The system model for LDS systems was presented for both the AWGN and frequency and frequency-nonselective channels. The design of spreading sequences and their important properties as well as the derivation of the MPA were also discussed. Simulation results show the MPA detector approaches the single user bound after a few iterations.

Chapter 3 introduced the proposed PIC-MMSE MUD technique. The PIC-MMSE detector combines the standard MMSE and PIC detectors, in a multistage manner. It is shown the PIC-MMSE detector offers a drastic reduction in computational complexity compared to the MPA detector and has computational complexity that is quadratic to the number of users in the systems. In addition, an approximate BER expression is derived and closely matches the simulated BER. Simulation results showed the PIC-MMSE detector is able to achieve reductions in multiplications and additions by over 65% while suffering a loss of a fraction of a dB.

In chapter 4, the proposed precoding scheme for multipath channels was introduced. The precoding applies an inverse channel frequency response to a block of spread chips. The received signal with precoding appears at the receiver with no ISI, and the multipath channel

is transformed into a single tap channel. The PIC-MMSE and MPA detectors in this channel model have a similar structure to the frequency-nonselective channel. Simulation results show the precoding scheme is effective and reliable communication is possible, even in harsh multipath conditions.

5.2 Potential Future Work

While this thesis presented an alternative MUD and precoding scheme to combat multipath channels, there are further areas to explore.

Error control coding was not studied in this thesis but is a necessity in all communication systems. It would be advantageous to explore how the PIC-MMSE and precoding impact the performance with error control coding. Typically, the channel decoding is done after the received signal is demodulated. A possibility would be to implement a soft decoder after the MMSE detector, just before the PIC detector. This way, the channel decoder and PIC detector could manipulate the bits, like a turbo decoder.

Minimal work has been done for LDS systems employing multiple-input multiple-output (MIMO) systems. MIMO has been researched with SCMA systems [51], to improve BER as well as spectral efficiency. Like the SCMA system proposed in [19], LDS can be used to employ permutation spreading, in which message bits are not spread to the same code, but instead are used to select a certain code from a group of codes of possible. While SCMA employs this same concept of selecting a codeword from a given codebook, what can be done instead is have this mapping extended to different spreading sequences chosen for each transmit antenna based on the message bits.

The spreading codes used in simulations were from other external sources and were not designed. The MPA and PIC-MMSE detectors use very different detection techniques, and the spreading codes used may be optimal for one detector but not another. The design of spreading codes specifically for the PIC-MMSE detector should look to minimize the cross correlations between codes, as this will help separate them and decrease the MAI. In addition, irregular indicator matrix designs could be implemented which would help the performance of the PIC part of the PIC-MMSE detector.

Bibliography

[1] J. Andrews, S. Buzzi, W. Choi, S. Hanly, A. Lozano, A. Soong and J. Zhang, "What Will 5G Be?," *IEEE Journal on Selected Areas in Communications,* vol. 32, no. 6, pp. 1065-1082, June 2014.

[2] F. Boccardi, R. Heath, A. Lozano, T. Marzetta and P. Popovski, "Five disruptive technology directions for 5G," *IEEE Communications Magazine,* vol. 52, no. 2, pp. 74-80, Dec. 2014.

[3] H. Zheng and L. Cao, "Device-centric Spectrum Management," in *First IEEE International Symposium on New Frontiers in Dynamic Spectrum Access Networks, 2005. DySPAN 2005.*, Baltimore, Nov. 2005.

[4] Y. Niu, Y. Li, D. Jin, L. Su and A. V. Vasilakos, "A Survey of Millimeter Wave (mmWave) Communications for 5G: Opportunities and Challenges," *Wireless Networks,* vol. 21, no. 8, pp. 2657-2676, Nov. 2015.

[5] W. Roh, J.-Y. Seol, J. Park, B. Lee, J. Lee, Y. Kim, J. Cho, K. Cheun and F. Aryanfar, "Millimeter-Wave Beamforming as an Enabling Technology for 5G Cellular Communications: Theoretical Feasibility and Prototype Results," *IEEE Communications Magazine,* vol. 52, no. 2, pp. 106-113, Feb. 2014.

[6] E. G. Larsson, O. Edfors, F. Tufvesson and T. L. Marzetta, "Massive MIMO for Next Generation Wireless Systems," *IEEE Communications Magazine,* vol. 52, no. 2, pp. 186-195, Apr. 2014.

[7] B. Di, L. Song, Y. Li and Z. Han, "V2X Meets NOMA: Non-Orthogonal Multiple Access for 5G Enabled Vehicular Networks," *IEEE Wireless Communications,* vol. 24, no. 6, pp. 14-21, Dec. 2017.

[8] L. Dai, B. Wang, Z. Ding, Z. Wang, S. Chen and L. Hanzo, "A Survey of Non-Orthogonal Multiple Access for 5G," *IEEE Communications Surveys & Tutorials,* vol. 20, no. 3, pp. 2294-2323, May 2018.

[9] Y. Cai, Z. Qin, F. Cui, G. Y. Li and J. A. McCann, "Modulation and multiple access for 5G networks," *IEEE Communications Surveys & Tutorials,* vol. 20, no. 1, pp. 626-646, Oct. 2018.

[10] Y. Saito, Y. Kishiyama, A. Benjebbour, T. Nakamura, A. Li and K. Higuchi, "Non-Orthogonal Multiple Access (NOMA) for Cellular Future Radio Access," in *2013 IEEE 77th Vehicular Technology Conference (VTC Spring)*, Dresden, Germany, June 2013.

[11] S. Chen, B. Ren, Q. Gao, S. Kang, S. Sun and K. Niu, "Pattern Division Multiple Access—A Novel Nonorthogonal Multiple Access for Fifth-Generation Radio Networks," *IEEE Transactions on Vehicular Technology,* vol. 66, no. 4, pp. 3185-3196, Apr. 2017.

[12] D. Fang, Y. Huang, Z. Ding, G. Geraci, S. Shieh and H. Claussen, "Lattice Partition Multiple Access: A New Method of Downlink Non-Orthogonal Multiuser Transmissions," in *2016 IEEE Global Communications Conference (GLOBECOM)*, Washington, DC, Dec. 2016.

[13] L. Dai, B. Wang, W. Yuan, S. Han, C. I and Z. Wang, "Non-Orthogonal Multiple Access for 5G: Solutions, Challenges, Opportunities, and Future Research Trends," *IEEE Communications Magazine,* vol. 53, no. 9, pp. 74-81, Sept. 2015.

[14] J. Choi, "Low Density Spreading For Multicarrier Systems," in *Eighth IEEE International Symposium on Spread Spectrum Techniques and Applications - Programme and Book of Abstracts (IEEE Cat. No.04TH8738)*, Sydney, Aug. 2004.

[15] R. Hoshyar, R. Wathan and R. Tafazolli, "Novel Low-Density Signature for Synchronous CDMA Systems Over AWGN Channel," *IEEE Transactions on Signal Processing,* vol. 56, no. 4, pp. 1616-1626, Apr. 2008.

[16] H. Nikopour and H. Baligh, "Sparse Code Multiple Access," in *2013 IEEE 24th Annual International Symposium on Personal, Indoor, and Mobile Radio Communications (PIMRC)*, London, Sept. 2013.

[17] M. Tahersadeh, H. Nikopour, A. Bayesteh and H. Baligh, "SCMA Codebook Design," in *2014 IEEE 80th Vehicular Technology Conference (VTC2014-Fall)*, Vancouver, Sept. 2014.

[18] L. Y, X. L. P. Fan and D. Chen, "An optimized design of SCMA codebook 7based on star-QAM signaling constellations," in *2015 International Conference on Wireless Communications & Signal Processing (WCSP)*, Nanjing, Oct. 2015.

[19] M. Kulhandjian and C. D'Amours, "Design of Permutation-Based Sparse Code Multiple Access System," in *2017 IEEE 28th Annual International Symposium on Personal, Indoor, and Mobile Radio Communications (PIMRC)*, Montreal, Oct. 2017.

[20] R. Gallager, "Low-Density Parity-Check Codes," *IRE Transactions on Information Theory,* vol. 8, no. 1, pp. 21-28, Jan. 1962.

[21] S.-Y. Chung, G. D. Forney, T. J. Richardson and R. Urbanke, "On the Design of Low-Density Parity-Check Codes Within 0.0045 dB of the Shannon Limit," *IEEE Communications Letters,* vol. 5, no. 2, pp. 58-60, Feb. 2001.

[22] T. Qi, W. Feng, Y. Chen and Y. Wang, "When NOMA Meets Sparse Signal Processing: Asymptotic Performance Analysis and Optimal Sequence Design," *IEEE Access,* vol. 5, pp. 18516-18525, 2017.

[23] J. v. d. Beek and B. M. Popovic, "Multiple Access with Low-Density Signatures," in *GLOBECOM 2009 - 2009 IEEE Global Telecommunications Conference*, Honolulu, Nov. 2009.

[24] K. Alishahi, S. Dashmiz, P. Pad and F. Marvasti, "Design of Signature Sequences for Overloaded CDMA and Bounds on the Sum Capacity With Arbitray Symbol Alphabets," *IEEE Transactions on Information Theory,* vol. 58, no. 3, pp. 1441-1469, Mar. 2012.

[25] F. Kschischang, B. Frey and H.-A. Loeliger, "Factor graphs and the sum-product algorithm," *IEEE Transactions on information theory,* vol. 47, no. 2, pp. 498-519, Feb. 2001.

[26] D. Guo and C.-C. Wang, "Multiuser Detection of Sparsely Spread CDMA," *IEEE Journal on Selected Areas in Communications,* vol. 26, no. 3, pp. 421-431, Apr. 2008.

[27] Y. Wu, S. Zhang and Y. Chen, "Iterative Multiuser Receiver in Sparse Code Multiple Access Systems," in *2015 IEEE International Conference on Communications (ICC)*, London, June 2015.

[28] Y. Du, B. Dong, Z. Chen, J. Fang and L. Yang, "Shuffled Multiuser Detection Schemes for Uplink Sparse Code Multiple Access System," *IEEE Communications Letters,* vol. 20, no. 6, pp. 1231-1234, June 2016.

[29] F. Wathan, R. Hoshyar and R. Tafazolli, "Dynamic Grouped Chip-Level Iterated Multiuser Detection Based on Gaussian Forcing Technique," *IEEE Communications Letters,* vol. 12, no. 3, pp. 167-169, Mar. 2008.

[30] D. Wei, Y. Han, S. Zhang and L. Liu, "Weighted Message Passing Algorithm for SCMA," in *2015 International Conference on Wireless Communications & SIgnal Processing (WCSP)*, Nanjing, Oct. 2015.

[31] X. Dai, S. Chen, S. Sun, S. Kang, Y. Wang, Z. Shen and J. Xua, "Successive Interference Cancelation Amenable Multiple Access (SAMA) for Future Wireless Communications," in *2014 IEEE International Conference on Communication Systems*, Macau, Nov. 2014.

[32] S. Verdu, Multiuser Detection, Cambridge: Cambridge University Press, 1998.

[33] R. L. a. S. Verdu, "Linear Multiuser Detectors for Synchronous Code-Division Multiple-Access Channels," *IEEE Transactions on Information Theory,* vol. 35, no. 1, pp. 123-136, Jan. 1989.

[34] U. Madhow and M. L. Honig, "MMSE Interference Suppression for Direct-Sequence Spread-Spectrum CDMA," *IEEE Transactions on Communications,* vol. 42, no. 12, pp. 3178-3188, Dec. 1994.

[35] M. K. Varanasi, C. T. Mullis and A. Kapur, "On the Limitation of Linear MMSE Detection," *IEEE Transactions on Information Theory,* vol. 52, no. 9, pp. 4282-4286, Sept. 2006.

[36] J. G. Proakis and M. Salehi, Digital Communications, 5th ed., New York: Mcgraw-Hill, 2008.

[37] M. K. Varanasi and B. Aazhang, "Multistage Detection in Asynchronous Code-Division Multiple-Access Communications," *IEEE Transactions on Communications,* vol. 38, no. 4, pp. 509-519, Apr. 1990.

[38] D. Divsalar, M. K. Simon and D. Raphaeli, "Improved Parallel Interference Cancellation for CDMA," *IEEE Transactons on Communications,* vol. 4, no. 2, pp. 258-268, Feb. 1998.

[39] R. Irmer, A. Nahler and G. Fettweis, "On the Impact of Soft Decision Functions on the Performance of Multistage Parallel Interference Cancelers for CDMA SystemsI," in *IEEE VTS 53rd Vehicular Technology Conference, Spring 2001*, Rhodes, Greece, May 2001.

[40] D. Divsalar, M. K. Simon and D. Raphaeli, "Improved Parallel Interference Cancellation for CDMA," *IEEE Transactions on Communications,* vol. 46, no. 2, pp. 258-268, Feb. 1998.

[41] D. R. Brown, M. Motani, V. V. Veeravalli, H. V. Poor and C. R. Johnson, "On the Performance of Linear Parallel Interference Cancellation," *IEEE Transactions on Information Theory,* vol. 47, no. 5, pp. 1957-1970, July 2001.

[42] H. V. Poor and S. Verdu, "Probability of Error in MMSE Multiuser Detection," *IEEE Transactions on Information Theory,* vol. 43, no. 3, pp. 858-871, May 1997.

[43] I. Gradshteyn and I. Ryzhik, Table of Integrals, Series, and Products Seventh Edition, Amsterdam: Elsevier/Academic Press, 2007.

[44] Y. Du, B. Dong, Z. Chen, J. Fang and X. Wang, "A Fast Convergence Multiuser Detection Scheme for Uplink SCMA Systems," *IEEE Wireless Communications Letters,* vol. 5, no. 4, pp. 388-391, Aug. 2016.

[45] R. Hoshyar, R. Razavi and M. AL-Imari, "LDS-OFDM an Efficient Multiple Access Technique," in *2010 IEEE 71st Vehicular Technology Conference*, Taipei, May 2010.

[46] R. v. Nee and R. Prasad, OFDM for Wireless Multimedia Communications, Norwood MA: Artech House, Inc., 2000.

[47] H. Ochiai and H. Imai, "On the Distribution of the Peak-To-Average Power Ratio in OFDM Signals," *IEEE Transactions on Communications,* vol. 49, no. 2, pp. 282-289, Feb. 2001.

[48] G. E. Bottomley, T. Ottosson and Y.-P. Wang, "A Generalized RAKE Receiver for Interference Suppression," *IEEE Journal on Selected Areas in Communications,* vol. 18, no. 8, pp. 1536-1545, Aug. 2000.

[49] D. Falconer, S. L. Ariyavisitakul, A. Benyamin-Seeyar and B. Eidson, "Frequency Domain Equalization for Single-Carrier Broadband Wireless Systems," *IEEE Communications Magazine,* vol. 40, no. 4, pp. 58-66, Apr. 2002.

[50] X. Wang and H. V. Poor, "Blind Equalization and Multiuser Detection in Dispersive CDMA Channels," *IEEE Transactions on Communications,* vol. 46, no. 1, pp. 91-103, Jan. 1998.

[51] H. Nikopour, E. Yi, A. Bayesteh, K. Au, M. Hawryluck, H. Baligh and J. Ma, "SCMA for Downlink Multiple Access of 5G Wireless Networks," in *2014 IEEE Global Communications Conference*, Austin, Dec. 2014.